ESL-TR-87-63

HYDRAZINE LOSS PROCESSES IN A TEFLON FILM REACTION CHAMBER: LABORATORY RESULTS AND KINETIC MODELS

D.A. STONE, F.L. WISEMAN

HQ AIR FORCE ENGINEERING AND SERVICES CENTER
AIR FORCE ENGINEERING AND SERVICES LABORATORY
TYNDALL AFB FL 32403-6001

MARCH 1988

FINAL REPORT

SEPTEMBER 1985-SEPTEMBER 1987

ENGINEERING & SERVICES LABORATORY
AIR FORCE ENGINEERING & SERVICES CENTER
TYNDALL AIR FORCE BASE, FLORIDA 32403

NOTICE

The following commercial products (requiring Trademark) are mentioned in this report. Because of the frequency of usage, the Trademark was not indicated. If it becomes necessary to reproduce any segment of this document containing any of these names, this notice must be included as part of that reproduction.

Pyrex
Teflon
Tedlar
Mylar
Plexiglas
Nylon
Tygon
Freon-12
NICOS

Mention of the products listed above does not constitute Air Force endorsement or rejection of this product, and use of information contained herein for advertising purposes without obtaining clearance according to existing contractual agreements is prohibited.

PLEASE DO NOT REQUEST COPIES OF THIS REPORT FROM HQ AFESC/RD (ENGINEERING AND SERVICES LABORATORY). ADDITIONAL COPIES MAY BE PURCHASED FROM:

NATIONAL TECHNICAL INFORMATION SERVICE
5285 PORT ROYAL ROAD
SPRINGFIELD, VIRGINIA 22161

FEDERAL GOVERNMENT AGENCIES AND THEIR CONTRACTORS REGISTERED WITH DEFENSE TECHNICAL INFORMATION CENTER SHOULD DIRECT REQUESTS FOR COPIES OF THIS REPORT TO:

DEFENSE TECHNICAL INFORMATION CENTER
CAMERON STATION
ALEXANDRIA, VIRGINIA 22314

REPORT DOCUMENTATION PAGE

Form Approved OMB No. 0704-0188

a. REPORT SECURITY CLASSIFICATION: UNCLASSIFIED	1b. RESTRICTIVE MARKINGS
a. SECURITY CLASSIFICATION AUTHORITY	3. DISTRIBUTION/AVAILABILITY OF REPORT: Approved for Public Release. Distribution Unlimited.
b. DECLASSIFICATION/DOWNGRADING SCHEDULE	
. PERFORMING ORGANIZATION REPORT NUMBER(S): ESL-TR-87-68	5. MONITORING ORGANIZATION REPORT NUMBER(S): ESL-TR-87-68
a. NAME OF PERFORMING ORGANIZATION: Air Force Engineering and Services Center; 6b. OFFICE SYMBOL (If applicable): RDVS	7a. NAME OF MONITORING ORGANIZATION
c. ADDRESS (City, State, and ZIP Code): HQ AFESC/RDVS, Tyndall AFB FL 32403-6001	7b. ADDRESS (City, State, and ZIP Code)
a. NAME OF FUNDING/SPONSORING ORGANIZATION: Air Force Engineering and Services Center; 8b. OFFICE SYMBOL (If applicable): RDV	9. PROCUREMENT INSTRUMENT IDENTIFICATION NUMBER: In-House
c. ADDRESS (City, State, and ZIP Code): HQ AFESC/RDVS, Tyndall AFB FL 32403-6001	10. SOURCE OF FUNDING NUMBERS

PROGRAM ELEMENT NO.	PROJECT NO.	TASK NO	WORK UNIT ACCESSION NO.
6.11 01	0100 0100	8314 8316	NA

1. TITLE (Include Security Classification)
Hydrazine Loss Processes in a Teflon Film Reaction Chamber: Laboratory Results and Kinetic Models

2. PERSONAL AUTHOR(S)
Daniel A. Stone and Floyd L. Wiseman

3a. TYPE OF REPORT	13b. TIME COVERED	14. DATE OF REPORT (Year, Month, Day)	15. PAGE COUNT
Final	FROM Sep 85 TO Sep 87	March 1988	129

6. SUPPLEMENTARY NOTATION
Availability of this report is specified on reverse of front cover.

7. COSATI CODES			18. SUBJECT TERMS (Continue on reverse if necessary and identify by block number)
FIELD	GROUP	SUB-GROUP	Hydrazine, Thrusters, Decay Processes in Environmental Chambers, Kinetic Modeling
07	04		
12	01		

9. ABSTRACT (Continue on reverse if necessary and identify by block number)

Experimental chamber studies and kinetic modeling of hydrazine vapor loss in a Teflon film chamber are presented in this technical report. Details of the experimental procedures employed to inject and monitor the decay of hydrazine and various tracer gases in the chamber are presented. A mathematical model is developed which explains and quantifies the experimental data. The decay data are plotted along with model curves which fit the observed data very well and offer a consistent explanation of their significance.

Kinetic data were generated using long-path Fourier transform infrared (FT-IR) spectroscopy to measure the appropriate absorbance values. Hydrazine liquid was vaporized and then flushed into a 320-L Teflon film chamber, equipped with a small mixing fan. The vapor-phase hydrazine concentration was monitored by measuring the peak height of the amino wagging vibration at 958 wavenumbers. Beer's law was assumed to be obeyed in the concentration ranges studied.

0. DISTRIBUTION/AVAILABILITY OF ABSTRACT	21. ABSTRACT SECURITY CLASSIFICATION
☒ UNCLASSIFIED/UNLIMITED ☐ SAME AS RPT. ☐ DTIC USERS	UNCLASSIFIED
2a. NAME OF RESPONSIBLE INDIVIDUAL: Dr Daniel A. Stone	22b. TELEPHONE (Include Area Code): (904) 283-4298 / 22c. OFFICE SYMBOL: HQ AFESC/RDVS

Continuation of Block 19 (Abstract)

As internal standards, methane and sulfur hexafluoride were flushed into the cham and their concentrations were monitored as a function of time. The vapor-ph half-lives of these compounds varied from about 40 to 60 hours, three to four ti longer than hydrazine. Experiments were also conducted with ammonia, Freon-12, methan water, and oxygen.

Kinetic studies revealed that the hydrazine loss rate in Teflon chambers independent of the oxygen content of the chamber matrix gas. Hence, vapor-ph autoxidation of hydrazine was ruled out. However, a small amount of ammonia was detec in the hydrazine studies, indicating some chemical reaction, probably surface-catalyz was occurring. The amount of ammonia formed was independent of the oxygen content of matrix gas in the chamber.

Other studies revealed that the hydrazine loss rate was strongly dependent on relative humidity (RH). At 50 percent RH, the initial loss rate was reduced by a fac of two to four. Moreover, there was a substantial deviation of the data from sim first-order behavior when compared to dry conditions. Since there was no spectrosco evidence for a vapor-phase hydrazine hydrate complex, it seems likely that the init hydrazine vapor loss rate was increased by enhanced adsorption on wetted surfaces in chamber.

Finally, studies revealed that the chamber system showed a conditioning effect tow hydrazine. That is, kinetic runs performed back-to-back showed an increase in half-life which tended toward an asymptotic level. The chamber could be deconditioned allowing it to remain unused for a few weeks. This conditioning effect was str evidence for hydrazine-surface interactions in the chamber.

Even though it was apparent that the vapor-phase loss of hydrazine invol predominantly physical rather that chemical processes, a comprehensive kinetic mod taking into account both physical and chemical processes, was developed. The mo included the following processes: simple second-order reactions, adsorption desorption, permeation through polymeric film, effusion (i.e., leakage through undetec holes of various sizes), and surface catalysis. The model was much more complex than needed, so abridged versions were used to fit single and sequential data sets. general, the permeation portion of the model was used to fit single data sets, althoug coupled version which included effusion and first-order adsorption and desorption co fit data sets equally well. Sequential data sets had to be fit using effusion coup with second-order adsorption and desorption. Making the adsorption process seco rather than first-order was designed to account for conditioning. The fits of the mo versions to the data sets were generally very good.

The three processes which could lead to loss of hydrazine from the system w permeation through the chamber walls, effusion, and chemical reactions. Chem reactions were ruled out in these experiments but the relative importance of effu versus permeation could not be determined from the model.

Continuation of Block 19 (Abstract)

As internal standards, methane and sulfur hexafluoride were flushed into the chamber and their concentrations were monitored as a function of time. The vapor-phase half-lives of these compounds varied from about 40 to 60 hours, three to four times longer than hydrazine. Experiments were also conducted with ammonia, Freon-12, methanol, water, and oxygen.

Kinetic studies revealed that the hydrazine loss rate in Teflon chambers was independent of the oxygen content of the chamber matrix gas. Hence, vapor-phase autoxidation of hydrazine was ruled out. However, a small amount of ammonia was detected in the hydrazine studies, indicating some chemical reaction, probably surface-catalyzed, was occurring. The amount of ammonia formed was independent of the oxygen content of the matrix gas in the chamber.

Other studies revealed that the hydrazine loss rate was strongly dependent on the relative humidity (RH). At 50 percent RH, the initial loss rate was reduced by a factor of two to four. Moreover, there was a substantial deviation of the data from simple first-order behavior when compared to dry conditions. Since there was no spectroscopic evidence for a vapor-phase hydrazine hydrate complex, it seems likely that the initial hydrazine vapor loss rate was increased by enhanced adsorption on wetted surfaces in the chamber.

Finally, studies revealed that the chamber system showed a conditioning effect toward hydrazine. That is, kinetic runs performed back-to-back showed an increase in the half-life which tended toward an asymptotic level. The chamber could be deconditioned by allowing it to remain unused for a few weeks. This conditioning effect was strong evidence for hydrazine-surface interactions in the chamber.

Even though it was apparent that the vapor-phase loss of hydrazine involved predominantly physical rather that chemical processes, a comprehensive kinetic model, taking into account both physical and chemical processes, was developed. The model included the following processes: simple second-order reactions, adsorption and desorption, permeation through polymeric film, effusion (i.e., leakage through undetected holes of various sizes), and surface catalysis. The model was much more complex than was needed, so abridged versions were used to fit single and sequential data sets. In general, the permeation portion of the model was used to fit single data sets, although a coupled version which included effusion and first-order adsorption and desorption could fit data sets equally well. Sequential data sets had to be fit using effusion coupled with second-order adsorption and desorption. Making the adsorption process second- rather than first-order was designed to account for conditioning. The fits of the model versions to the data sets were generally very good.

The three processes which could lead to loss of hydrazine from the system were permeation through the chamber walls, effusion, and chemical reactions. Chemical reactions were ruled out in these experiments but the relative importance of effusion versus permeation could not be determined from the model.

PREFACE

This report was prepared by the Engineering and Services Laboratory of the Air Force Engineering and Services Center (AFESC), Tyndall Air Force Base FL 32403-6001. This work was sponsored by AFESC. Dr Daniel A. Stone and 1Lt Floyd L. Wiseman (AFESC/RDVS) were the government project officers. This report summarizes work accomplished between October 1985 and September 1987 under program element 61101F.

This report has been reviewed by the Public Affairs Office (PA) and is releasable to the National Technical Information Service (NTIS). At NTIS, it will be available to the general public, including foreign nationals.

This technical report has been reviewed and is approved for publication.

DANIEL A.STONE, PhD
Research Chemist

THOMAS J. WALKER, Lt Col, USAF, BSC
Chief, Environics Division

FLOYD L. WISEMAN, 1Lt, USAF
Chemistry R&D Project Officer

LAWRENCE D. HOKANSON, Col, USAF
Director, Engineering and Services Laboratory

KENNETH T. DENBLEYKER, Maj, USAF
Chief, Environmental Sciences Branch

(The reverse of this page is blank.)

TABLE OF CONTENTS

TABLE OF CONTENTS
(Continued)

LIST OF FIGURES

LIST OF FIGURES
(Continued)

LIST OF TABLES

(The reverse of this page is blank.)

SECTION I

INTRODUCTION

A. OBJECTIVE

The research described in this report was undertaken to extend our knowledge of the chemical transformations of hydrazine vapor in the environment. It is known that both gas-phase and surface-catalyzed reactions can occur with this fuel. In the immediate vicinity of the ground, other surface processes, such as adsorption, can also be important.

To determine the eventual fate of hydrazine vapors which escape into the atmosphere through normal operations or during accidental liquid spills, all of these processes must be investigated. This study was undertaken in a chamber designed to simulate atmospheric conditions, but allowing for some control over important variables to address some of the potential chemical transformations.

B. BACKGROUND

Hydrazine is used extensively in small thrusters for satellites, as a fuel cell reactant, in emergency power generating units, and as a liquid rocket fuel component. Both routine handling operations and accidental spills can produce fuel vapors which constitute a substantial health risk. Hydrazine is classified as an animal carcinogen (Reference 1) and a suspect human carcinogen (Reference 2). This toxicity is reflected in its low threshold limit value, 0.1 parts per million (ppm) (Reference 3), and has prompted numerous studies of the fate of hydrazine in both atmospheric and terrestrial environments.

The autoxidation of hydrazine vapor has been the subject of several previous studies. Bowen and Birley investigated what they believed to be the vapor-phase reaction between hydrazine and oxygen in a Pyrex reaction vessel (Reference 4). They concluded that from 100 °C to 160 °C the reaction

was first order in both hydrazine and oxygen and that it proceeded by a five- or six-step successive chain reaction. The overall reaction stoichiometry was shown to be:

$$N_2H_4 + O_2 \longrightarrow N_2 + 2H_2O \qquad (1)$$

They further noted that the rate of the reaction was a function of the surface area of the reaction vessel.

Winning (Reference 5) conducted a similar study in 2-L and 0.5-L quartz reaction vessels from 20 °C to 185 °C. He also found that the rate of the reaction was directly proportional to the surface area of the reaction vessel. His results also showed that the reaction was first-order with respect to both hydrazine and oxygen. He determined that neither added nitrogen or water vapor had any effect on the reaction rate. However, he interpreted his results by invoking a nonchain bimolecular surface reaction. He also noted the production of some ammonia at temperatures above 115 °C.

Stone conducted two studies of the autoxidation of hydrazine vapor in various-sized Pyrex containers (References 6 and 7). All experiments were conducted at 25 °C. These studies gave a reaction stoichiometry in agreement with equation (1). They also showed the dependence of reaction rate on surface-to-volume ratio and on the surface composition. Small amounts of ammonia were produced in most experimental runs.

Bellerby (References 8 and 9) analyzed the studies of earlier researchers and deduced a mechanism which accounts for their major experimental observations. He proposed that the initial formation of a hydroperoxide by a chain process was followed by wall reaction to give the observed products.

An entire doctoral study, "The Vapor Phase Oxidation of Hydrazine," was recently completed by Moody (Reference 10). He studied the effects of temperature, surface-to-volume ratio, total reaction pressure, and the composition of the surface of the reaction vessel. The reaction vessels used in this work were relatively small, 0.3 - 1.9 L, and constructed from Pyrex.

In these vessels, Moody found that there was an unusual negative temperature coefficient in the reaction rate. He concluded that the surfaces of the reaction vessels play a dominant role and that there is ample evidence for a free-radical chain reaction mechanism.

Pitts and co-workers conducted two studies of the reactions of hydrazines under simulated urban tropospheric conditions (References 11 and 12). These studies were conducted in large Teflon film reaction chambers (volumes were 30,000, 6,400, and 3,800 liters) at room temperature. The reactions of hydrazine and various derivatives with hydroxyl radicals, oxides of nitrogen, ozone, nitric acid, and formaldehyde were studied. It was determined that hydrazine has an expected gas-phase lifetime of about 30 minutes under typical urban atmospheric conditions. These investigators also used radical traps and chemical tracers to determine details of the reaction mechanisms involved in the atmospheric oxidation of hydrazines.

Naik and co-workers also conducted a study of hydrazine air oxidation in a Teflon film reaction chamber (References 13 and 14). The chamber they used was smaller (about 320 L) and their studies centered on the effects of added surfaces on the rate of hydrazine oxidation in air. They determined that among the added metal surfaces studied, copper was by far the most reactive, followed by painted aluminum, aluminum foil, stainless steel, and aluminum plate. They also noted that the half-life of the hydrazine was a strong function of the relative humidity of the air in the chamber.

Two additional studies have been conducted in smaller (~100-L) synthetic film bags. The first was conducted by Lin (Reference 15), who determined the decay rates of hydrazine in nitrogen and in dry air in Teflon and Tedlar bags. The half-life of the hydrazine was notably shorter in the Tedlar bag. In a follow-up to some of his earlier work, Naik studied the decay of hydrazine in a Teflon bag (Reference 16). In this study, he determined the half-life of hydrazine in dry air as a function of the surface-to-volume ratio of the Teflon bag. By extrapolating to a surface-to-volume ratio of zero, he estimated that the homogeneous half-life of hydrazine in air is about 60 hours.

Previous studies have shown that the relative magnitudes of humidity, surface adsorption, permeation through walls, surface-to-volume ratio and actual oxidation as factors affecting the decay of hydrazine in Teflon film reaction chambers are still questionable. This study was undertaken to further investigate these effects with the aim of attempting to clarify the relative importance of these various loss processes.

C. SCOPE

The study included a thorough examination of the behavior of hydrazine vapor in a Teflon film reaction chamber. It included the design and construction of the chamber and a determination of its optimum operating conditions. It also included the development of a comprehensive, kinetic model to account for all potential molecular transformations, both chemical and physical. Finally, it included chamber studies of the decay of hydrazine vapor under four types of experimental conditions: dry and humid nitrogen, and dry and humid air.

SECTION II

EXPERIMENTAL PROCEDURES

A. REACTION CHAMBER

The reaction chamber was constructed by heat-sealing pieces of DuPont FEP Teflon film. The film thickness was .005 inches and the resulting chamber dimensions were approximately 0.87 by 0.66 by 0.56 meters, giving a volume of about 320 liters. The chamber was assembled by technicians at the NASA White Sands Test Facility, White Sands, NM. One of the longer sides of the bag had a 0.3- by 0.3-meter access port which was constructed by the same heat-sealing technique. This port extended out from the side of the chamber about 0.5 meter in the form of a square sleeve. The access port was sealed during chamber experiments by carefully folding the Teflon sheets and tightly clamping them between two wooden supports. The corners of the chamber were reinforced with strips of 2-inch Mylar tape (3M core series 2-0300, 3M Co., St. Paul, MN), including the access port. The chamber is shown schematically in Figure 1.

The chamber was supported by securing its two longer upper edges to 0.5-inch aluminum rods with Mylar tape. The aluminum rods were then suspended with wire from structural members of a supporting rectangular frame which measured 0.75 meters by 1.18 meters by 1.37 meters. The frame members were hollow, 1.0-inch square aluminum bar stock welded together. The aluminum frame was covered with 1/8-inch Plexiglas and placed on a wooden table, completely enclosing the Teflon chamber. A 1/6 hp motor (Lightning Model L, 1550 R/min) was mounted on the structural aluminum frame members above the Teflon chamber. The shaft of the motor was connected to a 6-inch, Teflon-coated fan blade (located inside the Teflon chamber) with a sealed, rotatable feed through. The Plexiglas box was fitted with four 1/4-inch Nylon bulkhead fittings with 1/4-inch PVC tubing leading to the system gas distribution manifold. These ports were used to direct gas flow into the annular space between the Plexiglas box and the Teflon chamber. One end of the Plexiglas was hinged for access to the optical components. The other end

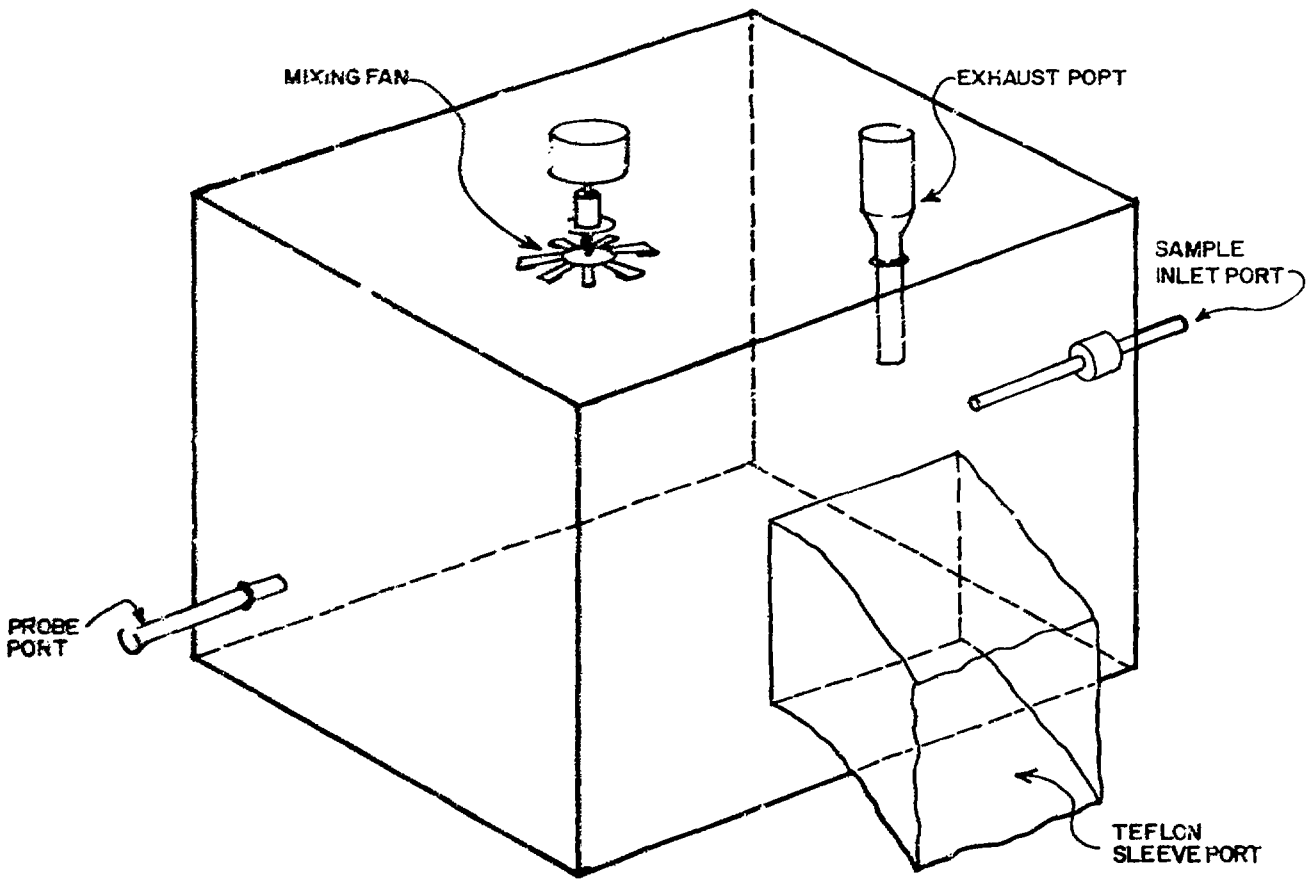

Figure 1. Schematic Drawing of the Teflon Chamber.

of the box had a 15 by 40 cm hinged opening for both beam path and path length adjustments. There was an additional hinged opening, 40 by 40 cm for access to the Teflon chamber sample port. There were other openings for the infrared beam, electrical cords, gas lines, and the exhaust port. The Plexiglas-covered aluminum frame is shown in Figure 2.

The chamber had three other access ports. One was a standard 24/40 ground glass joint located in the lower corner of the chamber and extended through the Plexiglas shell. This port was used for inserting a thermistor probe for temperature measurements of the chamber contents. The temperature inside the chamber was continuously monitored by recording the signal from a thermistor (Yellow Springs Instruments Model 401) thermometer (Yellow Springs Instruments Model 44TD) with a strip chart recorder (Varian Model 9176). The recorder response was calibrated using known water bath temperatures.

The second port was a 0.5-inch glass tube, located in the upper surface of the chamber and connected to a butterfly valve on the top Plexiglas surface of the chamber cover. This valve was connected to the PVC fume hood extension through a 2-inch piece of Tygon tubing. The third port, the sample inlet port, was a piece of 10 mm OD Pyrex tubing which entered the Teflon chamber from the side opposite the temperature probe port. Each of these glass ports was inserted through the chamber wall and sealed with carefully placed strips of Mylar tape.

The chamber was checked for leaks by first being flushed with helium gas, then inflated to slightly over its equilibrium pressure. A gas leak detector (Gow Mac Model 21-150) was then used to inspect the seams and corners for leaking helium. A number of leaks found in the chamber were repaired by pressing small strips of Mylar tape over the leaking areas. At some of the corner joints, silicon glue was squeezed into an area whose geometry did not allow the efficient use of tape. Later, pressure-sensitive tape made from unsupported Teflon TFE film (Berghof/America, Inc., Type 15078) was used to repair leaks. This tape was more flexible and provided better seals than the Mylar tape.

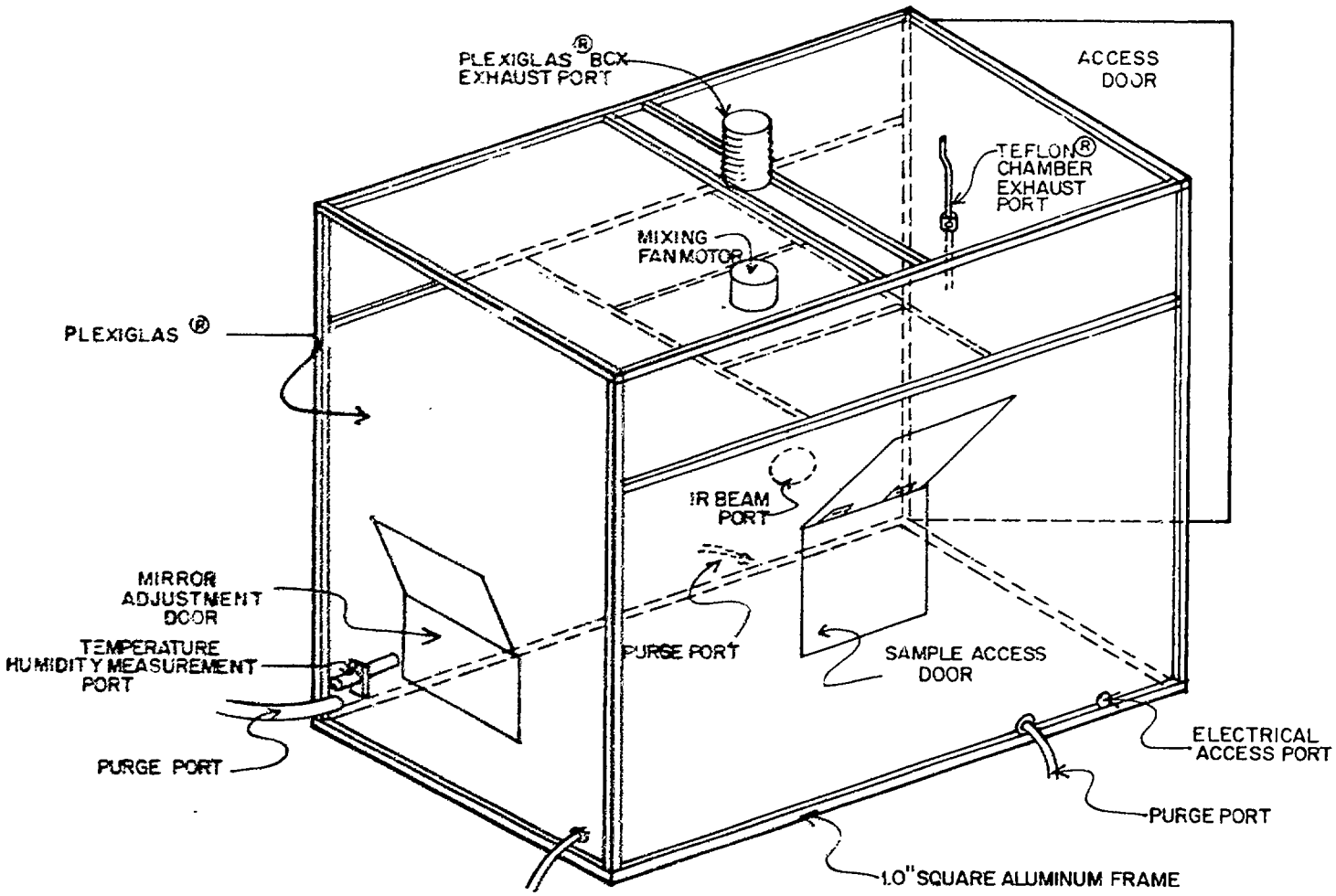

Figure 2. Schematic Drawing of the Plexiglas-Covered Aluminum Support Structure for the Teflon Chamber.

Also contained within the Plexiglas-covered aluminum frame was the sample inlet manifold. This manifold consisted of three Kontes 10 mm high vacuum valves with Teflon seals for admitting gaseous samples and a silicon septum inlet for injecting liquid or gas samples. The manifold was connected to a 500 mL mixing bulb and then proceeded through 10 mm Pyrex tubing to the Teflon chamber. The sample manifold was heated with heating tape controlled by variable autotransformers. The sample manifold is shown in Figure 3.

B. PURE AIR SYSTEM

Pure, dry air for chamber purging and filling was generated by a locally constructed system. A 7.5 hp air compressor (Ingersoll-Rand Model T30) was used to deliver compressed air to a noncycling refrigerated air dryer (Zeks-Therm Model 35NCA). This unit delivered air at a dew point of 35 ^{o}F to a catalytic air purifier (Aadco Model 737-15A). The air-purifier unit was capable of delivering 250 L/min of air with a less than one part-per-billion ozone, methane, hydrocarbons, carbon monoxide, hydrogen sulfide, sulfur dioxide, or fluorocarbons at a dewpoint of -60 ^{o}F. The pure air was delivered to the chamber through 1/2-inch PVC tubing (Imperial Eastman "Poly-Flo" tubing, type 88-P-1/2). The pure air system and distribution manifold are shown schematically in Figure 4.

C. FT-IR SPECTROMETER AND LONG-PATH CHAMBER OPTICS

Molecular species of interest in this study were monitored by Fourier transform infrared (FT-IR) spectroscopy using a Pimentel-type (Reference 17) multiple-reflection mirror system. The principal mirrors were located within the Teflon film chamber. These mirrors consisted of an in-focus (nesting) mirror cut from an 8-inch spherical mirror and two 4-inch out-of-focus (collecting) spherical mirrors, all with a common radius of curvature of 31.5 inches. These mirrors were standard 1/4-wave, first-surface Pyrex mirrors aluminized and overcoated with silicon monoxide (A. Jaegers Co.). They were used as received. The corner reflector was made by cutting a section of the nesting mirror and gluing it at right angles to a section of flat mirror with epoxy. The corner reflector was glued on a standard optical post assembly

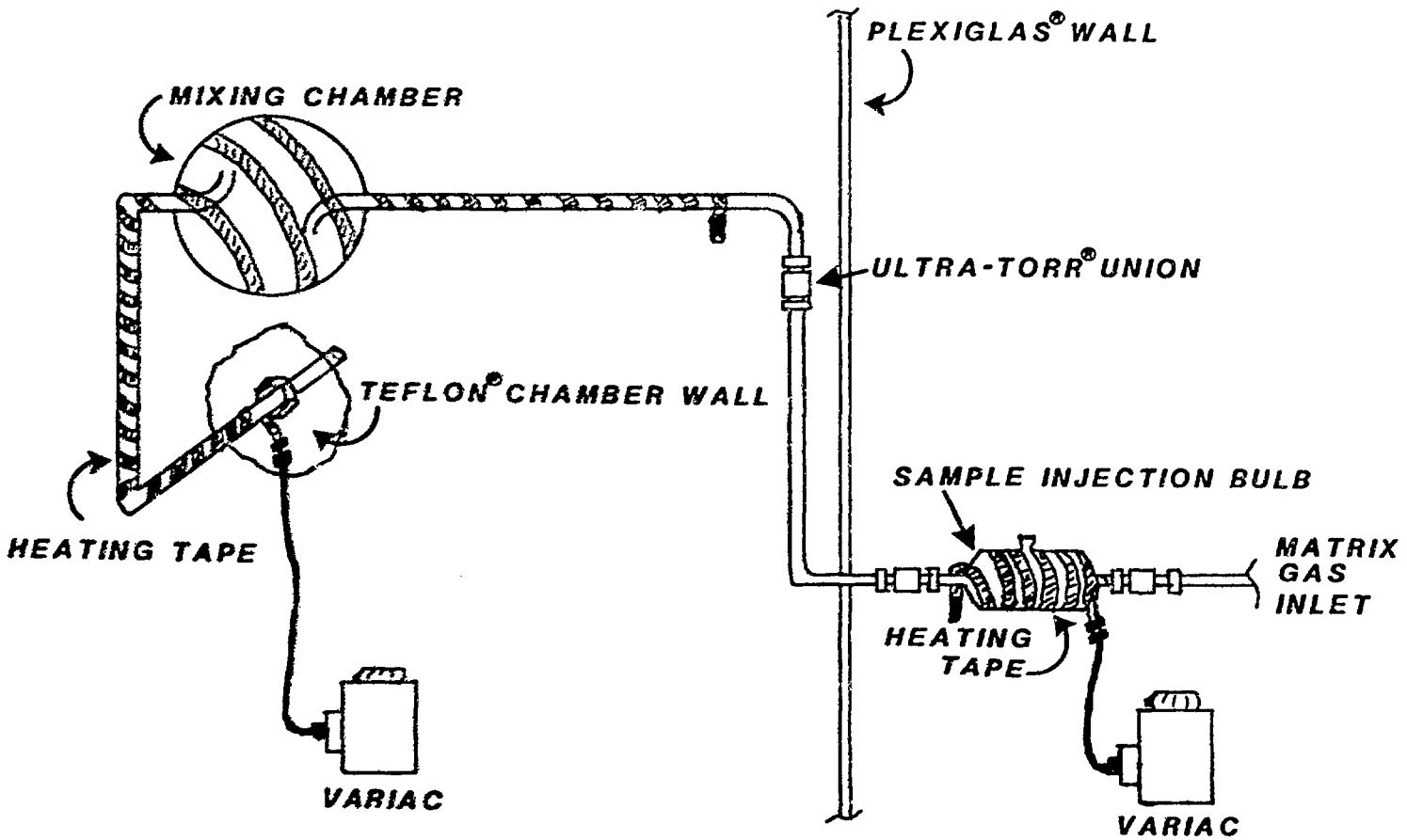

Figure 3. Schematic Drawing of the Chamber Sample Injection and Introduction System.

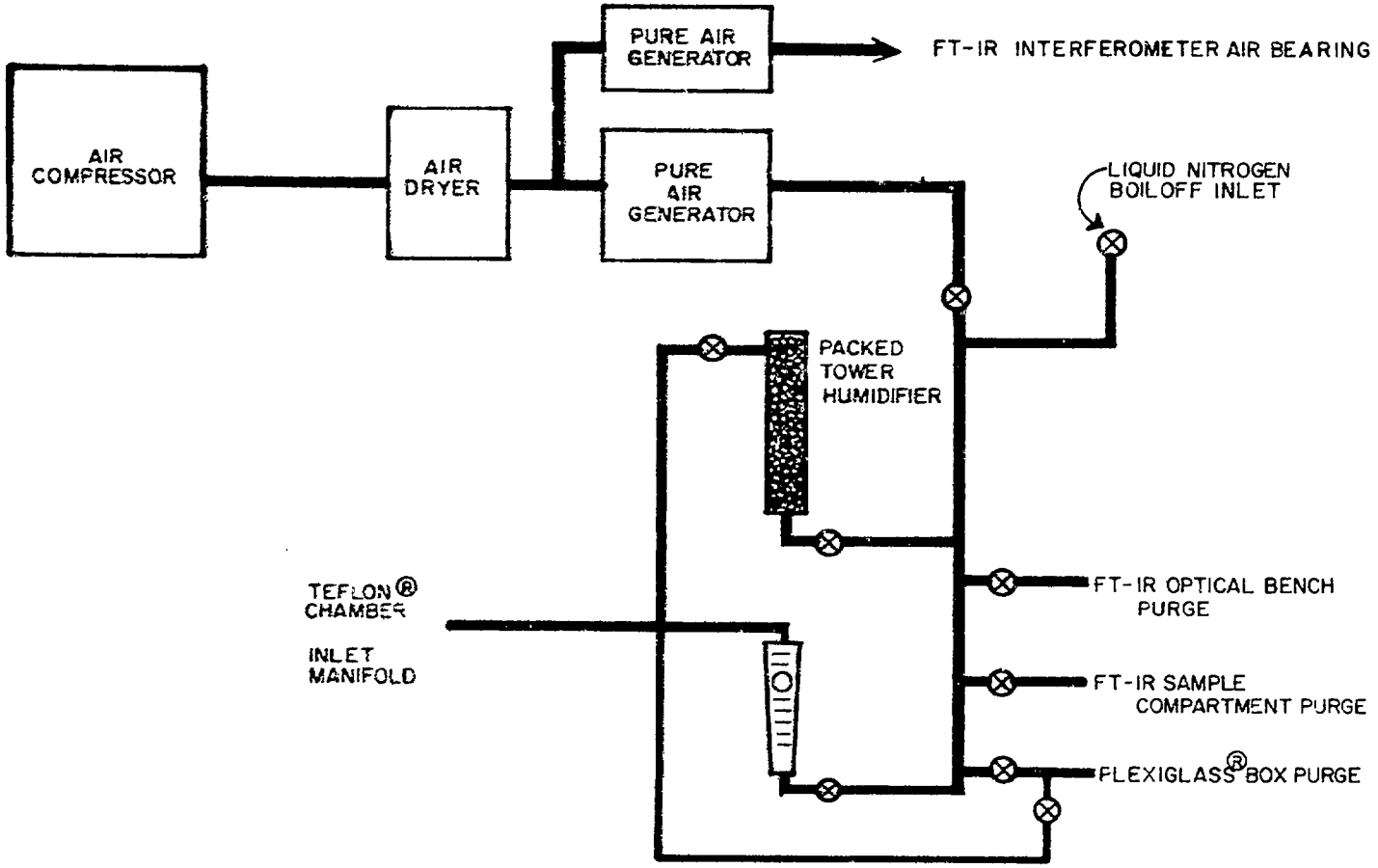

Figure 4. Schematic Drawing of the Laboratory Pure Air Generation and Delivery System.

for rotational and height adjustability. The other mirrors were glued to positioning mounts (Newport Model MM-2) fastened to standard optical posts, enabling the required x-y-z adjustments.

The total infrared beam path within the chamber was determined by counting the red image dots from a helium-neon laser whose optical path was coincident with that of the infrared beam from the FT-IR system. The long-path optical system was operated at 46 passes, giving a path length of 36.8 meters.

The incoming infrared beam was directed into the chamber and then onto a mercury-cadmium-telluride detector, operated at 77 K by a series of external mirrors, as shown in Figure 5. The FT-IR spectrometer employed was a Nicolet Model 6000C. This spectrometer has a maximum resolution of 0.06 cm^{-1}, and was upgraded to include a raster scan display, 24-Mbyte hard disk, 1-Mbyte, 8-inch floppy disk, digital plotter, and RS-232 dot matrix printer. Thus, configured, it operated on the more recent NICOS software.

D. MATERIALS

The hydrazine was anhydrous, fuel grade (98 percent pure) from Rocky Mountain Arsenal. It was used as received. Methane (CH_4) gas was Fisher high-purity grade (99.99 percent) and sulfur hexafluoride (SF_6) was Air Products instrument grade (99.99 percent).

E. METHODS AND PROCEDURE

1. Sample Introduction

To conduct an experiment in dry air, the following procedure was used. The annular space between the Plexiglas box and the Teflon film bag was purged with dry, purified air from the pure air system at 20 L/min for at least 60 minutes. At the same time, the Teflon film chamber was purged with a separate, 10 L/min flow of pure, dry air. The chamber mixing fan was operated during the entire purging process. The flow of air into the chamber

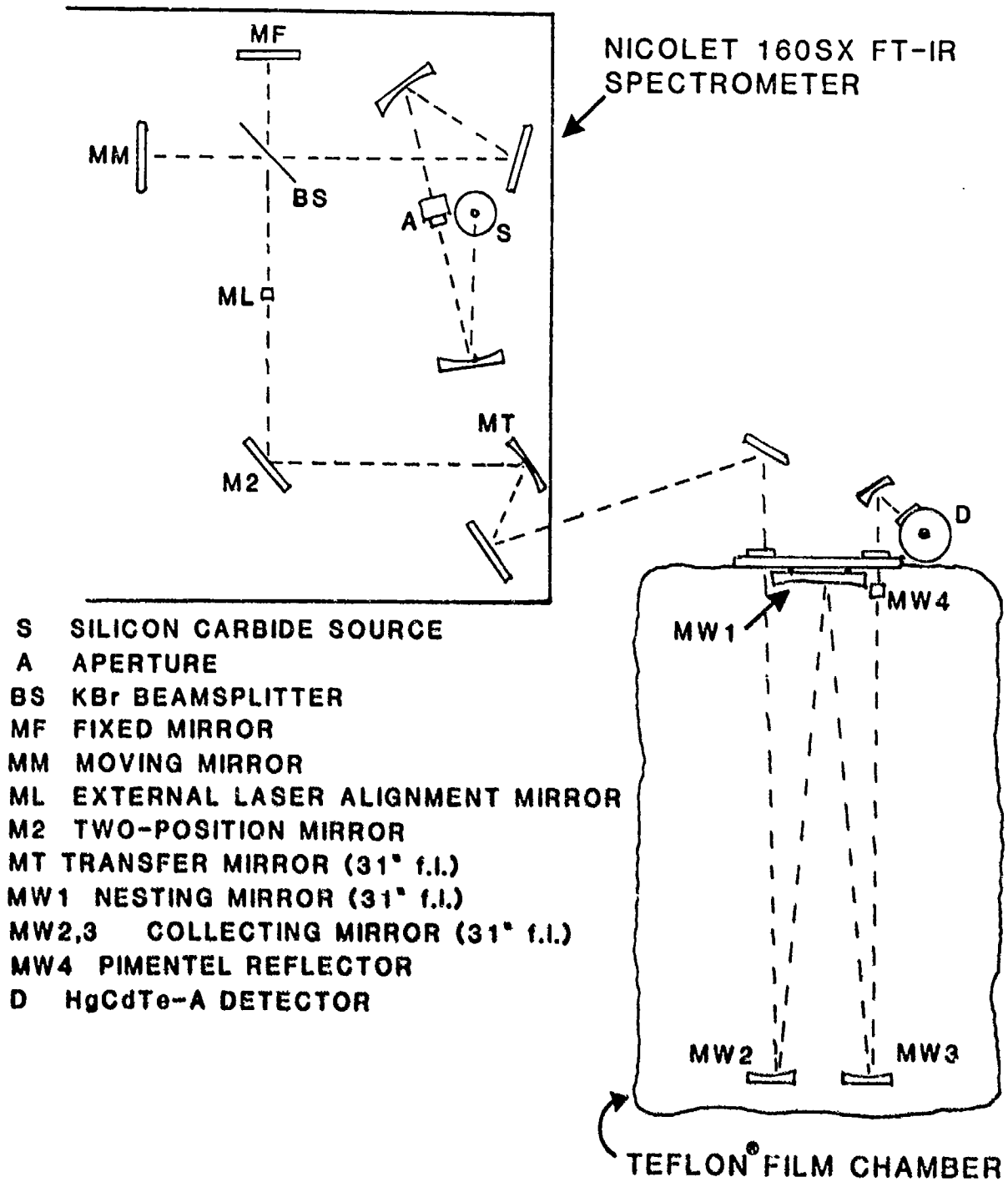

Figure 5. Schematic Drawing of the FT-IR and Chamber Optical Systems.

was manually balanced with the removal of air from the chamber via the exhaust port. After 60 to 90 minutes of purging, the humidity in the annular space of the box and the humidity in the chamber were measured electronically with a thin film capacitance device (Vaisala Model HMI 31 humidity and Model HMP 31 UT probe). The readings were always less than 2 percent relative humidity. The chamber was now ready for sample introduction.

To inject a sample, the purge flow in the annular space was lowered to about 10 L/min to maintain the low humidity, and flow to the chamber was stopped. The volume of the chamber was lowered by about 20 percent by opening the exhaust port. At this point, a reference spectrum was taken with the FT-IR system (see the following section for details on how the FT-IR spectrometer was operated). Both gas and liquid samples were injected with syringes through a silicon septum in a cylindrical, flow-through Pyrex sampling vessel. The sampling vessel was heated to about 50 ^{o}C with heat tape for hydrazine injections. Samples were flushed into the chamber with pure air flowing at about 2 L/min. The mixing fan was run continuously during sample injections. Pure air flow was maintained until the chamber was reinflated. Care was taken to see that the chamber was actually somewhat underinflated to prevent any physical force being exerted by the walls of the chamber which might have unnecessarily promoted various loss processes.

To conduct an experiment in humid air, the procedure outlined above was followed, except that the pure air flows for both the annular box space and the chamber were routed through a 10 cm diameter by 75 cm high Plexiglas column filled with Norton 16 mm, polypropylene Pall rings, and distilled water. Flow through this column resulted in relative humidity levels of about 60 percent in the chamber and box system.

Experiments which used dry nitrogen also used the same procedure outlined in the beginning of this section. The nitrogen was obtained from the boiloff of liquid nitrogen.

2. FT-IR Spectrometer Operation

Molecular species of interest in this study were monitored by recording their absorption spectra as a function of time with FT-IR spectroscopy. A pathlength of 36.8 meters was set in the Teflon chamber and a resolution of 1.0 cm^{-1} was employed. Data were recorded in the mid-infrared from 4000 - 700 cm^{-1} using a mercury-cadmium-telluride (MCT) photoconductive detector (Infrared Associates Model G-2229).

A background spectrum for a particular experiment was obtained by co-adding 256 instrument scans and then storing the result. Immediately after the injection of a sample, the instrument was placed under software control for automatic data acquisition, processing, storage, and plotting. This gave a spectrum within 2 to 5 minutes of sample injection. Three additional spectra were acquired in the same manner at 10-minute intervals. The instrument was then directed to increase the data acquisition interval to a longer, operator-controlled value, and continue to acquire, process, store, and plot data for up to 100 additional intervals. Generally, these longer intervals were 30 to 60 minutes, using 60 instrument scans. Experiments were conducted for periods of 12 to 60 hours.

The spectral acquisition software, written using a series of Nicolet MACRO commands, produced single-beam spectra stored in successive files in the "scratch" area of the system hard disk. These single-beam spectra were ratioed against the background spectrum, converted to absorbance mode, and analyzed to determine the absorption at specified analytical wavelengths for each molecular species of interest. Finally, the absorption values were printed out, along with time and wavelength information. All these operations were handled automatically by the instrument's MACRO software. (See Appendix A for program listings).

The automation of data acquisition enabled long experiments to be conducted without constant operator attention. However, this automation also caused a false temperature dependence to be observed in the data. By using the instrument's peak pick routine to determine absorption values, shifts in the absorption baseline caused by temperature variations in the room were not accounted for. When the absorbance values obtained from the peak pick

routine were compared with those obtained from manually plotting the spectra, drawing a consistent baseline and measuring the absorption, it was clear that a different approach would be necessary to correctly acquire data under instrument control.

To properly account for the shift in baseline, the following approach was used. For each molecular species, a point was chosen on either side of the analytical wavelength, essentially the same points one would choose to draw a baseline for a manual determination of the absorbance from a plotted spectrum. The absorbance values at these two points were determined from the instrument's peak pick routine. The absorbance value at the analytical wavelength was also determined, as before, using the peak pick routine. However, now it was scaled by a linear interpolation between the two points on either side (Reference 18). This procedure was implemented by using a short FORTRAN program, which was called from the instrument's MACRO software. The programs are listed in Appendix B. The procedure was checked against absorbance values obtained by manually drawing baselines and measuring absorbances. The results were essentially identical. Once this latter program was finished, some earlier spectral data were reprocessed to correct for baseline drift.

This procedure, while providing the correct absorbance values, was operator-intensive. Because of the display-intensive data manipulation required in this MACRO program, the instrument could not keep up with the software unless distinct software pauses were inserted. Each pause required the operator to physically press the RETURN key on the spectrometer keyboard.

To alleviate this situation, a software development effort was undertaken with the goal of accomplishing the analysis by using a FORTRAN program. The basis for this program was the availability of an existing FORTRAN subroutine called FGETOF written by Nicolet which allowed FT-IR scratch file data to be read by a FORTRAN program. The result was a program called GET2 which would take a predetermined wavelength interval on one side of an analytical peak and average the absorbance values over that interval. It would do the same for an equal interval on the other side of the

analytical peak. These two average points would then be used to baseline-correct the absorbance at the analytical peak.

This later program was run from another MACRO (see Appendix C). The program GET2 was used to correct the data files which remained uncorrected from earlier runs (i.e., those which had not been done manually, using the earlier MACRO called MPK).

3. Oxygen Concentration Measurements.

One series of experiments was conducted to measure the permeation of oxygen into the chamber. Oxygen concentration was measured by an indirect method, using a dissolved oxygen (DO) meter (Yellow Springs Instruments, Model 58). A 400-mL beaker containing about 250 mL of water was placed on a magnetic stirrer in the chamber. The DO meter was also placed in the chamber and its probe (Yellow Springs Instruments, Model 5720A) was supported in the water. The water was vigorously stirred. The resulting dissolved oxygen reading was assumed to have a linear proportionality relationship with the concentration of oxygen vapor in the chamber. The DO meter readings were recorded continuously on a strip-chart recorder (Esterline-Angus, Model T171B). The chamber mixing fan was operated continuously during these oxygen concentration measurements.

(The reverse of this page is blank.)

SECTION III

MODEL DEVELOPMENT

As already mentioned, the overall reaction of gaseous hydrazine in air at room temperature up to 160 °C has been proposed to be:

$$N_2H_4 + O_2 \longrightarrow N_2 + 2H_2O \qquad (1)$$

In addition to the fact that chamber surface-to-volume ratios affect the loss processes, many unexplained experimental results in hydrazine studies have also been obtained. Most notably, some results show hydrazine approximately obeying pseudo-first-order kinetics; others clearly do not (Reference 13).

Studies presented in this report have been geared to investigate whether Equation (1) is the dominant process, and if not, to determine what kinetic processes, chemical or physical, are occurring and to successfully model these processes. This chapter will show that Equation (1) is not the most important gaseous process, and will develop a model which takes into account many possible processes; including gaseous reactions, surface-catalyzed reactions, leakages, gaseous aerosol formation, surface adsorption, and permeation through chamber walls.

To test the possibility that Equation (1) might not be significant, an experiment was conducted in which the Teflon chamber was initially filled with dry nitrogen (N_2). Hydrazine was then vaporized and flushed into the system and its absorbance was monitored with time. The results of this and other experiments showed essentially no difference in the hydrazine loss rate for runs in N_2 and in air.

Because the box surrounding the Teflon chamber was not completely oxygen (O_2)-free, oxygen leakage had to be taken into account. Before the hydrazine experiments (which seem to show no major oxygen involvement) could prove to be conclusive, a model describing how O_2 might leak into the chamber and how this process can affect the loss rates of hydrazine (if it reacts with oxygen) was developed.

Two possible mechanisms for leakage through walls are effusion and permeation. The former is described by molecules passing through holes having cross-sectional areas that are small when compared with the mean free path of the gas. The latter is described by molecules jumping from one active site to another on the chamber walls or by simple diffusion caused by a concentration gradient (Reference 19). Both permeation and effusion will be incorporated into a later model. Described below is the kinetic model for a simple effusion process. Although results shown in the next chapter indicate permeation is probably a significant process in Teflon chambers, the effusion model is sufficient to account for gas leakage into the chamber.

The number of collisions, v, per unit area per unit time for an ideal gas is:

$$v = C\sqrt{RT/(2\pi M)}, \tag{2}$$

in which C is the molecular concentration, M is the molecular weight, R is the gas constant, and T is the absolute temperature. The number of molecules passing through an aperture of area, A, in time Δt is $CA\sqrt{RT/(2\pi M)}\Delta t$. If this quantity is divided by NV, in which N is Avogadro's number and V is the chamber volume, then the resultant quantity would be the change in moles per unit volume, or the change in molar concentration. If a leaking chamber is initially evacuated of a gas and there is an infinite reservoir of that gas outside the chamber (Figure 6), then the change in the molar concentration inside the chamber is:

$$\Delta C_m = (C_{mo} - C_m)(A/V)\sqrt{RT/(2\pi M)}\Delta t, \tag{3}$$

in which C_m is C/N, the chamber molar concentration, and C_{mo} is the reservoir molar concentration. Taking the limit as Δt approaches zero and integrating yields:

$$C_m = C_{mo}\{1 - \exp[-(A/V)\sqrt{RT/(2\pi M)}]t\}. \tag{4}$$

If the chamber is initially filled with the gas and the infinite reservoir has none of the gas, C_m can be shown to be:

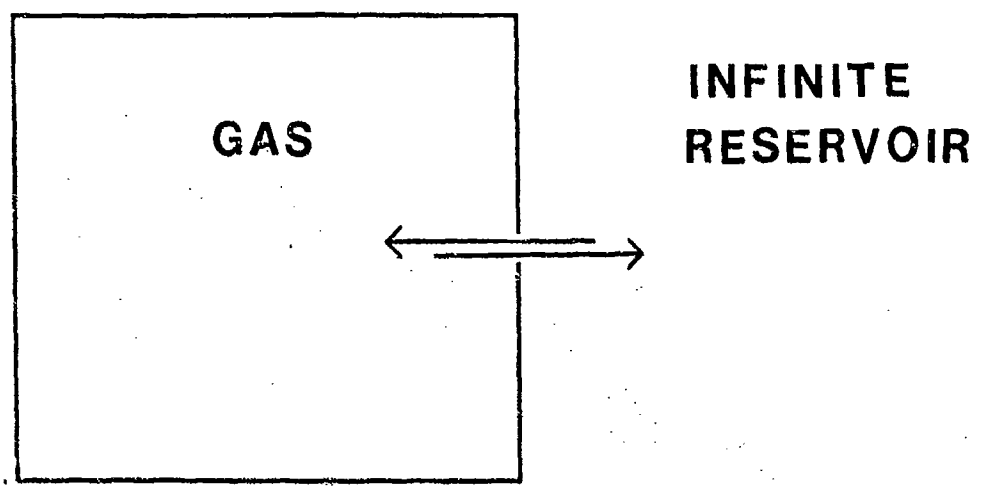

Figure 6. Diagram Showing Passage of Gas Through a Hole in the Chamber Wall.

$$C_m = C_{mo}\exp[-(A/V)\sqrt{RT/(2\pi M)}]t, \quad (5)$$

in which C_{mo} is now the initial chamber concentration. Equations (4) and (5) strictly apply if the mean free path is large compared to the cross section of the aperture. This insures that all molecules passing through the holes will not be deflected back into the chamber via collisions. At 25 °C and 1 atm, the mean free path of O_2 is 7×10^{-8} meter, which is much smaller than most holes which might exist in the chamber walls. However, assuming that a constant fraction of molecules passing through the holes are not deflected back into the chamber, the concentration change can still be described exponentially.

The differential rate equation describing the process in Equation (1), assuming simple second-order kinetics, is:

$$d[N_2H_4]/dt = -k[N_2H_4][O_2], \quad (6)$$

in which k is the second-order rate constant. If the chamber is initially evacuated of O_2 and hydrazine is promptly injected into the chamber, then Equations (4) and (6) can be combined to yield an applicable equation,

$$d[N_2H_4]/dt = -k[N_2H_4][O_2]_o[1 - \exp(-k_e t)], \quad (7)$$

in which k_e is the effusion rate constant and $[O_2]_o$ is the reservoir O_2 concentration. Equation (7) assumes the initial chamber O_2 concentration is zero and that reaction with hydrazine is negligible relative to O_2 effusion into the chamber. Since $[O_2]_o \gg [N_2H_4]$, this latter approximation is good so long as k_e is sufficiently large. Integrating Equation (7) yields:

$$[N_2H_4] = [N_2H_4]_o\exp\left(-k[O_2]_o\{t - [1 - \exp(-k_e t)]/k_e\}\right), \quad (8)$$

in which $[N_2H_4]_o$ is the initial concentration of hydrazine. Figure 7 shows plots of $[N_2H_4]/[N_2H_4]_o$ vs t for the cases $k_e = k[O_2]_o = .05$ hour^{-1}, and $k[O_2]_o = .05$ hour^{-1} and k_e = infinity; and a plot of $[O_2]/[O_2]_o$ vs t for $k_e = .05$ hour^{-1}. If Equation (1) describes

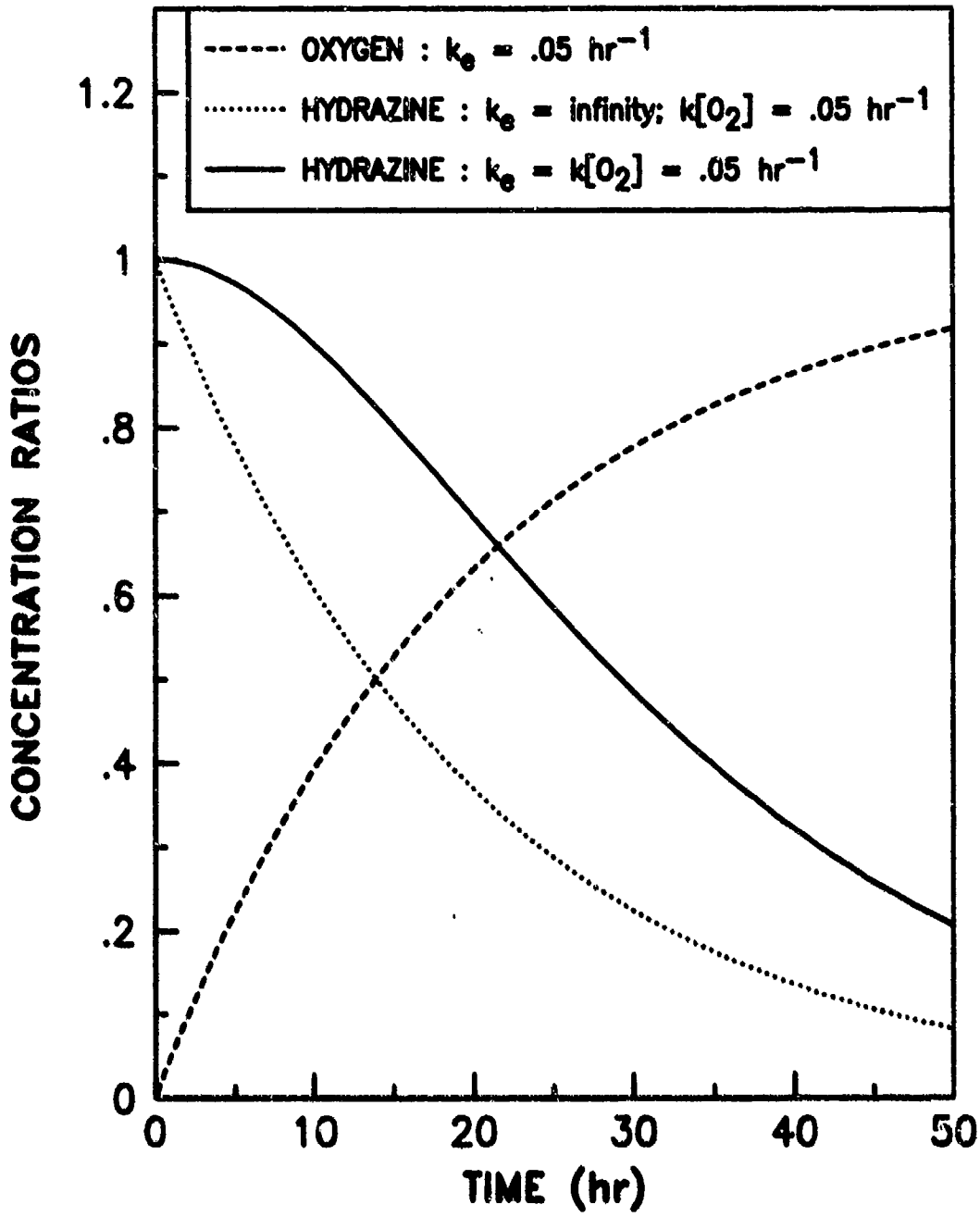

Figure 7. Plots of Equations (4) and (8).

the predominant kinetic process for hydrazine in the Teflon chambers, then curve 1 of Figure 7 should depict the general shape if the chamber is initially filled with N_2 and $k[O_2]_o$ is comparable to or larger than k_e.

Figure 8 shows data points for an experiment in which $[O_2]$ was monitored indirectly as a function of time following evacuation of O_2 from the chamber. The O_2 concentration approximately follows curve 3 of Figure 7. The effusion rate constant is 0.105 (.005) $hour^{-1}$. The details of this experiment are given in the Experimental Section.

Figure 9 shows data points for experiments in which hydrazine was monitored in the chamber filled with dry air and in the chamber initially filled with dry N_2. As indicated previously, there is little difference in the plots. These two experiments were conducted in the same 5-mil bag just days apart. Hence, physical factors which may have a gradual affect on changing kinetic behavior, such as the creation of more holes, were minimized. In addition, the fact that the points follow a general decay pattern and not a sigmoidal pattern predicted by Equation (8) lends further evidence that hydrazine is not reacting with O_2. The decay processes must, therefore, be one or more of the following: effusion, permeation through the chamber walls, simple physical adsorption, or surface-catalyzed reactions. Since it is difficult to postulate how Teflon surfaces might catalyze reactions, one or more of the other processes must be predominating. Before the idea that surface interactions are important can be tested quantitatively, a comprehensive model which fits the data must be developed.

The following kinetic model considers all likely gas and surface interactions which might occur in a Teflon chamber:

$$G \xrightarrow{k_e} \text{effusion}$$

$$G + S_1 \underset{k_{-s}}{\overset{k_s}{\rightleftharpoons}} G\text{-}S_1$$

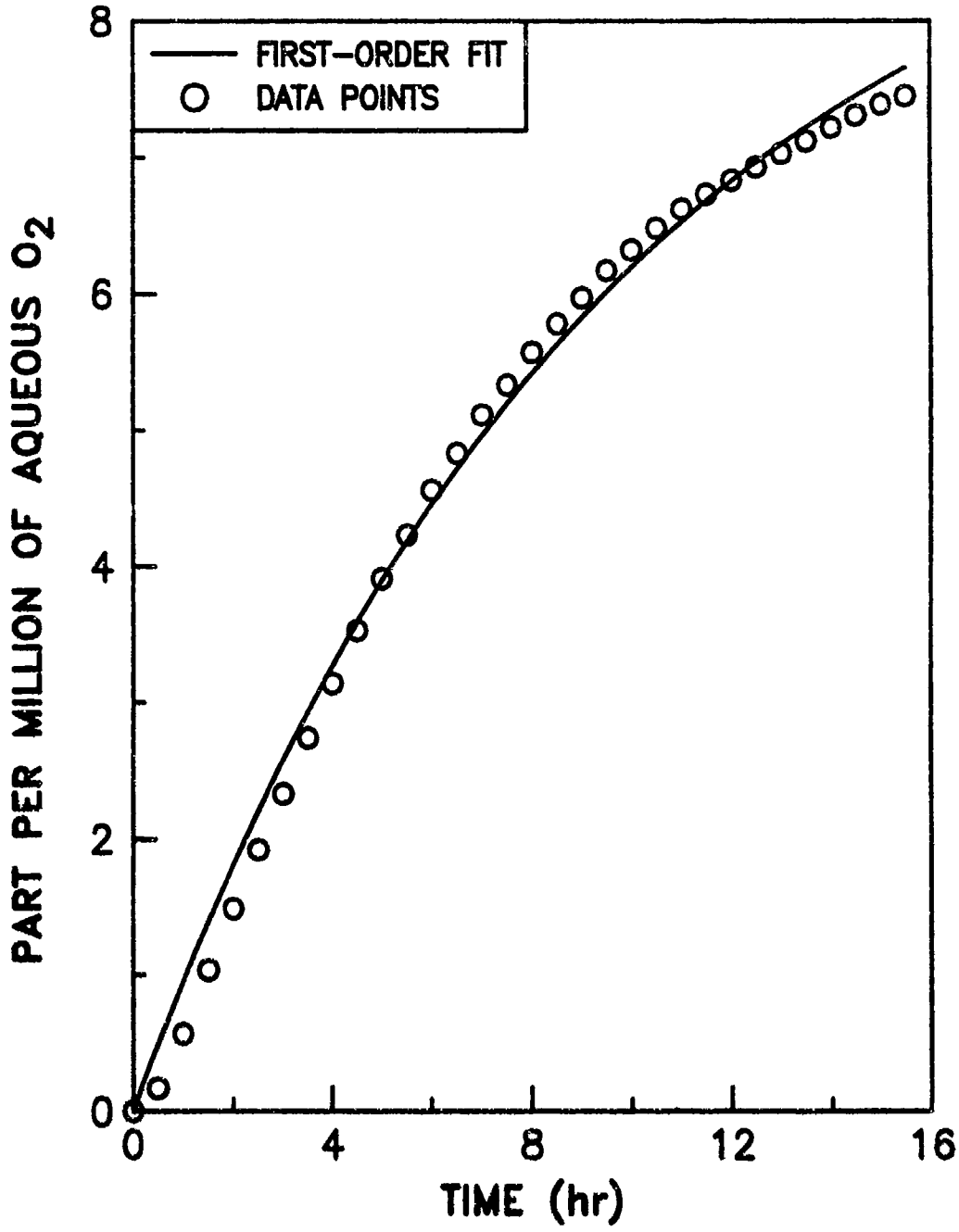

Figure 8. First-Order Fit to O_2 Permeation Data.

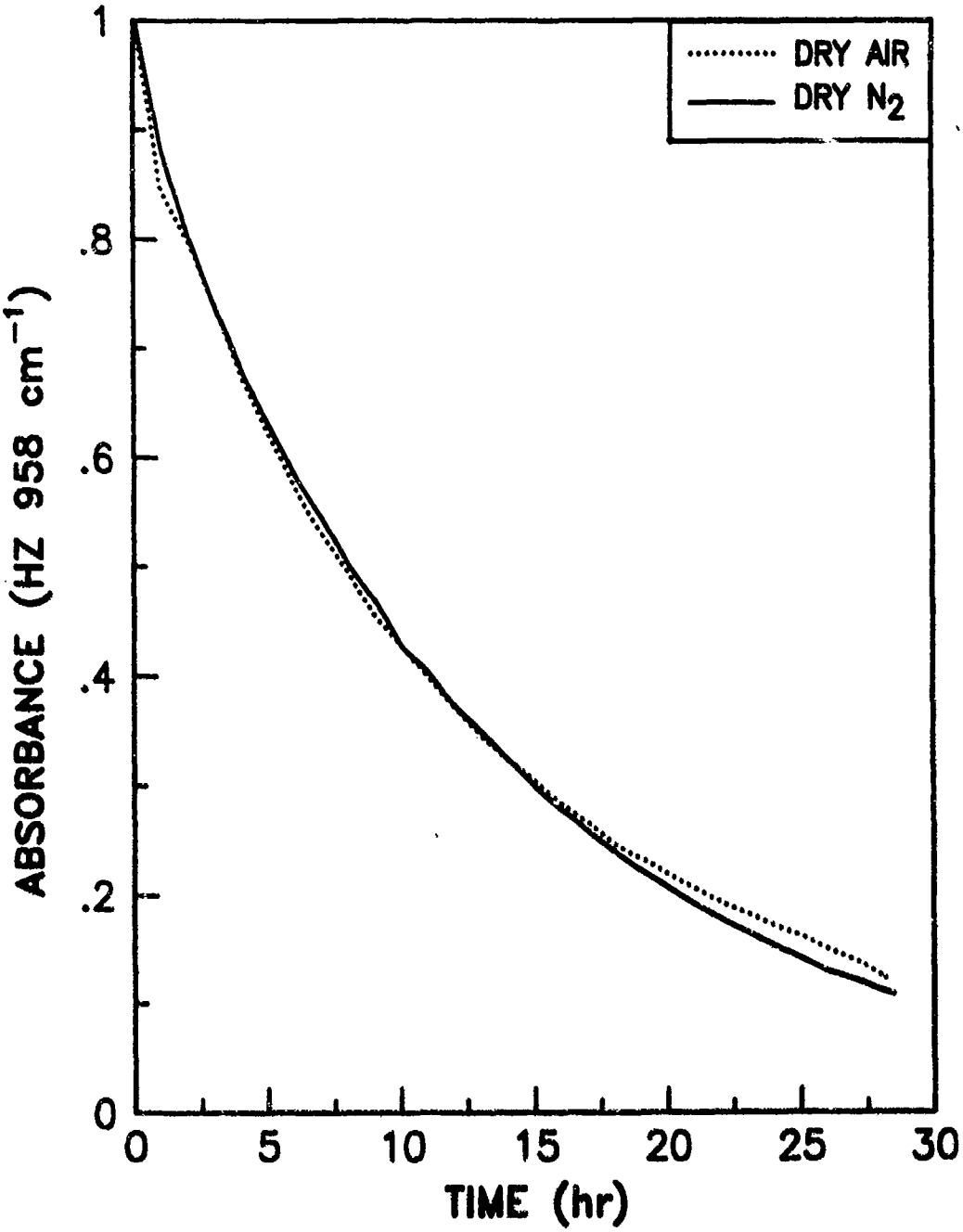

Figure 9. Decay of Hydrazine Vapor in Dry Air and Dry N_2.

For i = 1 to f;

$$G + F_i \underset{k_{-i}}{\overset{k_i}{\rightleftharpoons}} G\text{-}F_i$$

For i = 1 to p;

$$G + P_i \xrightarrow{k_{pi}} \text{reaction products}, \qquad (9)$$

in which G is the gas species being monitored, S_1 is the first polymeric film pore layer (defined below) on the inside surface of the Teflon chamber wall, F_i is the Ith interacting surface, other than Teflon, P_i is the Ith gaseous species which reacts irreversibly in a simple second-order process with G, f is the number of F-type surfaces, and p is the number of P-type gas species. The corresponding rate constants are self-explanatory. F_i can also be a gas species, such as H_2O, which reversibly complexes with G. Here a pore layer is defined as the distance, perpendicular to the plane of the wall, that a molecule must travel to move from one pore site to an adjacent site. A pore layer which comprises the surface of the film is called a surface pore layer, and a pore layer inside the film is called a subsurface pore layer (Figure 10). There are two surface pore layers, one comprising the inside surface and one comprising the outside surface of the film. In addition, there are numerous subsurface pore layers. The number of pore layers is that number comprising the thickness of the walls. Delocalization occurs if a molecule jumps from one pore site to another within the same layer (Figure 10).

There are three classifications of pores: micropores (less than 15 Å in width), mesopores (15 to 1000 Å in width), and macropores (greater than 1000 Å in width) (Reference 20). It is unlikely, because of the low concentrations of hydrazine in the chamber, that more than one molecule will occupy a pore site at any given time. Hence, the kind of pore which will occur i Teflon is irrelevant to the model. Moreover, whether or not delocalization occurs is also irrelevant since it will not affect the model. After the gas molecules become adsorbed onto the surface pore layer, permeation and eventual loss can occur by the following process:

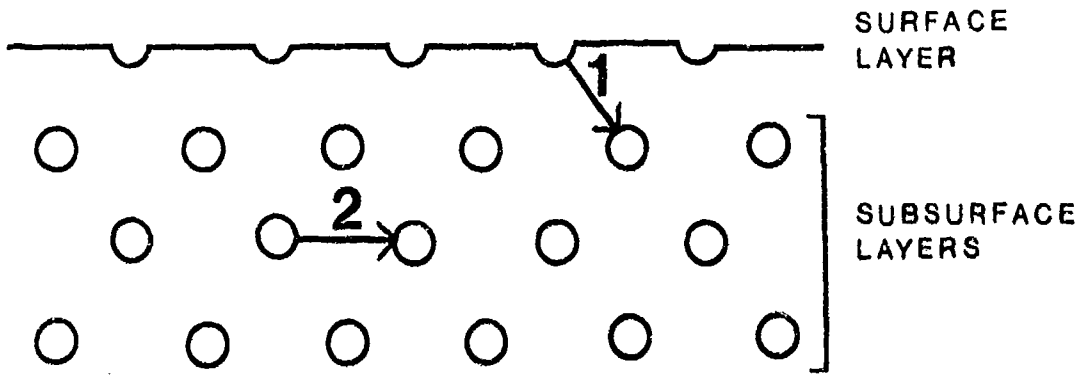

Figure 10. Diagram Showing How Permeation Can Occur. Molecules Can Migrate From One Layer to Another (Arrow 1), or Migrate Within the Same Layer (Arrow 2).

For i = 2 to N;

$$G\text{-}S_{i-1} + S_i \underset{k_D}{\overset{k_D}{\rightleftharpoons}} G\text{-}S_i + S_{i-1}$$

$$G\text{-}S_N \xrightarrow{k_{-s}} \text{loss to the outside,} \qquad (10)$$

in which S_i is the Ith pore layer, k_D is the diffusion rate constant, and N is the number of pore layers. The differential rate equations describing the processes shown in Equations (9) and (10) are:

$$d[G]/dt = -(k_e + k_s[S] + \sum_{i=1}^{f} k_i[F_i] + \sum_{i=1}^{p} k_{pi}[P_i])[G] + k_{-s}[G\text{-}S_1] + \sum_{i=1}^{f} k_{-i}[G\text{-}F_i]$$

$$d[G\text{-}S_1]/dt = k_s[S][G] - k_{-s}[G\text{-}S_1] + k_D[S]([G\text{-}S_2] - [G\text{-}S_1])$$

For i = 2 to N-1;

$$d[G\text{-}S_i]/dt = k_D[S]([G\text{-}S_{i-1}] + [G\text{-}S_{i+1}] - 2[G\text{-}S_i]),$$

$$d[G\text{-}S_N]/dt = k_D[S]([G\text{-}S_{N-1}] - [G\text{-}S_N]) - k_{-s}[G\text{-}S_N]$$

For i = 1 to f;

$$d[G\text{-}F_i]/dt = k_i[F_i][G] - k_{-i}[G\text{-}Fi], \qquad (11)$$

in which the brackets refer to the concentrations, and [S] is the concentration for each pore layer. If [G] becomes comparable to $[F_i]$, then the pseudo-first-order term, $k_i[F_i][G]$, must be replaced by the second-order term, $k_i([F_i]_o - [G\text{-}F_i])[G]$, in which $[F_i]_o$ is the initial concentration for the Ith kind of surface. All surface concentrations, [S], $[F_i]$, $[G\text{-}S_i]$, and $[G\text{-}F_i]$, are in the same units as the gas concentrations, [G] and $[P_i]$, and, for convenience, are defined as absorbance units, which is proportional to the gas phase concentration.

In general, the series of differential equations above cannot be analytically integrated. However, they can easily be numerically solved in the following manner. If the variables, x and t, in the general expression, $\Delta x = g(x,t)\Delta t$, cannot be separated, then each infinitesimal increment in x can be calculated by the expression:

$$x' = x + g(x,t)\Delta t. \tag{12}$$

All one needs to know from the physical problem are the initial values for x and t. Each increment in t is given by:

$$t' = t + \Delta t. \tag{13}$$

A computer routine can be written to calculate each incremental value for x until the desired value of t, the independent variable, is reached. The routine requires initial conditions, determined by the physical problem, and a value for Δt. No certain value for Δt is required, provided it is small enough to insure the numeric integration converges. As it becomes smaller, more computer time is required to complete the integration.

Although this technique has been illustrated for just one differential equation, it can in theory be applied to an infinite number of dependent differential equations. Hence, the model which has been presented can be modified and expanded to any degree and still be solved numerically, provided the computer can do the integration in reasonable time.

This model can be fitted to actual data by the same methods used to fit simple expressions to data. The only modification is that the estimated values for the dependent variable are generated from a numeric integration rather than a simple function. The parameters, in this case the rate constants, are adjusted to give the best estimates in the same manner. The Marquardt nonlinear least squares approach (run on a Tektronix computer, Model 4054) was used to fit the models to the data. The program used was Statistics Volume 4, Tape 1. This program allows the user to define the function and set initial values for the parameters. Although the program is

not designed for the user-defined function to be a series of differential equations requiring numeric integration, the program is able to fit the differential equations to the data. In place of a single equation, a user-written subroutine which iteratively performs the numeric integration is required. The subroutine may vary, depending on how the model is used. Appendix IV lists the source code for the permeation version of the model and explains the code.

The experimental data presented in this report include monitoring of temperature, but not temperature control. At the beginning of this study, it was thought that temperature fluctuations affected the decay of hydrazine, hence a method for incorporating temperature fluctuations into the model was devised. After making corrections due to spectral baseline shifts caused by temperature fluctuations, it was found that temperature fluctuations had no effect. Nevertheless, the method for accounting for temperature fluctuations is outlined below, as it may be important for some processes yet to be studied. Because the equations are numerically integrated, it is an easy task to include temperature variations in the model.

For moderate temperature changes, temperature effects can be incorporated into the rate constants by the Arrhenius expression:

$$k = A \exp[-E_a/(RT)], \tag{14}$$

in which A is the pre-exponential factor, E_a is the activation energy, and T is the temperature. In order for the differential equations to be integrated with time, the temperature must be expressed as a function of time. The general expression used for this is:

$$T = T_1[1 + f(t)], \tag{15}$$

in which T_1 is the temperature where $f(t) = 0$ and $f(t)$ is some function of time, t. The use of the subscript "1" in T_1 will become apparent below. Since it is true in this report that $1 \gg f(t)$, Equation 14 can be rearranged using Equation (15) to yield

$$k = k_o \exp[E_a f(t)/(RT_1)], \tag{16}$$

in which k is k_o where f(t) = 0. The functional form of f(t) is empirical. Generally, though not always, T varies sinusoidally, being a maximum around 4 p.m. and a minimum around 7 a.m. in the Environics Laboratory.

The function, f(t) is generated one of two ways. One way is to fit T to an expression such as a polynomial. However, T can sometimes vary in some parts of the kinetic run, but remain constant over several hours in other parts. In these cases a simple empirical equation will not fit. What can be used instead will hereafter be called "finite linear functions." In this approach, T is assumed to vary linearly in t between any two consecutive data points. This approach will be accurate so long as drastic temperature fluctuations do not occur between points. The procedure for applying this approach to the model is as follows. Let T_i and t_i be the temperature and time for the Ith data point, respectively. Now let T_i be given by the following general linear function:

$$T_i = T_1(1 + m_i t_i + b_i), \tag{17}$$

in which m_i and b_i are constants associated with the Ith data point. Since temperature varies linearly between t_i and t_{i+1}, m_i, b_i, and T can therefore be put in terms of T_1, t_i, t_{i+1}, T_i, T_{i+1}, and t as follows:

$$b_i = T_i/T_1 - 1 - t_i(T_{i+1} - T_i)/[T_1(t_{i+1} - t_i)]$$

$$m_i = (T_{i+1} - T_i)/[T_1(t_{i+1} - t_i)]$$

$$T = T_i + (T_{i+1} - T_i)(t - t_i)/(t_{i+1} - t_i). \tag{18}$$

Equation (18) applies in the range, $t_i \leq t \leq t_{i+1}$. Therefore, f(t), in the range $t_i \leq t \leq t_{i+1}$, is:

$$f(t) = (T_{i+1} - T_i)(t - t_i)/[T_1(t_{i+1} - t_i)] + T_i/T_1 - 1. \tag{19}$$

Temperature fluctuations have been as high as 6.5 ^{o}C during the course of an experiment. Still no significant effect due to temperature fluctuations was seen. Hence, no processes having even moderate activation energies are occurring.

Several kinetic reaction models which do lend themselves to analytical integrations have been derived in this study. Some of these models can be found in many advanced books on chemical kinetics. Appendix V shows the derivations of five kinetic models. Some of them have been used to fit data from this study. However, they did not fit the data well.

The oxygen permeation data was modeled using an adaptation of the permeation version of the model, which is given in Appendix VI.

Some experiments were done in which Teflon sheets were placed inside the chamber. Appendix VII shows an adaptation of the permeation model version which accounts for permeable sites inside the chamber. This adaptation has been used to fit data from the runs with added Teflon sheets.

(The reverse of this page is blank.)

SECTION IV

RESULTS AND CONCLUSIONS

A. SPECIES CONCENTRATION MEASUREMENTS

All species used in this study obeyed Beer's law in the concentration ranges used. Kinetic information, therefore, was processed by using absorbance versus time measurements.

B. THE STABILITY OF INTERNAL STANDARDS IN THE TEFLON CHAMBER

Both methane (CH_4) and sulfur hexafluoride (SF_6) were used to test the stability of inert gases in the Teflon chamber. Numerous experimental runs were conducted where these gases were introduced into the chamber under a variety of experimental conditions. Methane was used as the internal standard for most of the hydrazine runs so that any major changes in chamber leak rate could be detected and repaired.

1. SF_6

A total of 7 different runs were made with SF_6 between August 1985 and September 1986. These included six runs in dry air and one run in humid (50 percent relative humidity) air. The concentration of SF_6 was approximately equal to 1.5 parts-per-million by volume (ppm). The SF_6 was injected at atmospheric pressure in a 1.0-mL gas syringe as a 0.5 mL sample. All of the runs in both dry and humid air were made in combination with approximately 20 ppm CH_4.

The decay of SF_6 was erratic. A typical decay curve (a plot of SF_6 absorbance versus time) is shown in Figure 11. Further investigation of this behavior revealed that the majority of the peaks and valleys in the decay curve decreased considerably when the integrated band intensity rather than the absorbance was plotted versus time (see Figure 11). The revised data processing MACRO program is listed as a part of Appendix B. The erratic

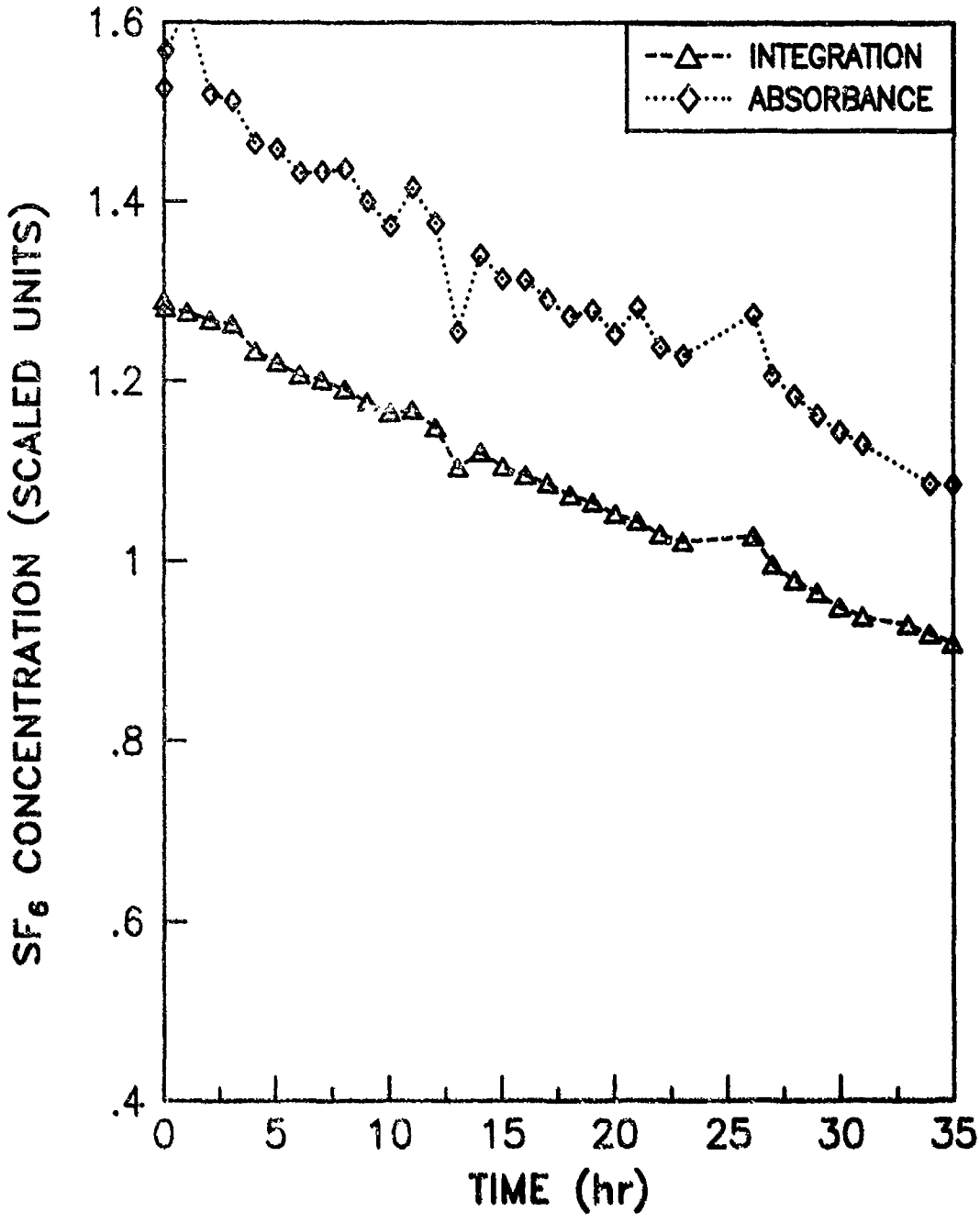

Figure 11. Comparison of SF_6 Plots by Integration and Absorbance.

behavior in the plots is understandable in view of the fact that the absorption coefficient for SF_6 is about 100 times greater than that of hydrazine. Plotting SF_6 absorbance versus time has the effect of amplifying small variations by a factor of 100 when compared with a similar hydrazine decay curve.

The SF_6 runs were analyzed by plotting the integrated absorbance of the SF_6 band between 900 and 1000 cm^{-1} versus time (normalized to a starting value of one for comparison). They are shown in Figure 12. The decay curves fall roughly into two groups. The upper four curves have an average half-life of about 60 hours. The lower three curves have an average half-life of about 40 hours.

An examination of the plot legend shows that the upper four curves were obtained in experiments from October 1985 through February 1986. The lower three curves were from experiments from July 1986 through September 1986. The 33 percent decrease in half-life is probably due to leaks from small holes created by mechanical stress on the Teflon bag as a routine part of other experiments conducted from March 1986 to June 1986. Repeated experiments, especially those where the bag was opened, often caused small holes along seams and at corners.

2. CH_4

Methane was used as an internal standard or an inert test gas in 22 separate experimental runs between 10 December 1985 and 19 September 1986. Five of these runs were conducted in humid air and the remainder in dry air. Six of the runs contained SF_6, three contained ammonia (NH_3), and one contained additional Teflon sheets.

In the runs made with SF_6, when normalized to a beginning absorbance of one, the CH_4 decay followed the same pattern as the SF_6. These curves are plotted in Figure 13. There were roughly two groups; those conducted early in the year had a half-life of roughly 60 hours and those conducted from July 1986 to September 1986 had a half-life of 35 to 45 hours.

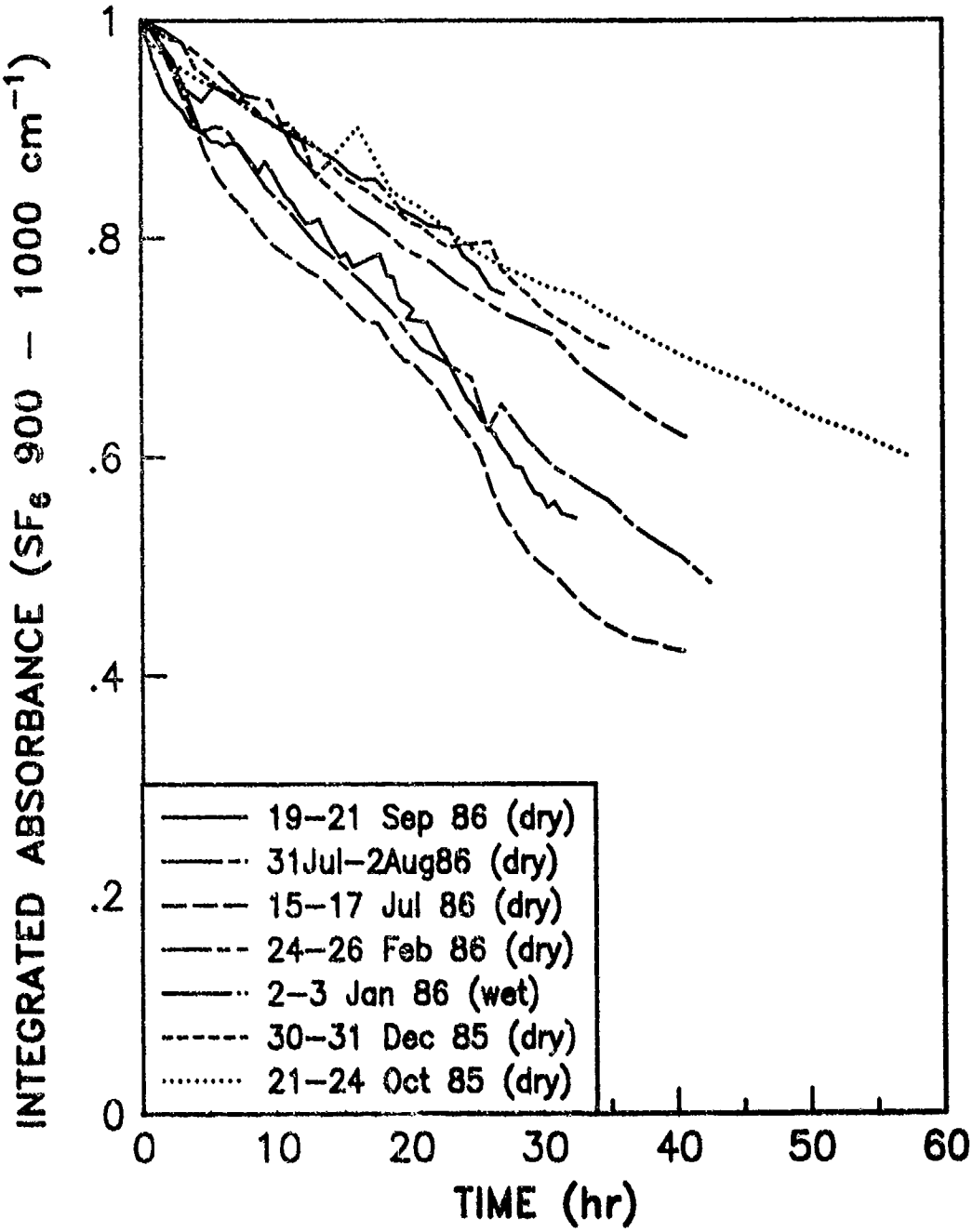

Figure 12. Plots of SF_6 Concentration Versus Time in the Teflon Chamber.

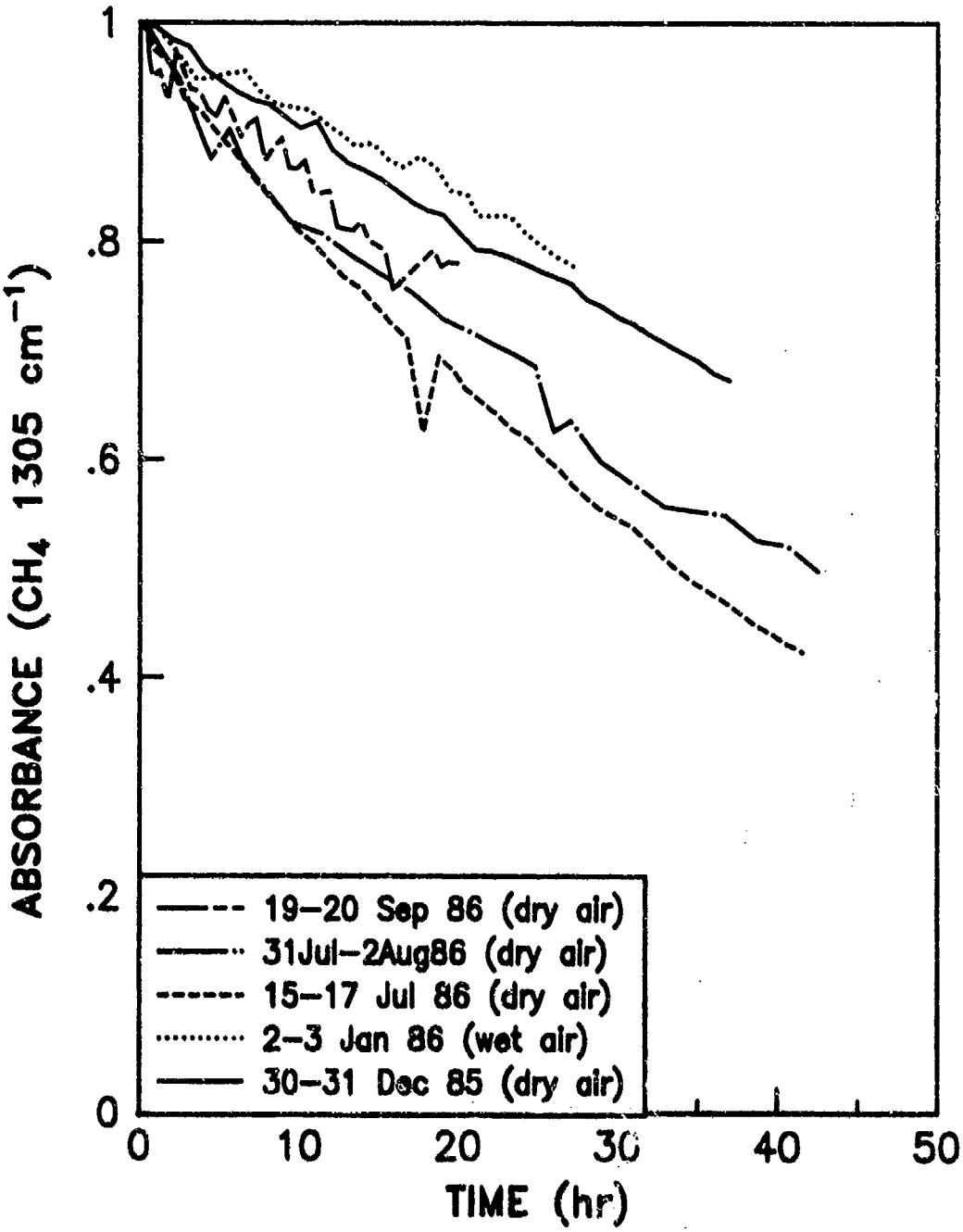

Figure 13. Plots of CH_4 Concentration Versus Time in the Teflon Chamber (with SF_6 Present).

The single run conducted under humid conditions showed a somewhat slower decay rate than the runs conducted under dry conditions. This pattern appears throughout the CH_4 runs and demonstrates that either there is a site competition between CH_4 and water or that the humid air is wetting the Teflon film, making it less receptive to CH_4 adsorption.

In experiments conducted with NH_3, the run conducted under humid conditions decayed somewhat more slowly than the two conducted under dry conditions (half-life 42 hours versus 35 hours). Even though these runs were all conducted early in the year, they did not follow the trend of slower decay rates observed in the SF_6/CH_4 system. The reason for this difference is not clear. These three runs are plotted in Figure 14.

In the experiments where hydrazine was run in combination with CH_4, the decay rates generally followed the same pattern observed in the SF_6/CH_4 system. Decay rates were generally slower in the runs conducted at the first part of the year and somewhat faster in runs conducted some months later. Again, the runs conducted under humid conditions decayed somewhat more slowly than any of the others. These runs are shown in Figure 15. CH_4 runs conducted with added Teflon sheets and added mirror surfaces were not distinguishable from others.

One other observation should be noted. In runs conducted under humid conditions (with the exception of the NH_3/CH_4 run), the CH_4 concentration increased for the first 4 to 6 hours of the run. It would then show a smooth gradual decrease. This behavior is shown in Figure 16.

3. Other Test Gases

Other runs were conducted with NH_3, methanol, dichlorodifluoromethane (Freon-12), atmospheric O_2, and water vapor to test ideas concerning properties of the Teflon film.

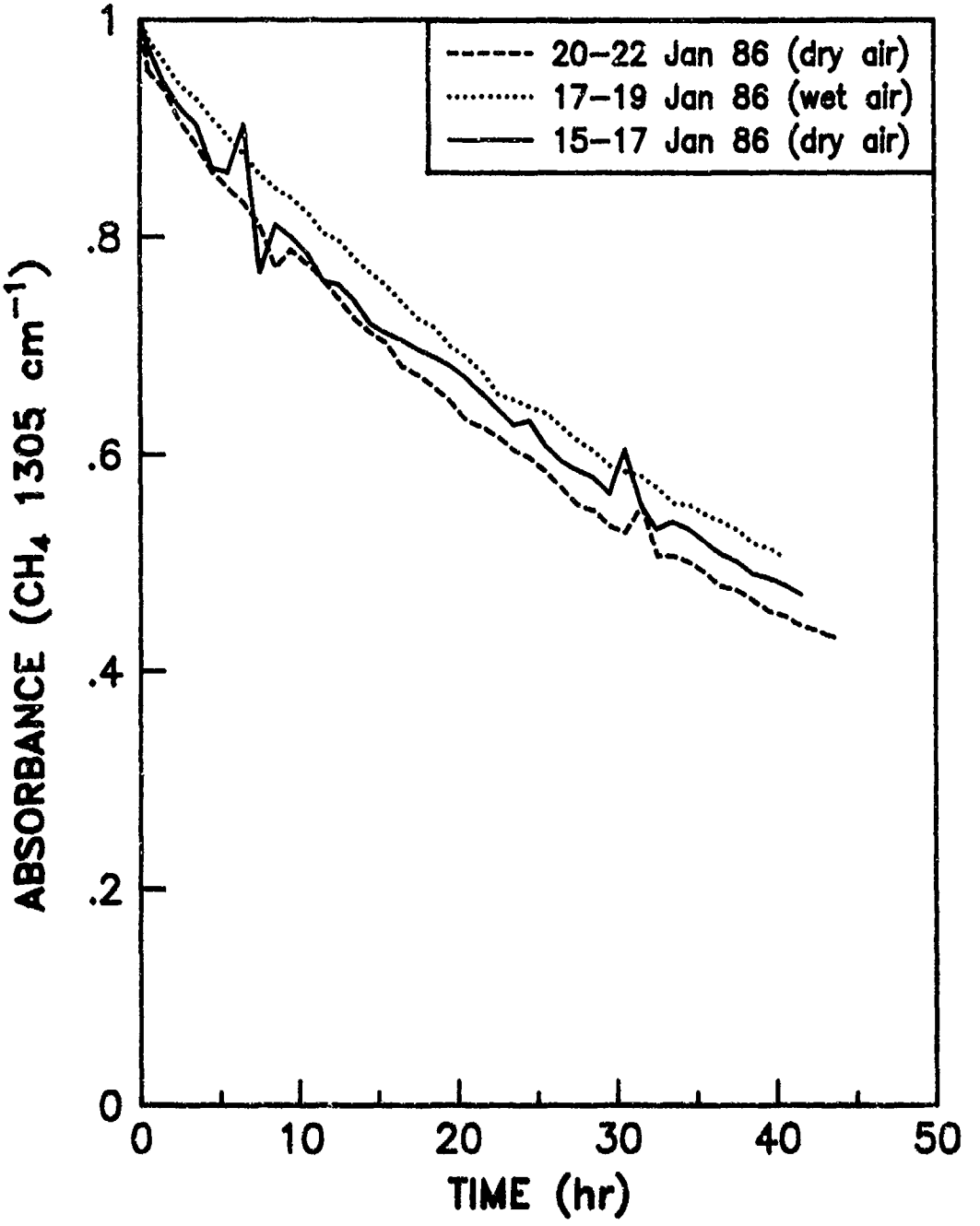

Figure 14. Plots of CH_4 Concentration Versus Time in the Teflon Chamber (with NH_3 Present).

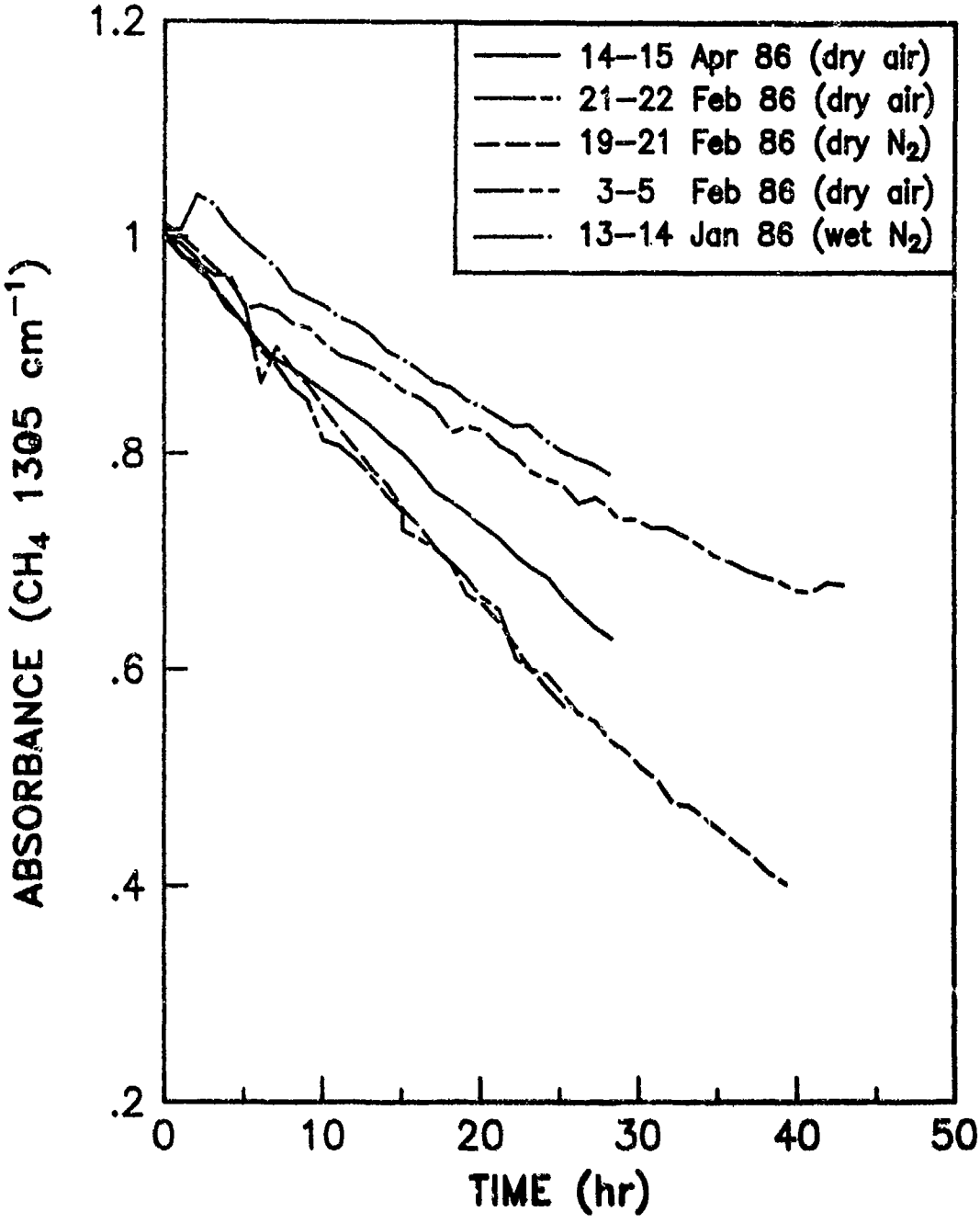

Figure 15. Plots of CH_4 Concentration Versus Time in the Teflon Chamber (with Hydrazine Present).

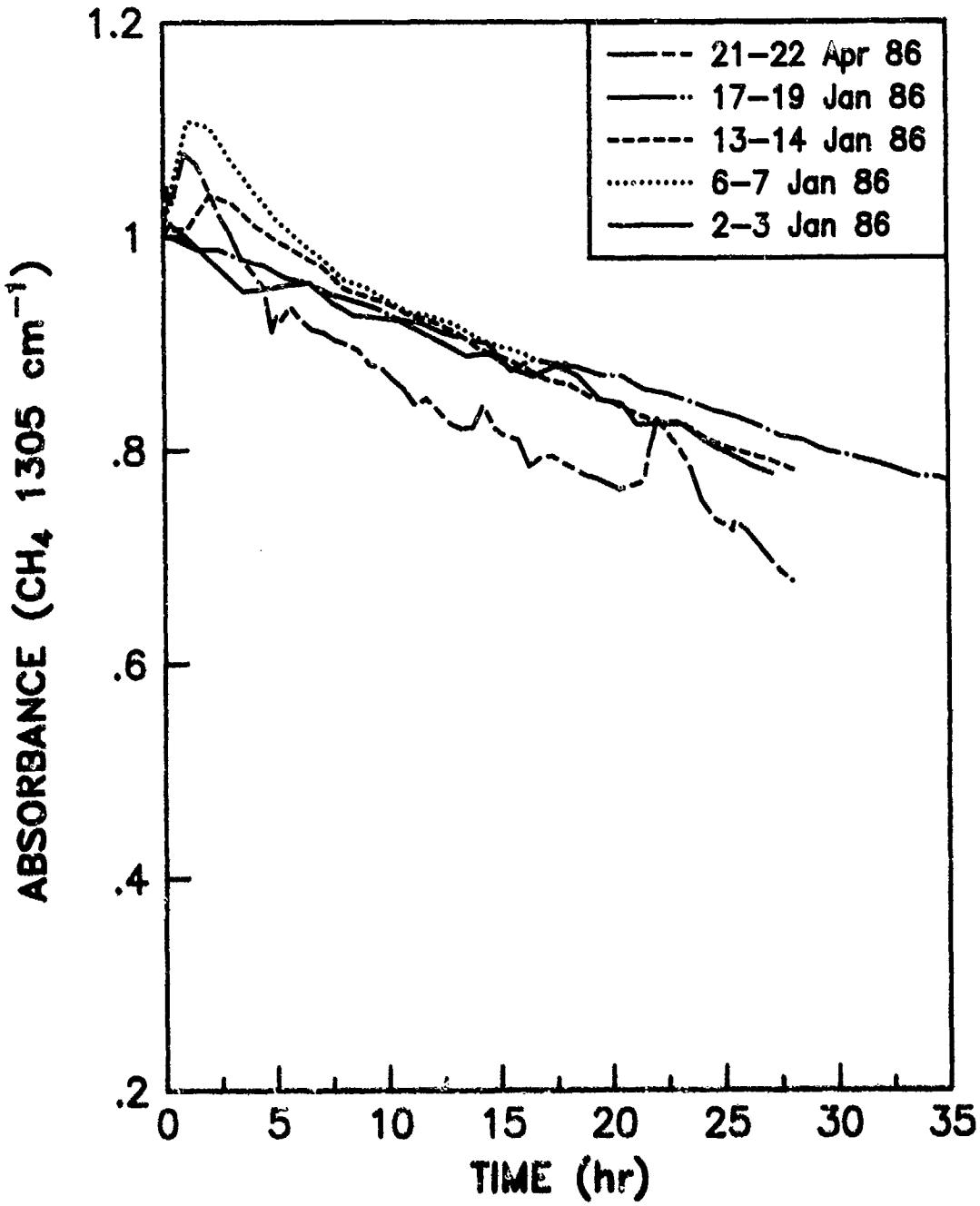

Figure 16. Plots of CH_4 Concentration Versus Time in the Teflon Chamber (under High Humidity Conditions).

a. NH_3

Since hydrazine may be considered as being derived from NH_3 by replacement of one hydrogen atom with an $-NH_2$ group (Reference 21), it was felt that NH_3 would exhibit behavior similar to hydrazine in the Teflon chamber. Three different experiments were run with NH_3, two in dry air and one in humid air. In each case, CH_4 was used as an internal standard.

These runs were normalized to an initial integrated absorbance of one and plotted in Figure 17. The NH_3 decay in humid air was a little slower than in dry air. The estimated half-life in humid air was about 41 hours, while the average half-life in dry air was about 36 hours.

In general, NH_3 behaved in the same way as the inert tracer gases had behaved. Despite its chemical similarity with hydrazine, its behavior in the Teflon chamber failed to indicate any hydrazine-like decay.

b. Methanol

Since NH_3 behaved essentially the same as CH_4 or SF_6 in the Teflon chamber, methanol was tried in one run to see if it would behave more like hydrazine. The run was conducted in dry air, and methanol, too, behaved like the inert gases. The run is plotted is Figure 18.

c. Freon-12

Technical data on the permeation rates of different gases through FEP Teflon film were obtained from DuPont (Reference 22). The permeation rate of Freon-12 was from 30 to 100 times greater than most other gases. One experiment was conducted with Freon-12 in dry air to determine its behavior in the Teflon chamber. The expectation was that the Freon-12 would rapidly permeate out of the chamber and have a relatively short half-life. However, it, too, behaved much the same as CH_4 or SF_6 (see Figure 19).

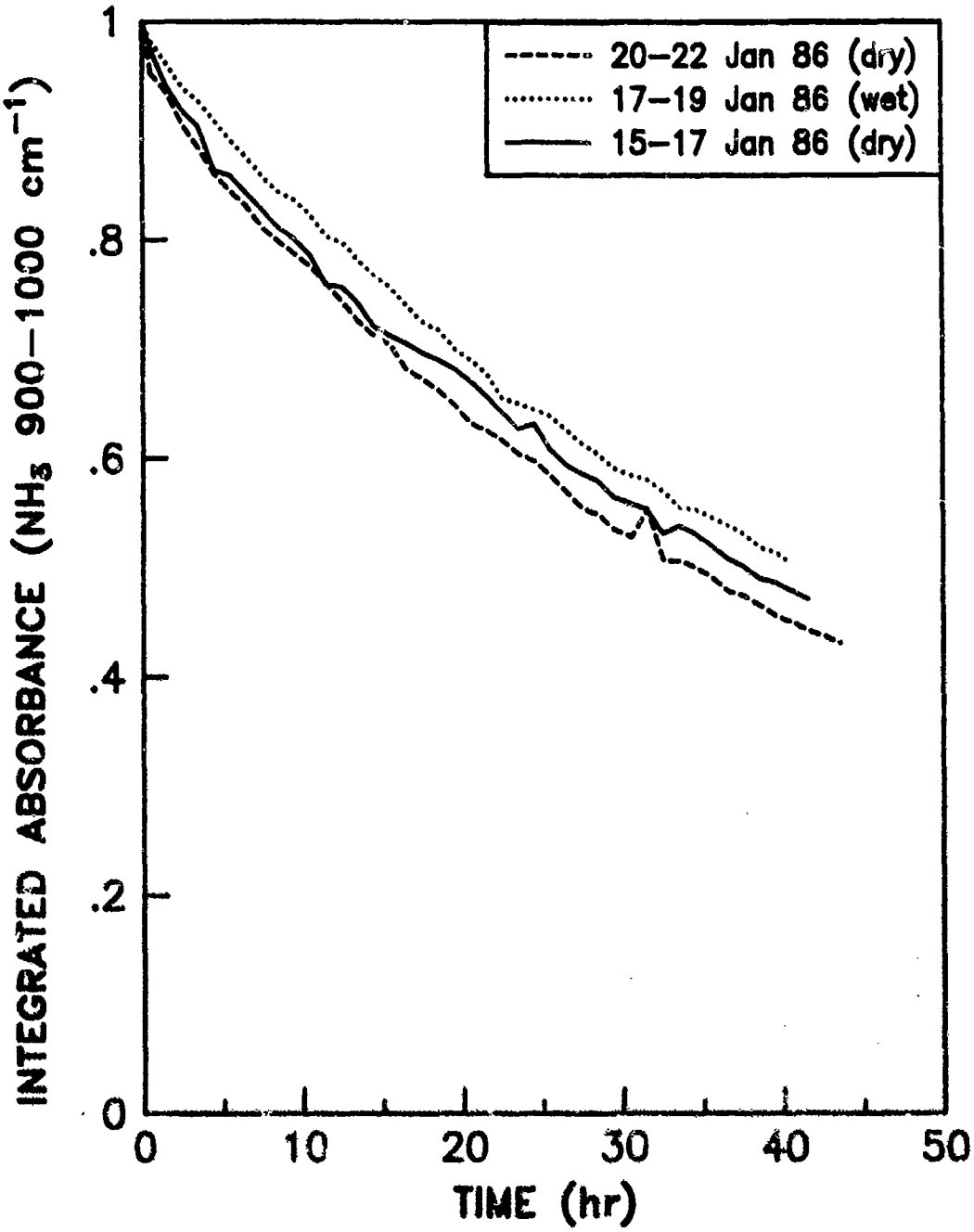

Figure 17. Plots of NH_3 Concentration Versus Time in the Teflon Chamber.

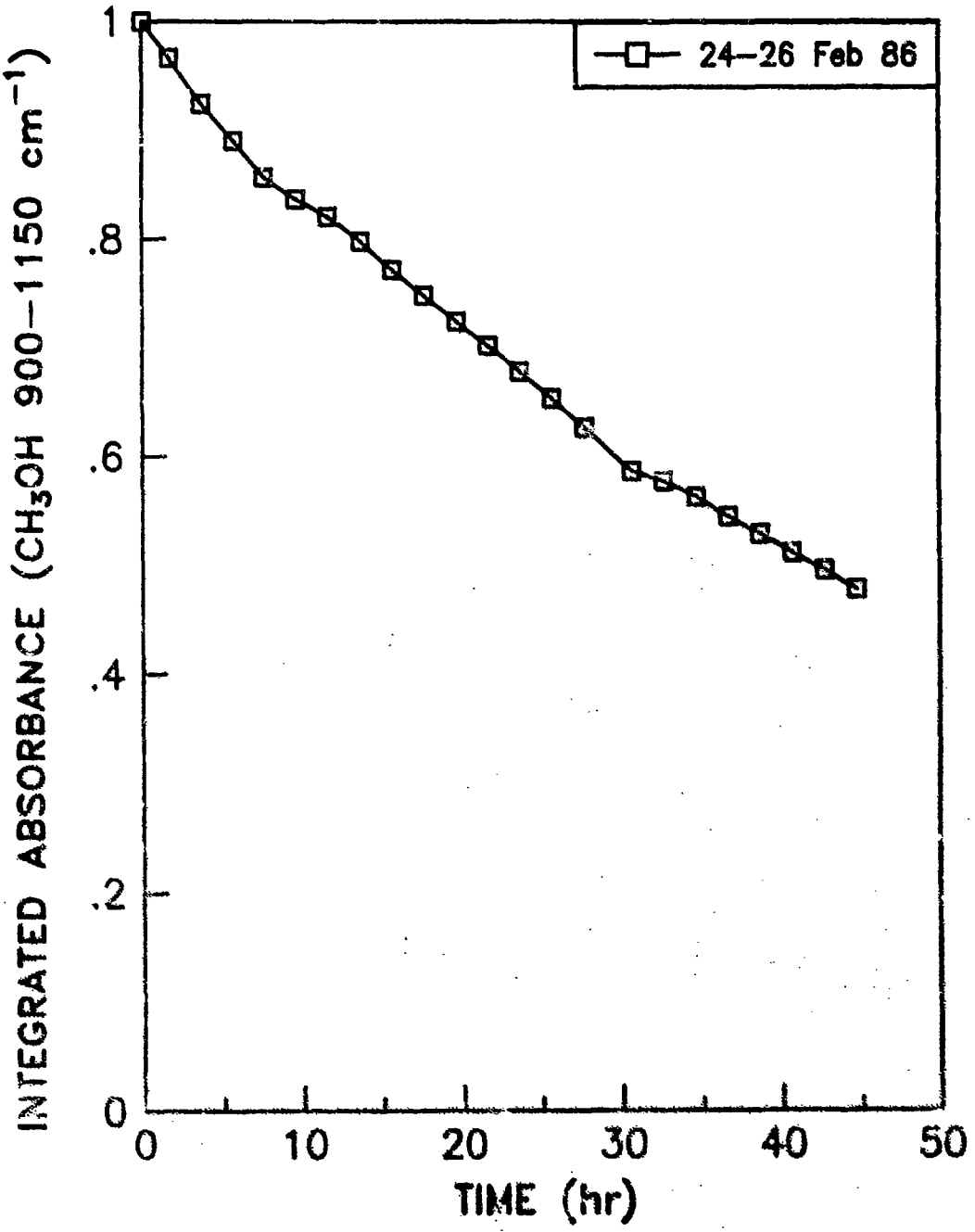

Figure 18. Plot of Methanol Concentration Versus Time in the Teflon Chamber.

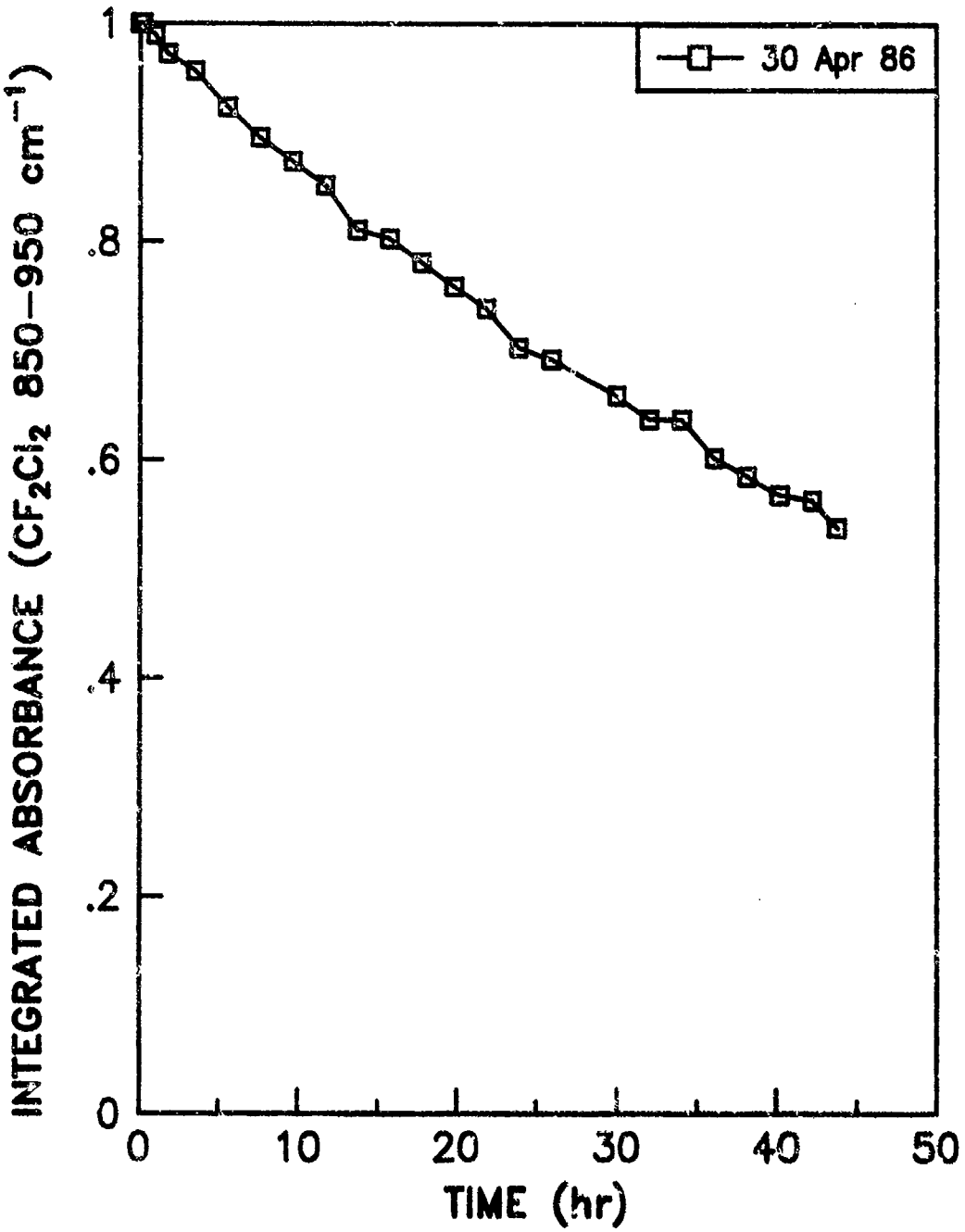

Figure 19. Plot of Freon-12 Concentration Versus Time in the Teflon Chamber.

The behavior of Freon-12 in the chamber is difficult to explain unless one invokes the idea that some gases in the chamber escaped predominantly from undetected macroscopic holes in the chamber walls or seams. This possibility cannot be totally ruled out, since small holes are very difficult to locate in the transparent Teflon film surface, especially at corners and seams.

d. Water Vapor

Water permeation studies were done in which the chamber was filled with dry air and the increase in water vapor was monitored with the FT-IR spectrometer. Figure 20 shows a first-order fit to a typical data set. The half-lives estimated from the various data sets varied somewhat. The data in Figure 20 showed a half-life of 19 hours. Most half-lives were smaller than this. Moreover, some data sets showed substantial scatter after 15 to 20 hours. This may have been due either to temperature fluctuations or changes in the absolute humidity in the laboratory.

Water vapor has a somewhat greater ability to go through Teflon film than most of the other gases studied. That water may have a substantial affinity for Teflon film is an important consideration in light of the hydrazine studies presented later in this report.

e. Atmospheric O_2

Oxygen permeation studies were done in which the chamber was filled with dry N_2 and the increase in O_2 was monitored with the FT-IR spectrometer, as described earlier. The estimated half-life for this process was 7 hours. This process was modeled using the simple effusion model in Section III, Model Development. Figure 21 shows a fit of the permeation version adapted for permeation into a chamber (see Appendix F). The fitted parameters with errors are: $k_s[S] = .7(.2)$, $k_D[S] = 2(?)$, and $k_{-s} = .8(.4)$ (all parameters in $hour^{-1}$). This model aptly explains the slight sigmoidal shape of the data. Oxygen behaves much like hydrazine toward Teflon film, despite the obvious structural and chemical differences.

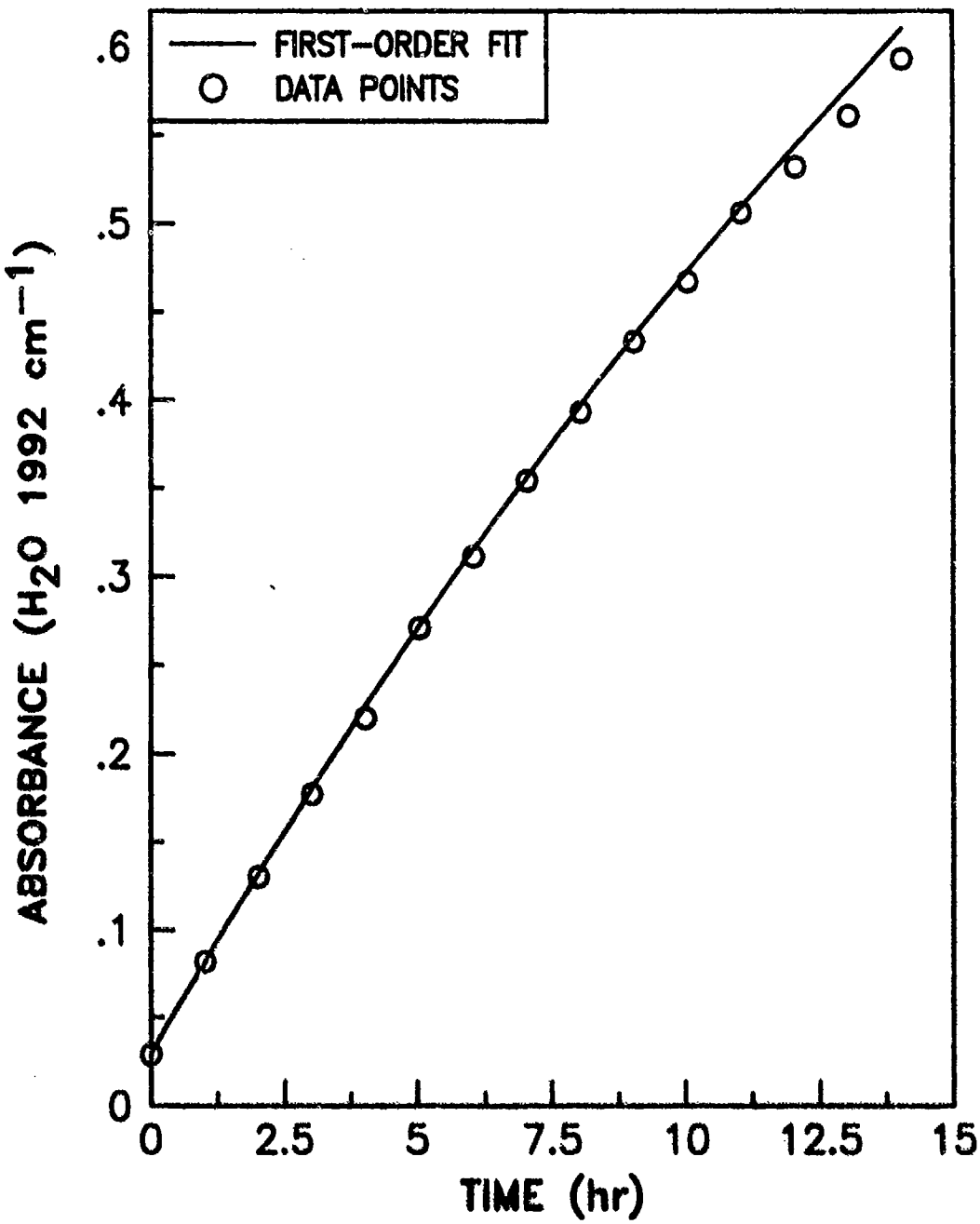

Figure 20. First-Order Fit to Water Permeation Data.

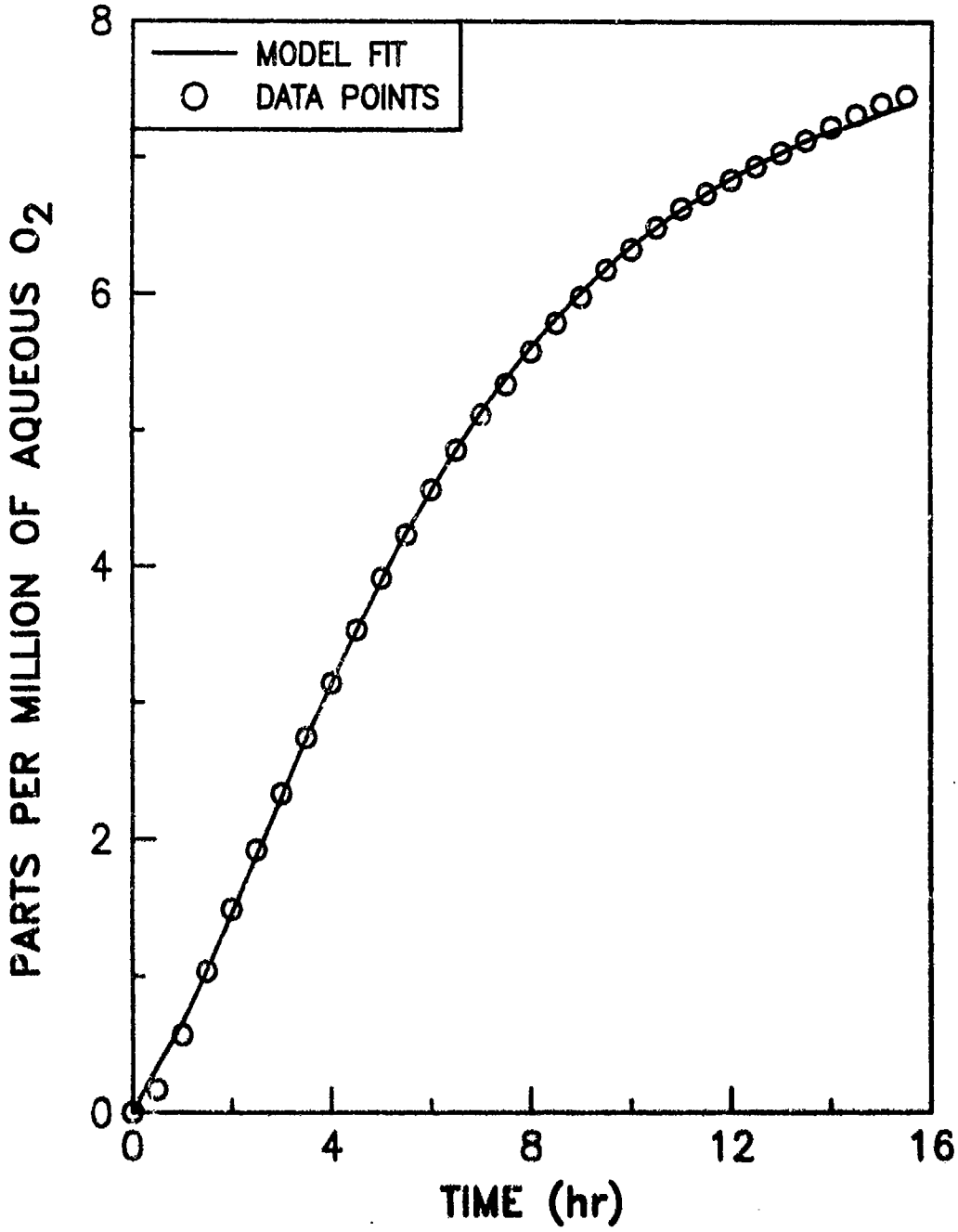

Figure 21. Permeation Model Fit to O_2 Permeation Data.

f. Discussion

There are two modes by which a gas can enter or leave the chamber: permeation and effusion. Experiments with inert gases conducted over a period of months seem to indicate that effusion is occurring to a larger extent. However, if effusion was the only mode of loss from the chamber, there would be a correlation between the square root of the mass of a chemical species and its loss rate. No such correlation was observed in this study. Therefore, permeation must also be an important loss mode. The degree of importance of permeation may be somewhat dependent on the chemical nature of the species. However, there is no apparent correlation between the structural and chemical nature of a species and its loss rate. There may be some less obvious structural or chemical feature, either inherent or induced, common to hydrazine, water, and oxygen, which accounts for the enhanced permeation rates of these species.

The fact that the O_2 permeation data can be fitted very well by the permeation version of the model may seem to lend support to the hypothesis that permeation is important for some species in Teflon film chambers. However, a model version in which simple effusion is coupled with surface adsorption onto nonpermeable sites inside the chamber fits the O_2 data equally well. Experimental results from all inert species studied indicate both effusion and permeation are taking place, but the model cannot be used to determine the relative importance.

C. HYDRAZINE EXPERIMENTS

Nearly 40 separate runs were conducted with hydrazine in the 5-mil Teflon chamber beginning in October 1985. These included runs in dry air, in humid air, in dry N_2, and in humid N_2. There were also runs made with added Teflon sheets and with added mirror surfaces in the chamber.

Various abridged versions of the model have been used to fit single runs and sequential runs. Versions used for single runs included the permeation version and the coupled effusion-adsorption version. These simple versions

fit data sets much better than the first-order equation, but do not account for conditioning. A simple modification of the effusion-adsorption version, however, can account for conditioning. Changing the adsorption process from first- to second-order is sufficient to handle the conditioning which is seen in sequential data sets.

1. Hydrazine in Dry N_2

A total of five different experiments were conducted. The runs were normalized to a starting absorbance of one for the hydrazine analytical band at 958 cm^{-1} and plotted on one graph in Figure 22. Four of the runs fell on nearly the same decay curve, while one (10-12 Jan 86) is considerably slower. A simple graphical determination of the half-lives for these runs gave the results shown in Table 1.

TABLE 1. HYDRAZINE DECAY IN DRY NITROGEN

Date of Run	Half-Life (hours)
6-8 Dec 85	8.0
11-12 Dec 85	8.1
10-12 Jan 86	16.8
19-21 Feb 86	6.9
8-9 Sep 86	9.5

In examining this data, it was found that the 10-12 Jan 86 run had only one observable difference from the other four runs. It was the last in a series of four experimental runs involving hydrazine decay which were conducted essentially back-to-back; that is, there was never more than a weekend between them. Even though each run was preceded by a thorough purge, there is apparently enough surface site attraction for hydrazine to maintain surface conditioning for at least several days. Thus, the chamber was conditioned by the earlier runs and, as a result, the decay rate was only about half that of the other runs. In fact, model fits shown later indicate that deconditioning is a relatively slow process in dry conditions.

Three of the other runs had been conducted after lengthy periods of no chamber activity: 5 weeks for the 6-8 Dec 85 run, 2 weeks for the 19-21

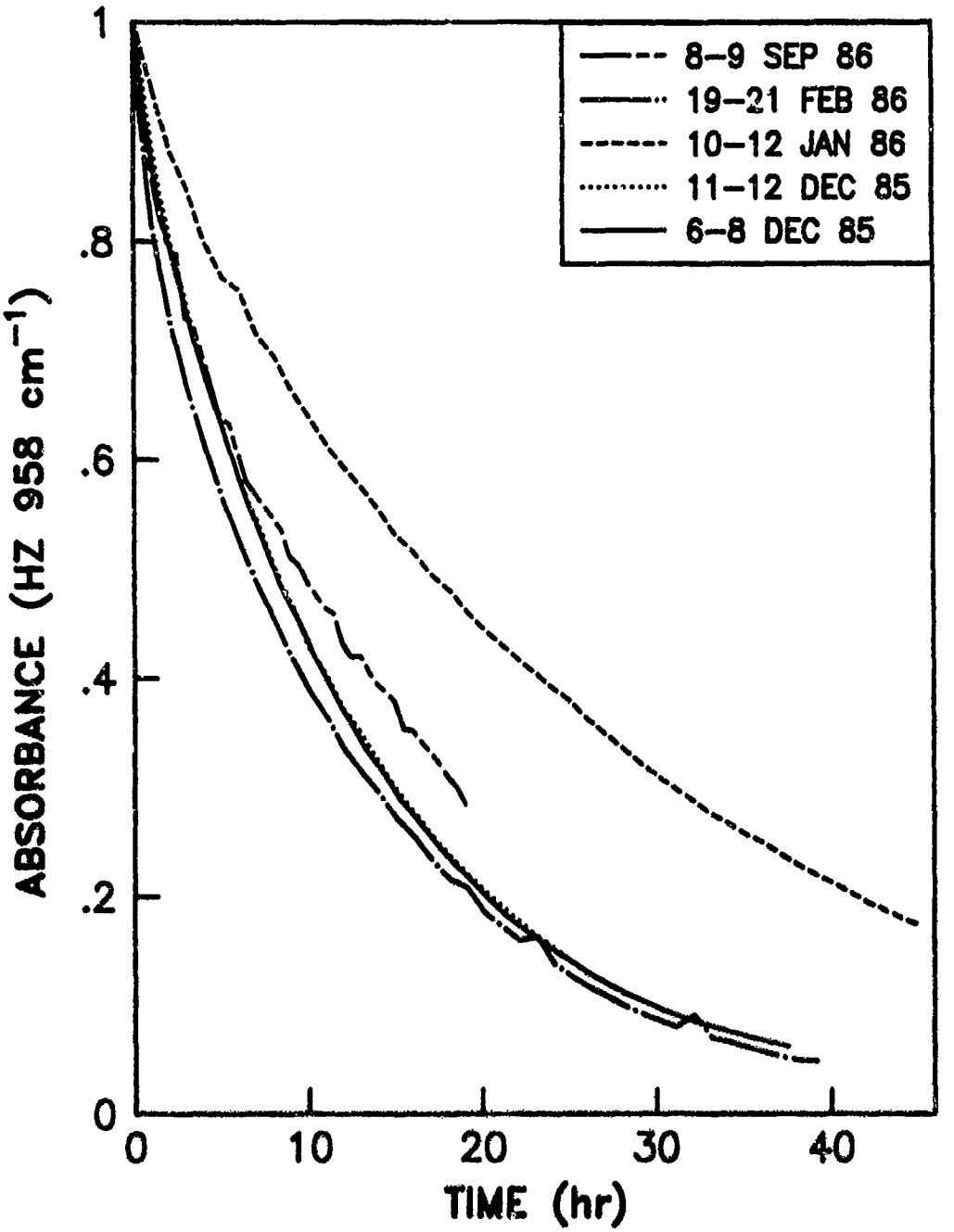

Figure 22. Plots of Hydrazine Concentration Versus Time (In Dry Nitrogen).

Feb 86 run, and 5 weeks for the 8-9 Sep 86 run. However, the 11-12 Dec 85 run was conducted only 3 days after the 6-8 Dec 85 run. There was, however, a dry SF_6/CH_4 run conducted between 6-8 Dec 85 and 11-23 Dec 85. This intervening run apparently affected the chamber deconditioning process, but it is not clear by what mechanism.

Figure 23 shows the data for the 8-9 Sep 86 run with model fits. The permeation version fits the data much better than a simple first-order fit. The fitted parameters are: $k_s[S] = .17(.01)$, $k_{-s} = .58(.07)$, and $k_D[S] = .9(.2)$ (all parameters are in $hour^{-1}$). The number of pore layers was set to two and the time step was .01 hour. This was generally the case for most of the permeation version fits.

2. Hydrazine in Dry Air

Beginning in October 1985 and continuing through December 1986, a total of 18 different experiments of hydrazine in dry air were conducted. Fifteen of these runs were normalized to a starting absorbance of one for comparison with each other (the remaining three were not successfully stored). These runs are shown in Figures 24, 25, and 26. The half-life for each run was again estimated by a simple graphical procedure. The results are tabulated in Table 2.

The first group of data is a summary of experimental runs conducted between October 1985 and February 1986. These runs are plotted in Figure 24. The 28-29 Oct 85 run was the first hydrazine run in the 5-mil Teflon bag. However, two characterization runs had been conducted earlier, one on 16 Oct and the other on 21 Oct. These runs were made with CH_4 and SF_6 to evaluate the stability of these inert gases in the chamber. Apparently these two runs affect the chamber conditioning (giving a half-life about 30 percent greater than later runs in a well-flushed chamber), but the exact mechanism is not yet established. The next run, conducted from 19-20 Dec 85 showed a half-life of only 7.8 hours. This decrease is explained by the fact that the Teflon chamber sat for 7 days before the run was started, giving the chamber time to partially decondition. The third run in the table, 23-24 Dec 85, was

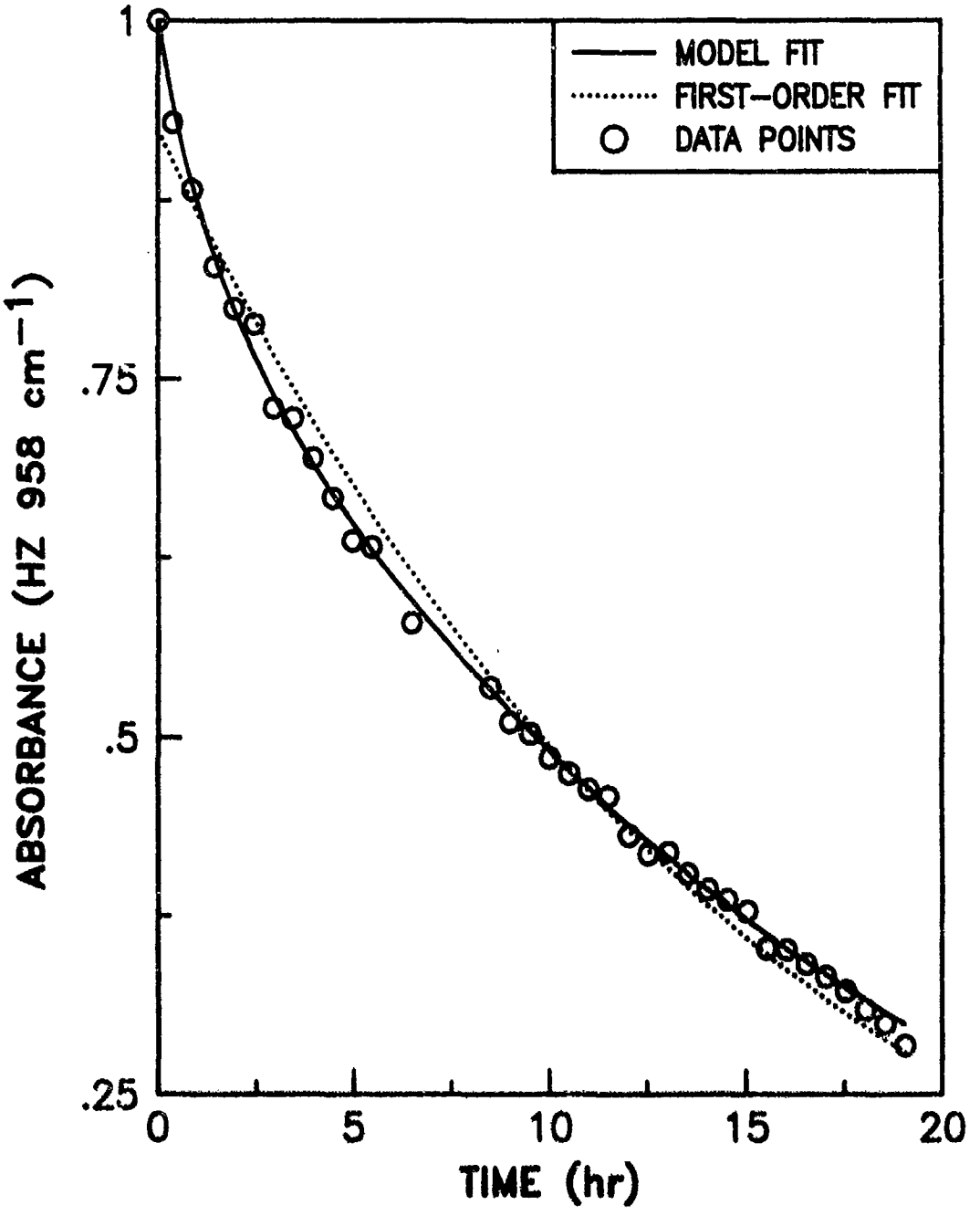

Figure 23. First-Order and Permeation Model Fits of Hydrazine Decay Data.

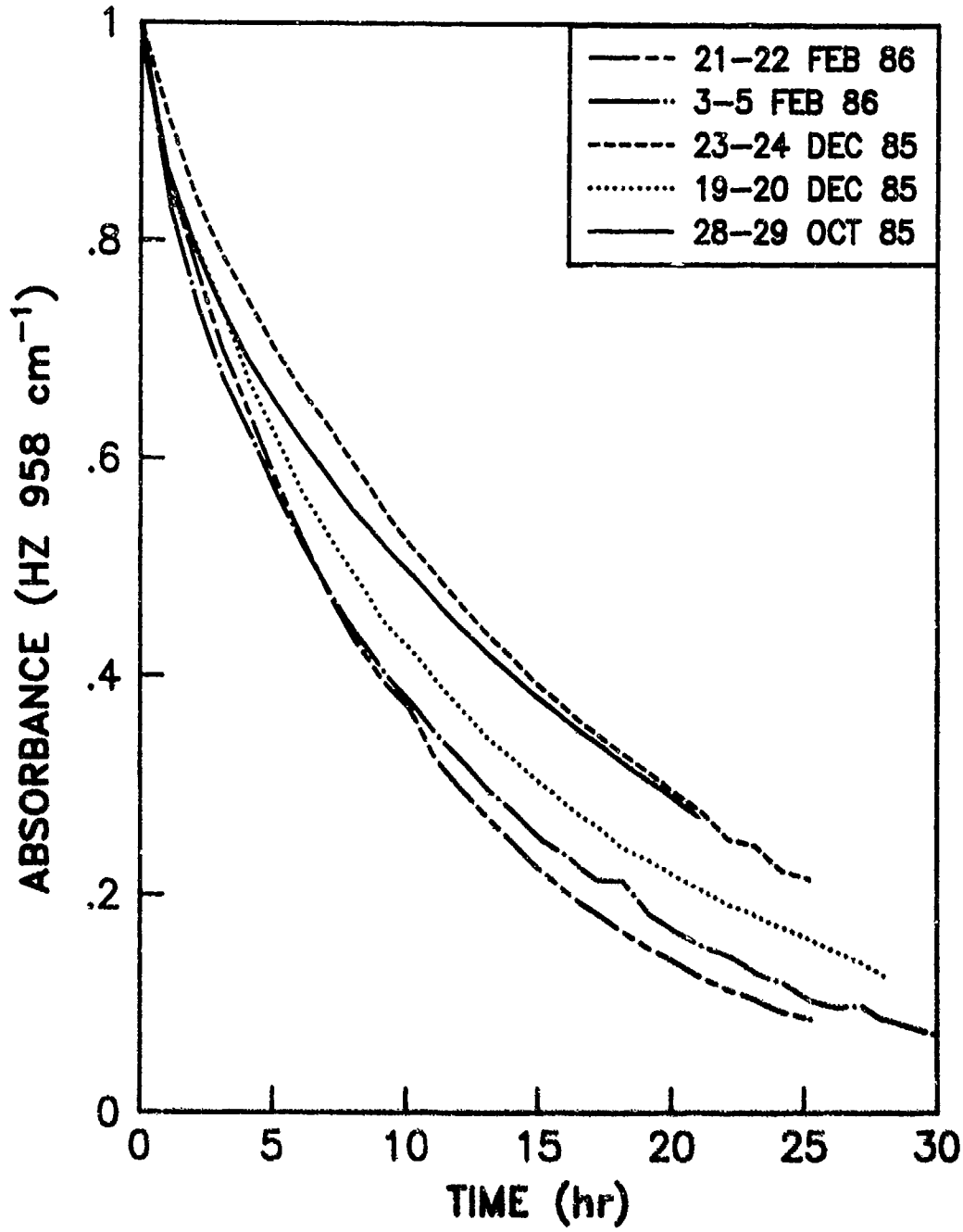

Figure 24. Plots of Hydrzine Concentration Versus Time in the Teflon Chamber (In Dry Air).

TABLE 2. HYDRAZINE DECAY IN DRY AIR

Date of Run	Half-Life (hours)
---------- Group 1 ----------	
28-29 Oct 85	10.0
19-20 Dec 85	7.8
23-24 Dec 85	10.8
3-5 Feb 86	6.6
21-22 Feb 86	6.5
---------- Group 2 ----------	
14-15 Apr 86	9.6
15-16 Apr 86	12.9
16-17 Apr 86	14.0
17-18 Apr 86	14.6
---------- Group 3 ----------	
3-5 Nov 86	6.7
12-14 Nov 86	8.6
24-26 Nov 86	10.4
1-3 Dec 86	10.3
8-9 Dec 86	10.3
9-11 Dec 86	8.7

conducted 2 days after the second run. This did not allow the chamber walls to desorb the hydrazine completely and the half-life increased to 10.8 hours. Prior to the fourth run, 8 sheets of 2-mil Teflon were hung from the interior ceiling of the chamber, effectively doubling the interior surface area. However, the chamber had also sat for 2 weeks before the run was made. The combination of added Teflon sheets and a 2-week rest period combined to give

a very short 6.6 hour half-life. The final run in the first group was made after eight Pyrex mirrors of various sizes were placed inside the chamber. The mirrors were of the same basic construction as those used in the chamber optical system. They were of Pyrex glass with a silicon dioxide overcoated aluminum surface. The run was made to test the effect of added mirrors on the decay of hydrazine. This run was preceded by a run with dry nitrogen; therefore, there had not been enough time for the chamber surfaces to desorb hydrazine completely. The added mirrors appear to have accelerated the decay process, since the half-life was the lowest of any run, 6.5 hours.

The third run in Group 1 was modeled using an adaptation of the permeation version of the model. This adaptation, derived in Appendix G, includes equations for a permeable surface within the chamber. Since 2-mil sheets were used in the chamber made of 5-mil sheets, the number of inside surface pore layers was set to two and the number of chamber wall pore layers was set to five. Table 3 shows results of the model fit to this data set, along with three more fits of data sets in dry conditions. Since long-term conditioning is not taken into account in the permeation version of the model, the fitted parameters shown in Table 3 are for rough comparisons only. The value of $k_s[S]$ for the run with the added sheets is slightly higher than for the runs with nothing added, reflecting the idea that the 2-mil sheets were unconditioned. The parametric values for the fit of the 28-29 Oct 85 run are somewhat different than for the other two fits. Since the run was the first run in the 5-mil bag, this discrepancy might be expected. However, because the permeation version is not an accurate model (it does not take into account conditioning), differences in the values for the fitted parameters cannot be confidently interpreted.

The value of $k_s[S]$ for the fit of the run with the added mirrors is larger than for the other fits. This lends support to the idea that the hydrazine is interacting with the mirrors, either by surface adsorption or surface-catalyzed oxidation. A more accurate version of the model would take these interactions into account by introducing an additional adsorption process, but would also require additional parameters. As it is, the simple permeation version fits the data quite well. Using more sophisticated

TABLE 3. RESULTS OF THE PERMEATION VERSION MODEL FITS FOR REPRESENTATIVE DATA SETS.*

Date of Run	Conditions	$k_s[S]$	k_{-s}	$k_D[S]$	SOS
28-29 Oct 85	dry air	.213(.007)	1.96(.09)	5.5(.2)	3×10^{-3}
3-5 Feb 86	dry air; 2-mil sheets	.24(.03)	3.2(.4)	28(13)	1×10^{-3}
21-22 Feb 86	dry N_2; 8 mirrors	.31(.02)	2.1(.2)	5.7(.4)	9×10^{-4}
14-15 Apr 86	dry air	.18(.03)	3.3(.8)	32(10)	5×10^{-4}

*The model was adapted as described in the text for the data set using the 2-mil Teflon sheets. The number of pore layers for the chamber film for all runs was set to 5. All parameters are in $hour^{-1}$. SOS is the residual sum of squares.

versions of the model requires fitting multiple data sets simultaneously rather than just single data sets. Fits of multiple-data sets have been done for sequential runs and the results are given later in this section.

The second group of data in Table 2 summarizes four sequential runs made in April 1986. These runs are shown in Figure 25. These runs were made to test the hypothesis that there was a conditioning effect when insufficient time was allowed between hydrazine decay runs. The first run in this series was conducted after the chamber had not been in use for almost 5 weeks. According to previous experience, the half-life should have been around 7 hours. However, it was measured at 9.6 hours. The reason for this behavior is not known. Each succeeding run in this series was conducted by adding hydrazine to the previous run with no additional flushing of the chamber. As expected, the half-life of runs 1, 2, 3, and 4 increased from 9.6 to 14.6 hours. This series of runs demonstrated that there is a definite conditioning process which occurs in this chamber.

The second group in Table 2 was modeled compositely, using the effusion-adsorption version modified by allowing adsorption to be second-order. The

parameters for this version are: k_1 (adsorption constant), k_{-1} (desorption constant), $[F_1]_o$ (initial concentration of nonpermeable surface sites), and k_e (first-order effusion constant). This version has been used for composite fits of sequential runs because no reasonable adaptation of the permeation version could fit a set of sequential runs very well. This is not to say that permeation does not occur, at least to some extent. In fact, the effusion constant serves as a catch-all term for any first-order process, which includes steady-state permeation. Figure 27 shows a normalized composite fit to the first three runs of the sequential data set. Initial absorbance readings for the second and third runs were adjusted to minimize the residual sum of squares. This was done because of the large systematic errors in the first data points of the second and third runs. Table 4 shows results of the composite fits for the second and third groups of hydrazine decay in dry air and two composite fits for runs in humid air. Since the effusion-adsorption version adapted for describing the conditioning process is likely a more accurate description of the truth than the simple permeation version, a meaningful interpretation of the fitted parameters is possible. Interpretation of these parameters is given later in the General Discussion Section.

The third group of data in Table 2 summarizes six sequential runs made between 3 Nov and 11 Dec 86 (Figure 25). These runs were designed to further test the model. The results of the composite fit are in Table 4. The first run was begun after a 2-week purge of the chamber with pure air. Every 30 minutes, the mixing fan was cycled on for 2 minutes and the annular space in the Plexiglas box was continuously purged with dry air. The expectation was that the initial run would be essentially the same as a run in a "new" Teflon chamber.

This turned out to be the case; the half-life was 6.7 hours. Runs 2-5 were conducted by adding additional hydrazine to the chamber. There was no purging between runs, but the chamber mixing fan was left on its automatic cycle. The second run saw an increase in half-life to 8.6 hours and the third run to 10.4 hours. The adsorption sites had become nearly saturated

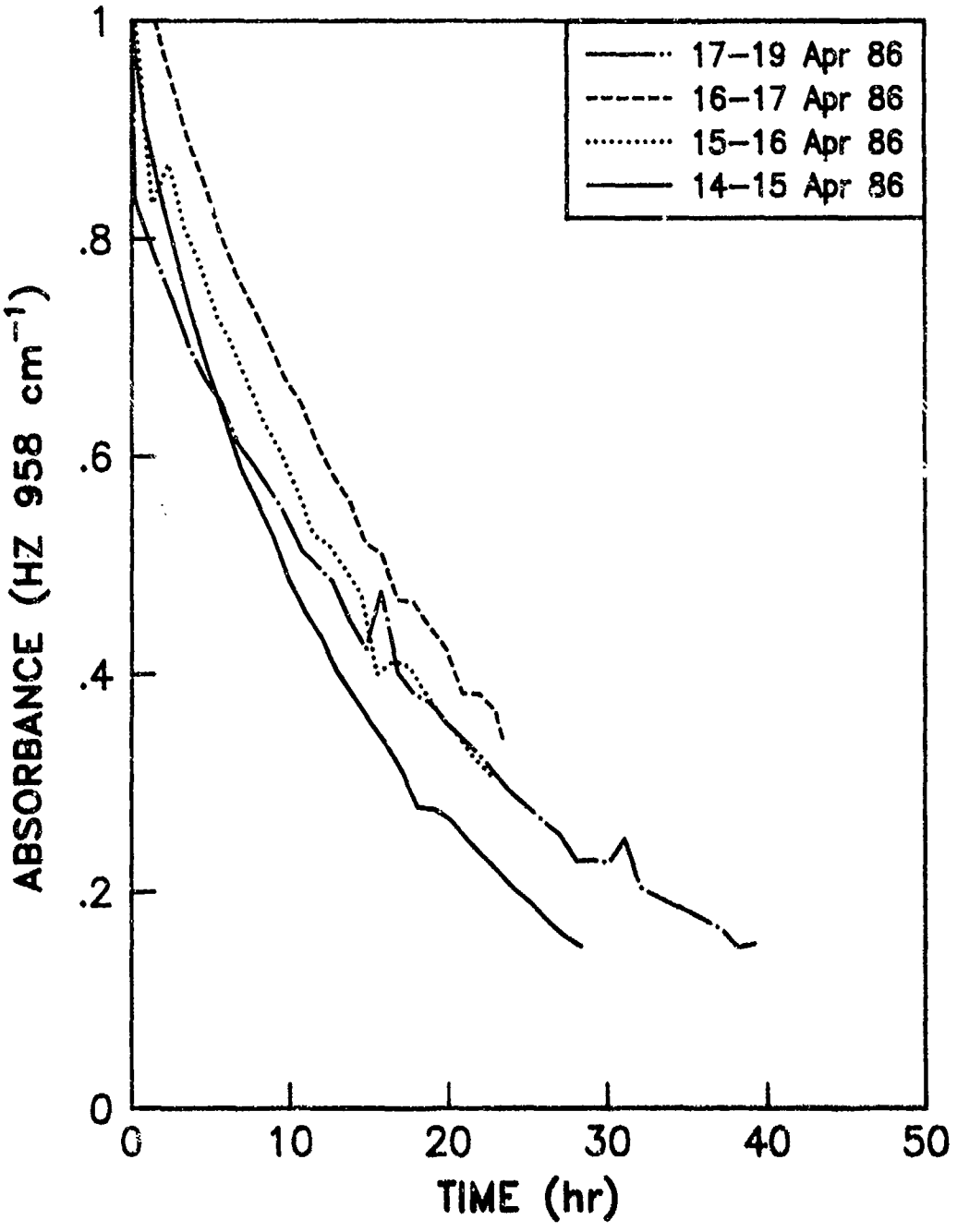

Figure 25. Plots of Hydrazine Concentration Versus Time in the Teflon Chamber (Sequential Runs in Dry Air).

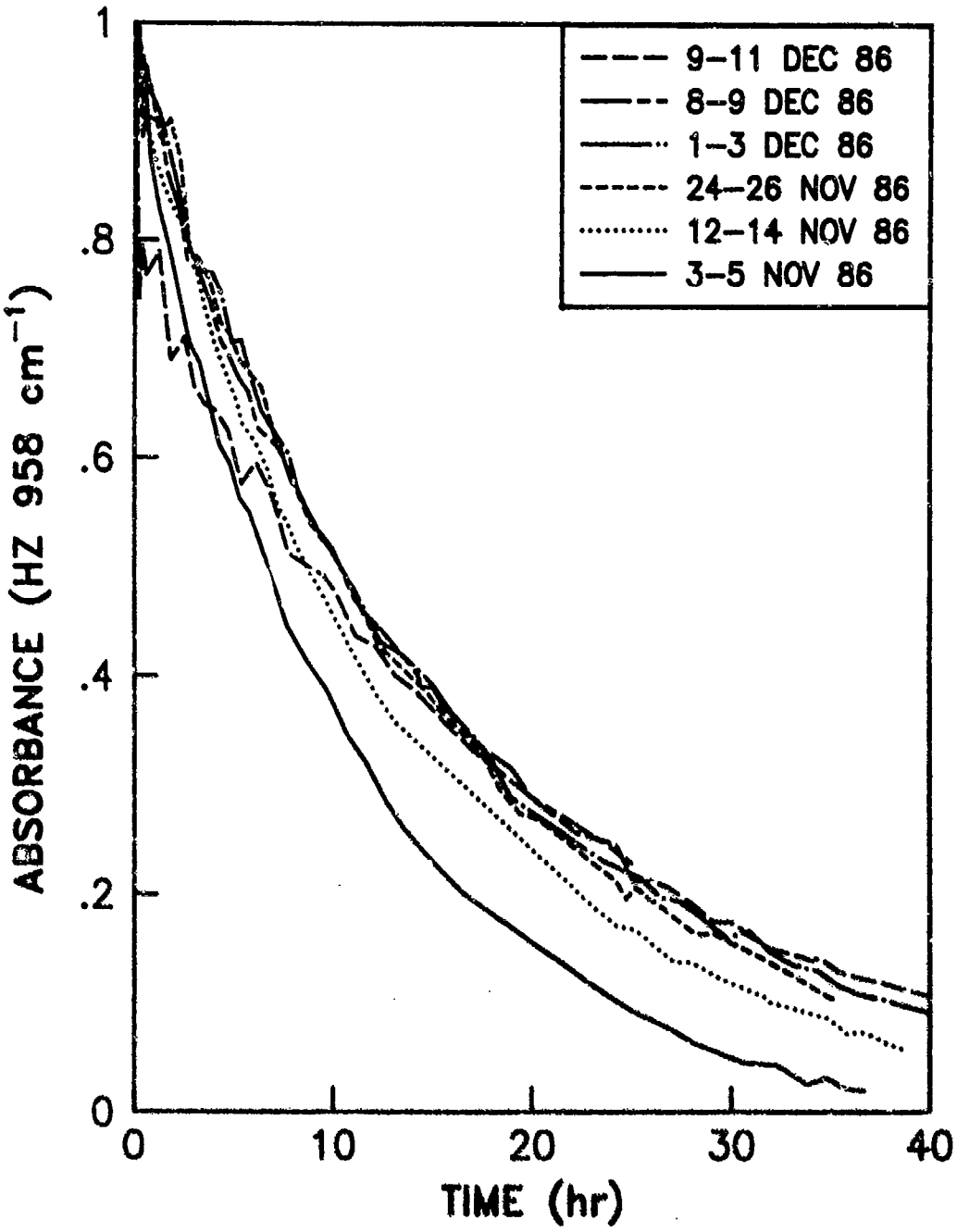

Figure 26. Plots of Hydrazine Concentration Versus Time in the Teflon Chamber (Six Sequential Runs in Dry Air).

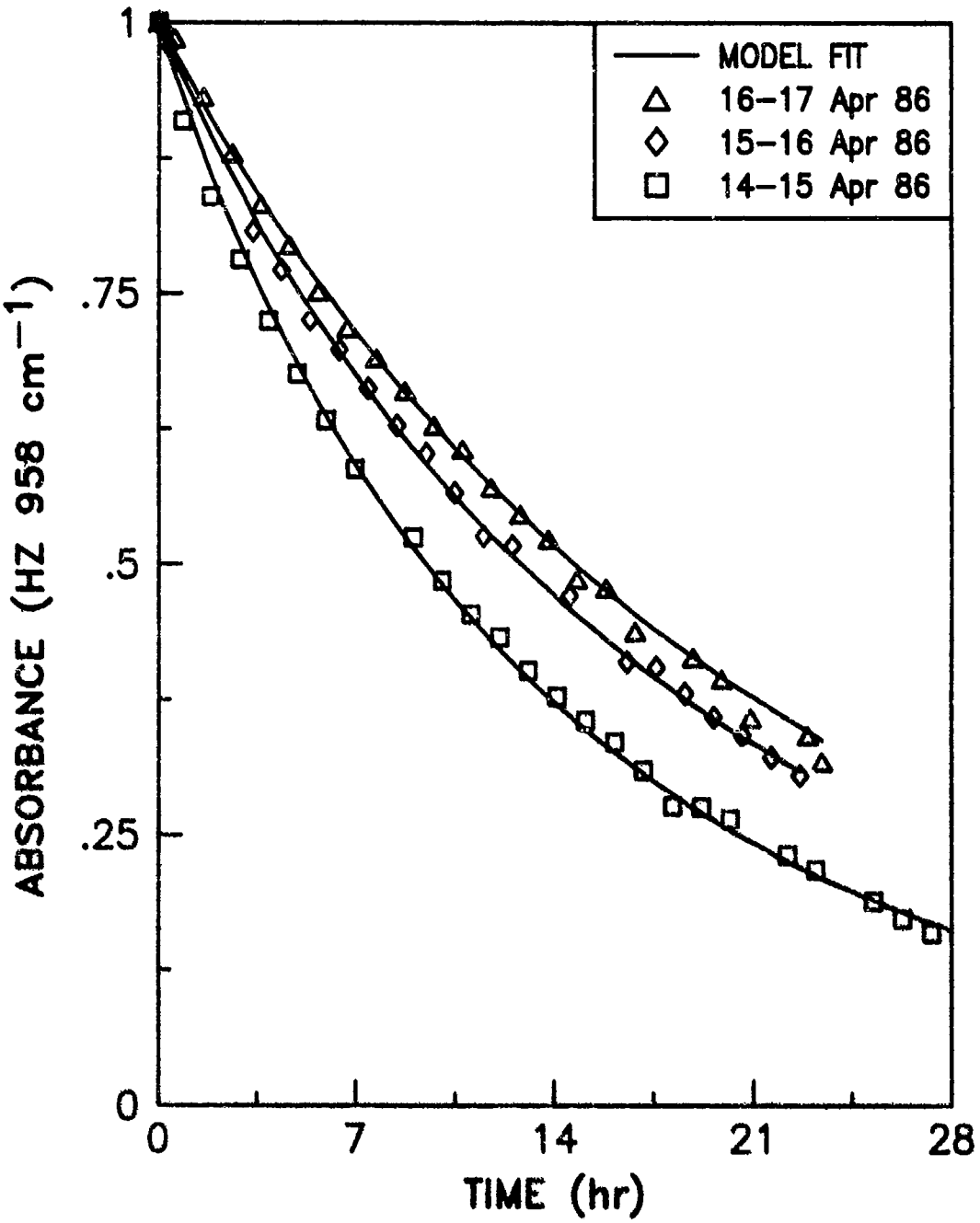

Figure 27. Effusion-Second-Order Adsorption Model Fit to a Sequential Set of Hydrazine Decay Runs in Dry Air.

TABLE 4. RESULTS OF COMPOSITE FITS OF THE EFFUSION-ADSORPTION MODEL VERSION TO SEQUENTIAL DATA SETS IN DRY AND HUMID AIR.*

Date of Run	Conditions	k_1	$[F_1]_o$	k_{-1}	k_e	SOS
14-18 Apr 86	Dry Air	.088(.004)	.44(.02)	.002(.001)	.0442(.0003)	.006
3 Nov - 3 Dec 86	Dry Air	.101(.007)	.63(.04)	$8(2) \times 10^{-4}$	.057(.001)	.018
21 Apr 86	50% humidity in air	1.44(.09)	.326(.009)	.046(.009)	.187(.002)	.001
10 Feb 87	60% humidity in air	1.4(.2)	.37(.04)	.24(.04)	.381(.009)	.003

*This version has been adapted to account for conditioning. The parameters are in the following units: k_1 - $hour^{-1} \cdot Au^{-1}$, $[F_1]_o$ - Au, k_{-1} and k_e - $hour^{-1}$ (Au = absorbance units).

after the third run, causing the half-lives for Runs 4 and 5 to be nearly the same.

Run 6 was conducted by adding hydrazine to Run 5 at the 24-hour point. The resulting decrease in half-life is somewhat misleading. A better understanding of the situation in this run is obtained by looking at the shape of the decay curve in Figure 26. The model predicted that the decay curve for this final run would lie just a little above that of Run 5. Instead, Run 6 began to decay more rapidly than any of the previous runs but then ended up with slower decay beyond about the 30-hour point. The explanation for this decay pattern is not known.

There was no readily observable difference between the runs conducted in dry nitrogen and the first group of those conducted in dry air. Succeeding groups in dry air showed decay half-lives which increased to an essentially constant level. No such experiments were conducted with dry nitrogen because of the large quantities required for continuous purging. If a difference between oxygen and nitrogen decay rate is to be observed in this particular chamber, it would probably require that long-term successive-addition hydrazine decay runs be made in a dry nitrogen atmosphere.

3. Hydrazine in Humid Nitrogen

Only a single experimental run was conducted under these conditions. The decay curve is shown in Figure 28. Several observations were noted in this system. First, the decay curve is not pseudo-first-order. (Figure 29 shows results of a first-order fit and the permeation version fit). Second, the decay rate is much more rapid, giving an approximate half-life of about 3.3 hours. Third, there is a fairly significant amount of NH_3 produced, about 4 ppm.

The explanation for the dramatic differences in the decay curves for this system versus the hydrazine-dry nitrogen system appears to lie in the ability of hydrazine to readily adsorb onto wetted Teflon film, just as in the case of humid air. In all likelihood, all of the "active sites" (both

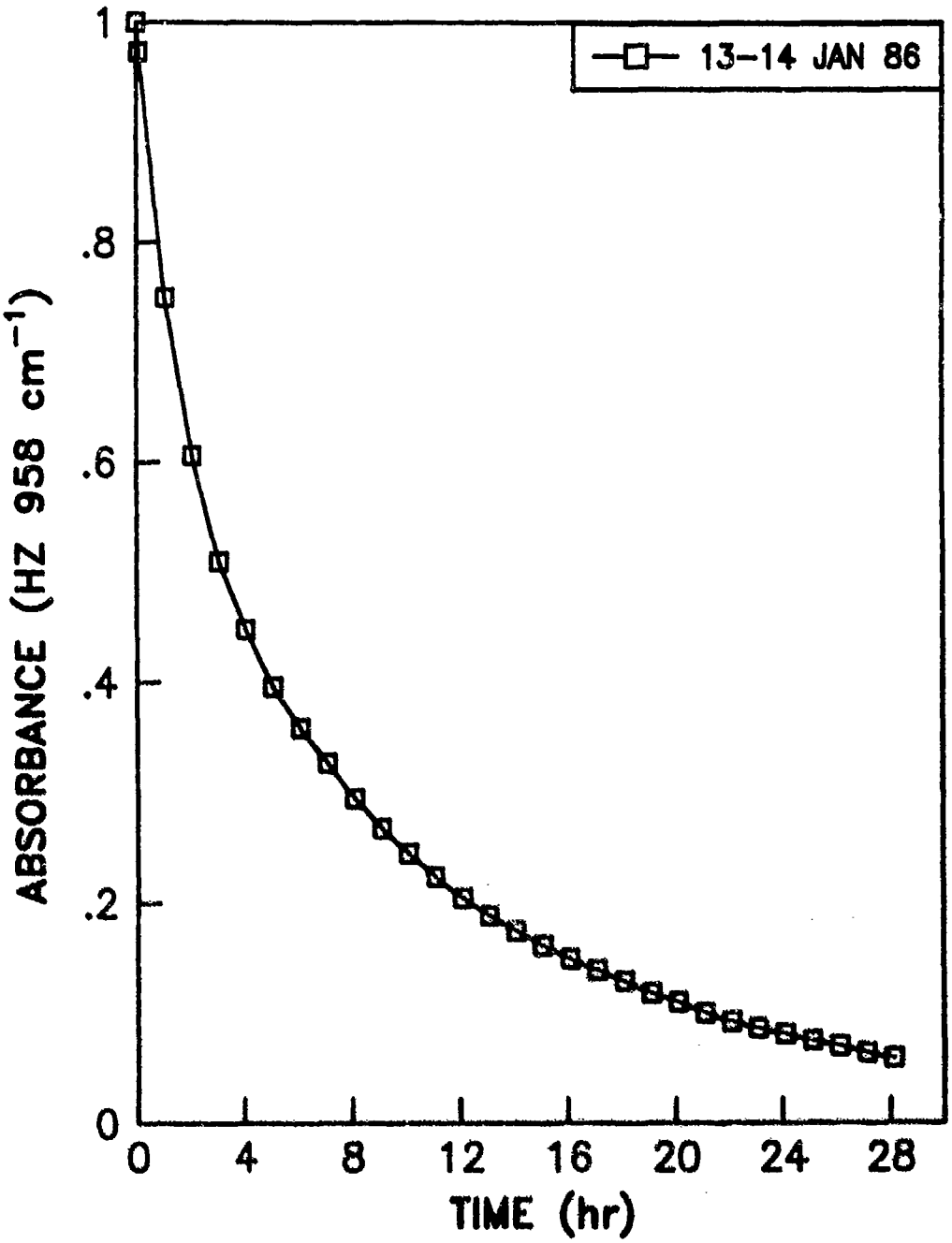

Figure 28. Plot of Hydrazine Concentration Versus Time in the Teflon Chamber (In Humid Nitrogen).

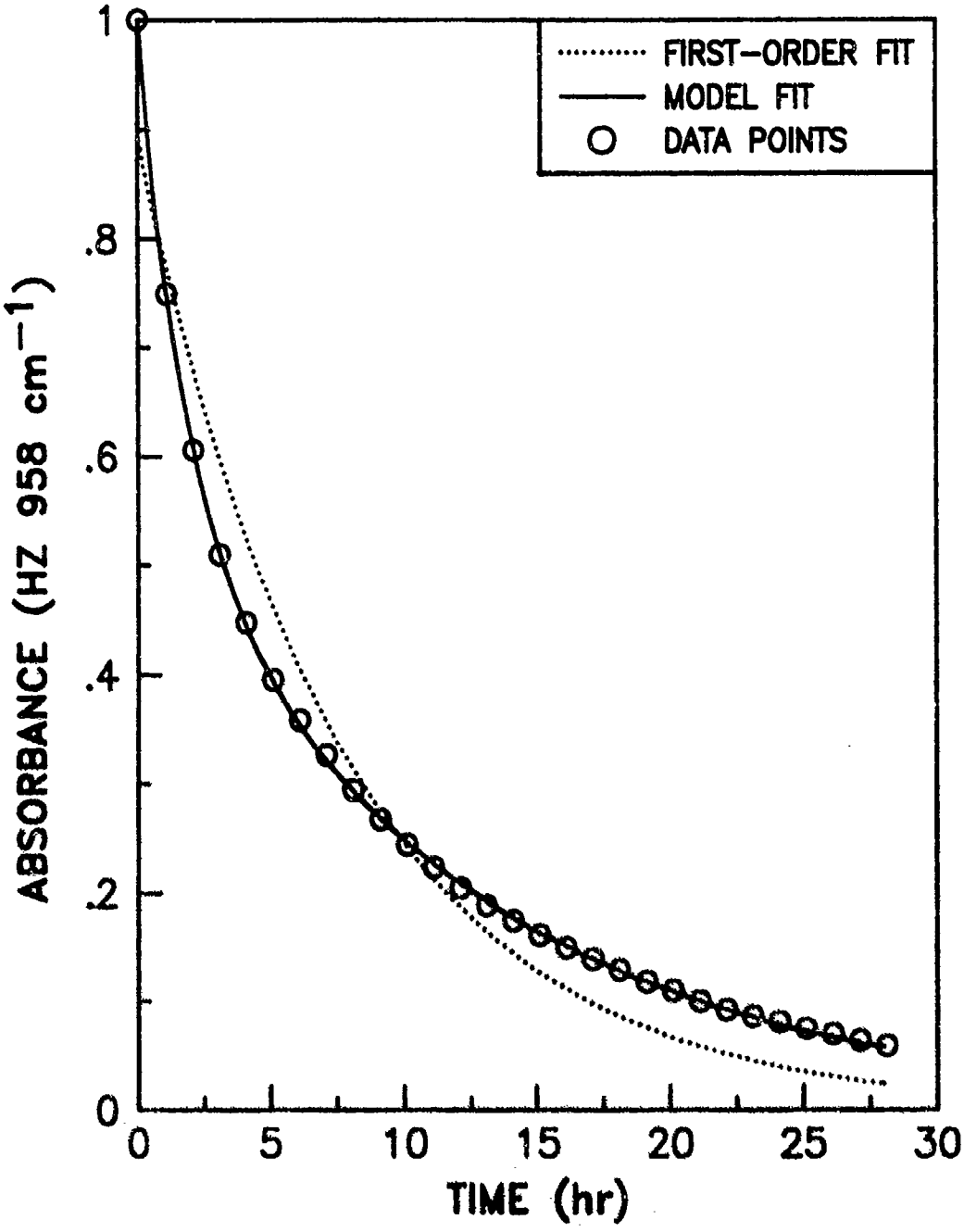

Figure 29. First-Order and Permeation Model Fits to Hydrazine Decay Data in Humid N_2.

surface sites and microvoids in the film itself) on the Teflon chamber surface are occupied by water when the hydrazine is added. As the hydrazine molecules strike the surface of the chamber, they encounter these adsorbed water molecules or microdroplets and stick. The presence of the adsorbed water apparently exerts a catalytic effect on the trapped hydrazine, causing the formation of small quantities of NH_3.

4. Hydrazine in Humid Air

A total of 12 runs were completed in humid air. The first two were conducted in sequences of runs involving several experimental conditions. The next four were run as a series with no purging of the chamber between them. The last six were conducted after 6 weeks of purging the chamber with humid air (with the mixing fan on a 30-minutes-off, 2-minutes-on cycle) and the Plexiglas box with humid air. This was designed to give conditions approximating those which would be found in a new Teflon bag which had been conditioned with water vapor. The first two runs in the sequential data sets were fitted using the effusion-adsorption version adapted for conditioning and results are given in Table 4. The dates and half-lives of these runs are shown in Table 5. Plots of typical data sets are shown in Figures 30 and 31 (decay curves are normalized to unit absorbance).

The 30 Oct 85 run was the first one in the 5-mil Teflon chamber involving high humidity. In this case, room air, measured at 74 percent relative humidity, was used. However, this run was preceded by a hydrazine run in dry nitrogen on 28 Oct and a hydrazine-conditioning run (i.e., an injection of four times the regular amount of hydrazine) on 29 Oct. Apparently the high-humidity room air negated the expected conditioning effects of the two preceding runs, resulting in the very short half-life observed in the 30 Oct experiment. Model fits on humid runs show that desorption is greatly enhanced in humid conditions (see Table 4).

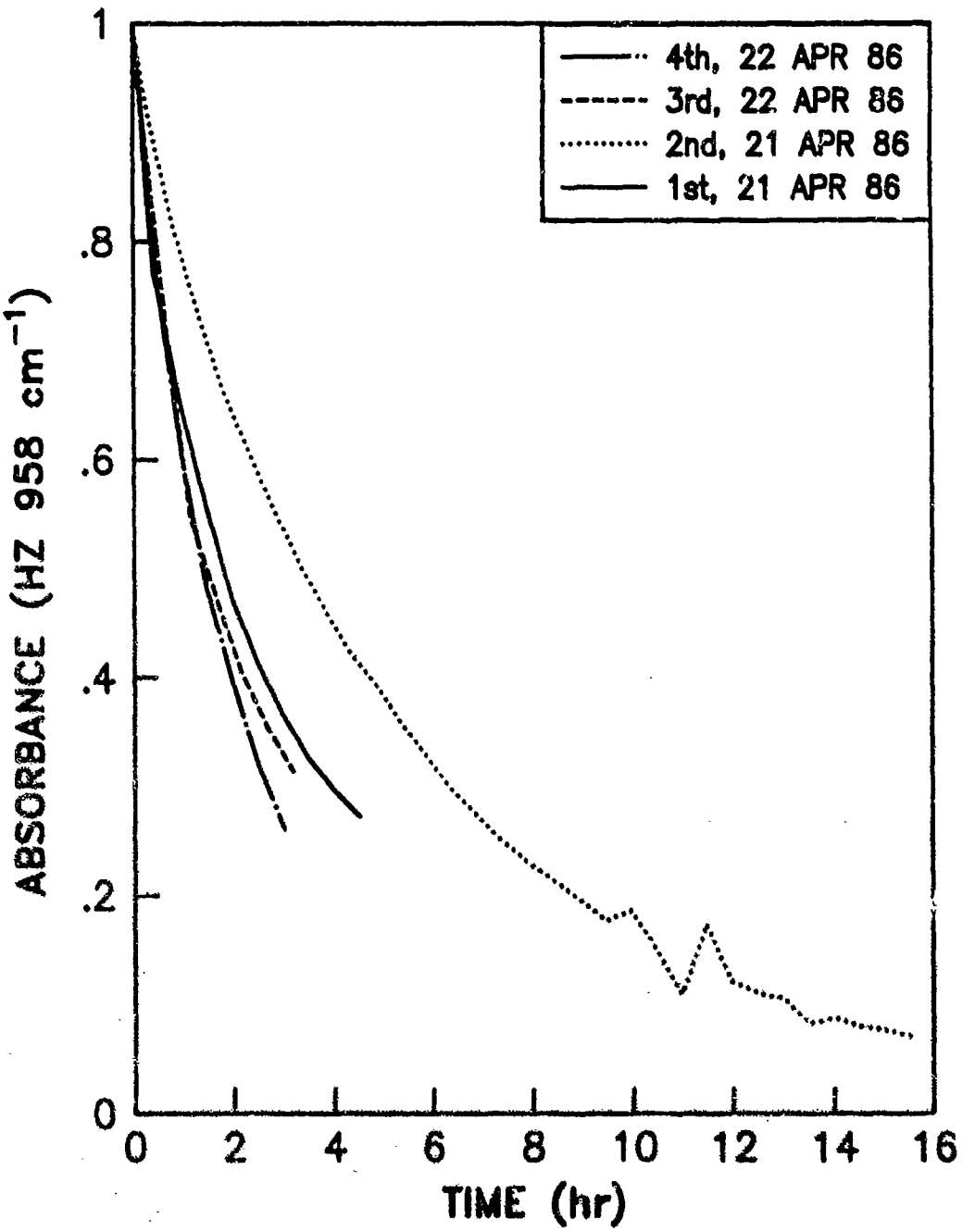

Figure 30. Plots of Hydrazine Concentration Versus Time in the Teflon Chamber (Four Sequential Runs in Humid Air).

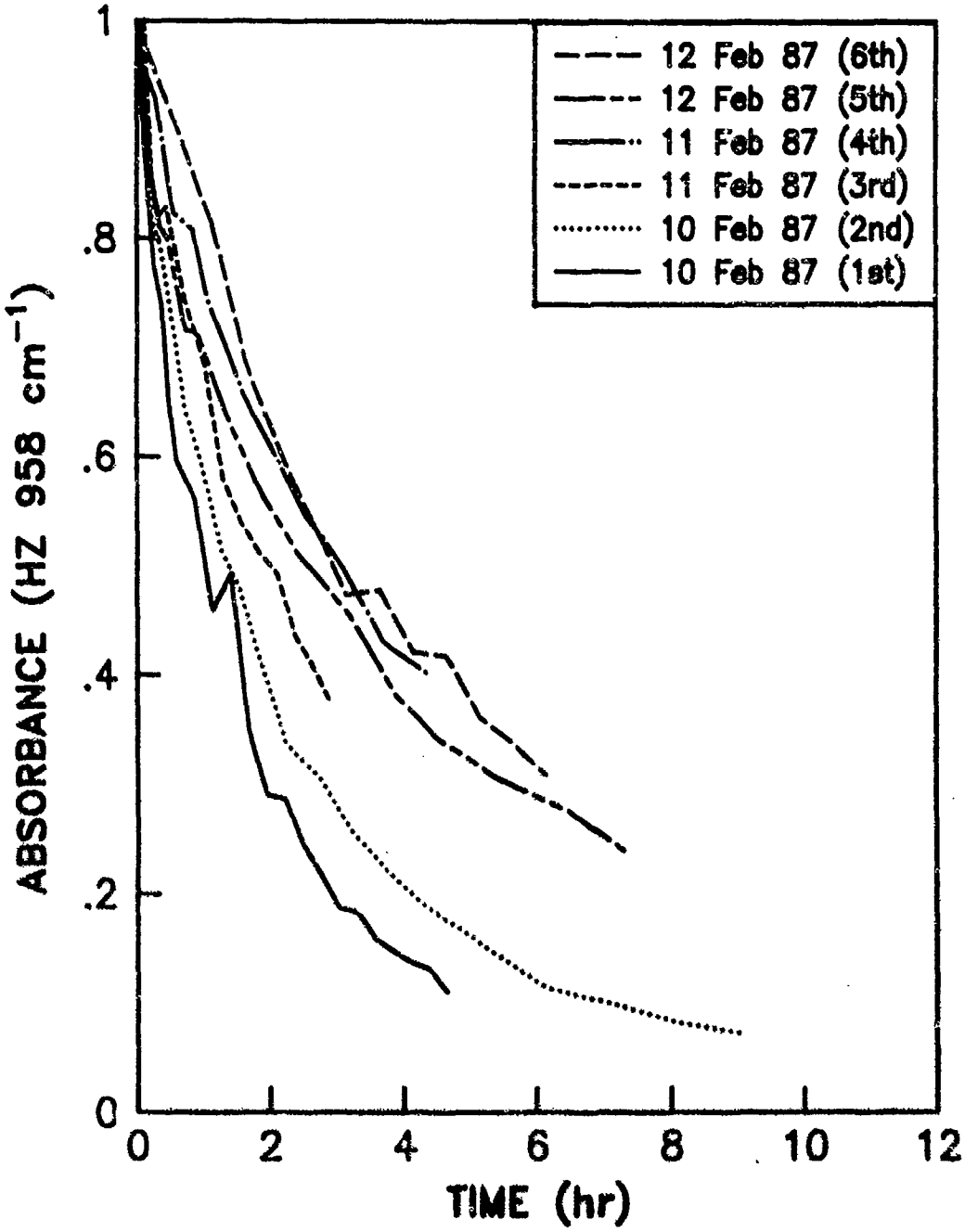

Figure 31. Plots of Hydrazine Concentration Versus Time in the Teflon Chamber (Six Sequential Runs in Humid Air).

TABLE 5. HYDRAZINE DECAY IN HUMID AIR

Date of Run	Half-Life (hours)
30 Oct 85	1.0
6-7 Jan 86	1.5
21 Apr 86 (1)*	1.8
21 Apr 86 (2)	3.3
22 Apr 86 (1)	1.5
22 Apr 86 (2)	1.5
10 Feb 87 (1)	1.0
10 Feb 87 (2)	1.3
11 Feb 87 (1)	2.1
11 Feb 87 (2)	3.1
12 Feb 87 (1)	2.7
12 Feb 87 (2)	3.0

*Denotes first run on this date, etc.

The 6-7 Jan 86 run was the 13th to be made in the 5-mil Teflon chamber. The previous 12 runs had little conditioning effect, as evidenced by the 1.5 hour half-life of the 6-7 Jan run. The humidity source in this run was pure air bubbled through distilled water. The humidity level was lower, about 40 percent, and the temperature of the room was unusually low, 16 ^{o}C.

The four sequential experiments conducted on 21 and 22 Apr 86 were made at about 50 percent relative humidity. There was an increase in half-life from the first run made on 21 Apr to the second run made on that same day. However, when the next run was made on 22 Apr, the half-life decreased by 50 percent, indicating rapid desorption. The final run on 22 Apr showed a slight further decrease in half-life. As in the high humidity run conducted in nitrogen, there was an approximately fourfold increase in ammonia

production in these experiments, compared with hydrazine decay in dry air. Figure 32 shows fits of the effusion-adsorption version to the first two runs in this sequence.

The final six sequential experiments conducted on 10-12 Feb 87 were run at about 60 percent humidity. Humidity variations during each experiment were less than 2 percent, except for the final two runs, where the humidity decreased about 8 percent over the course of the run. The first four experiments showed an expected increase in half-life as the chamber became conditioned by the hydrazine.

The possibility that the rapid loss of hydrazine in both humid nitrogen and humid air runs could be due to association of hydrazine with water in the vapor phase to form hydrazine hydrate was also considered. However, infrared spectra in either system show no absorbance features which cannot be accounted for in terms of hydrazine or water. This finding is supported by an early study of Coulter (Reference 23), who also found no spectroscopic evidence for hydrazine hydrate formation. Hence, hydrazine surface adsorption is most likely being enhanced under humid conditions. This being the case, the effusion-adsorption model version modified for conditioning closely describes what is actually occurring.

D. CONCLUSIONS

Experimental and modeling results show that gaseous hydrazine is not oxidizing at ambient conditions, but interacting strongly with surfaces in the Teflon chamber environment. The model described in this report takes into account all types of elementary reactions and surface interactions. Different versions of the model have been used to fit data runs. The most accurate version seems to be the effusion-adsorption version that allows for second-order rather than first-order adsorption. The sequential data sets show a conditioning effect aptly described by second-order adsorption. Binding sites become almost full after the second or third run in a

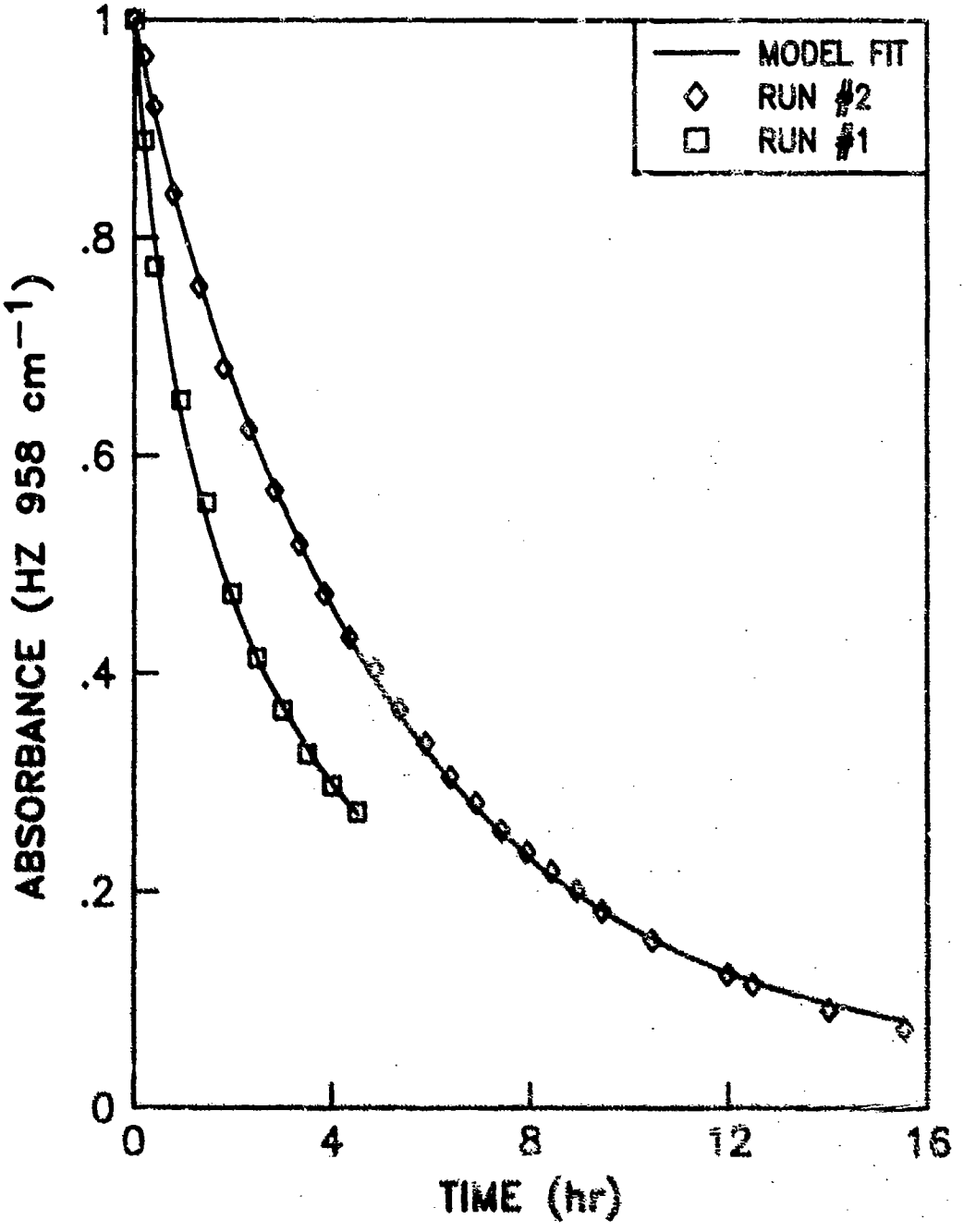

Figure 32. Effusion-Second-Order Adsorption Model Fit to a Sequential Set of Hydrazine Decay Runs in Humid Air (Both Runs Were Done the Same Day).

sequential set of runs in dry conditions. Of course, this process is reversible, so that the chamber can be deconditioned.

Table 4 shows results of the effusion-adsorption model version fits to sequential sets in dry and humid conditions. The reproducibility of the fitting parameters, k_1 and $[F_1]_o$, is good for the two dry runs and the two humid runs. The reproducibility of k_{-1} is not as good. This parameter may vary strongly with humidity and temperature. This seems to be the case, because there is a difference in the values of k_{-1} for the 50 percent and 60 percent humidity runs. The parameter, k_e, varies in the model fits for humid runs as well. Again, this parameter also appears to be sensitive to environmental conditions, which implies that k_e does not just represent effusion, but steady-state permeation, which no doubt is somewhat sensitive to humidity.

Interestingly, k_1, k_{-1}, and k_e increase substantially with humidity. That k_1 and k_e increase implies that hydrazine has a stronger affinity for a wetted surface. However, that k_{-1} increase shows that adsorbed hydrazine comes off the surface sites more easily in humid conditions. This may imply that with the wetted surfaces inside the chamber, hydrazine is binding more to the water molecules rather than the surface sites. Whereas the hydrazine has a strong affinity for wetted surfaces, it apparently binds more tightly with the dry surface. This can be described by a physical process in which hydrazine is becoming trapped in the structure of the surface, requiring more activation energy for adsorption. In terms of energetics, the adsorption and desorption activation energies are lower for wetted surfaces, as illustrated by Figure 33. This makes both k_1 and k_{-1} larger for humid conditions. That k_{-1} is much larger in humid conditions shows that deconditioning can be greatly expedited by flushing the chamber with humid air. This is reflected in Table 5 by the fact that allowing the chamber to be filled with humid air overnight essentially deconditions the chamber. Otherwise, using dry air for purging would require a few weeks of purging to decondition the chamber. The half-life for deconditioning in dry air is about 3 weeks, whereas in 60 percent humid air, the half-life for deconditioning is 3 hours. As might be expected, $[F_1]_o$ is slightly

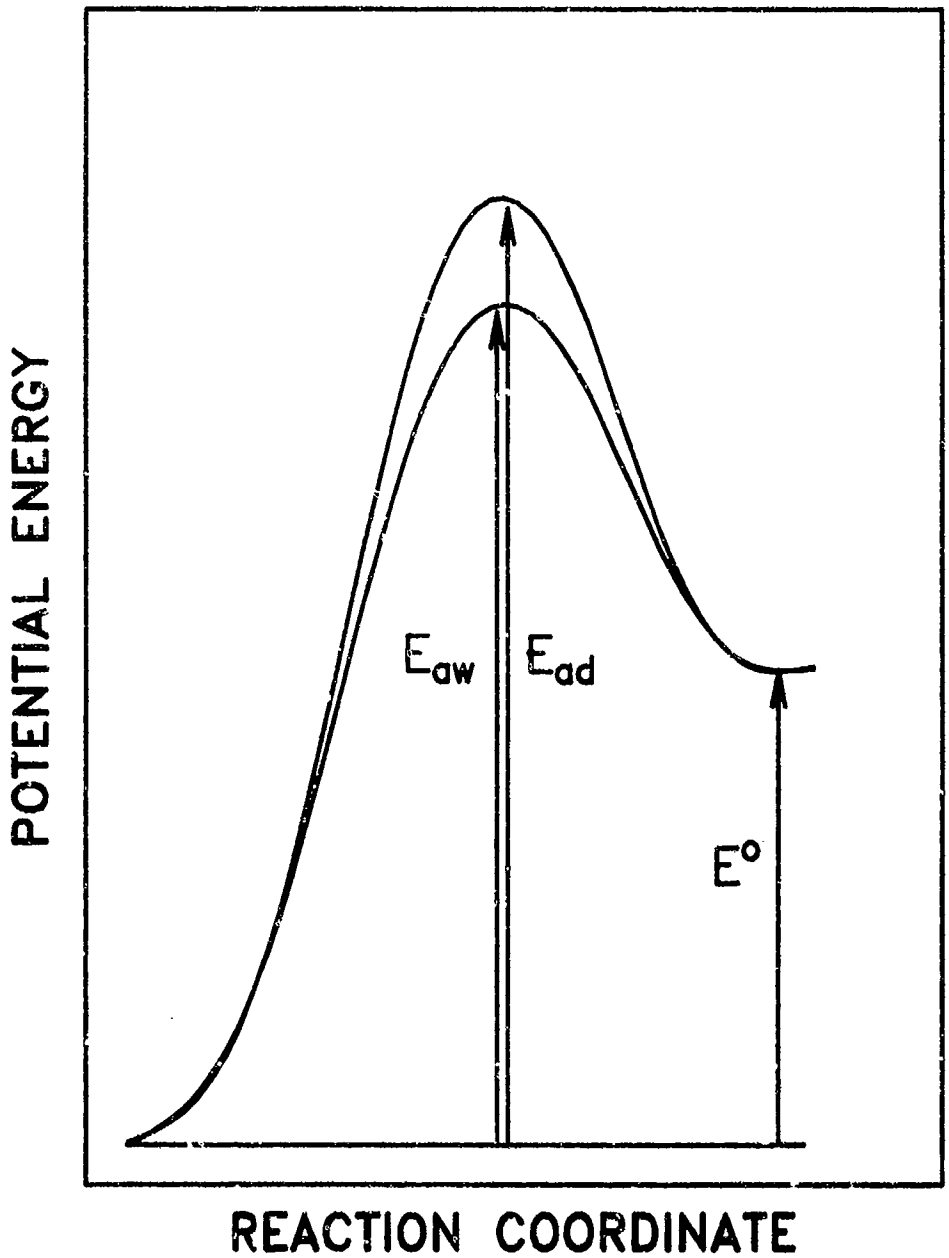

Figure 33. Diagram Showing the Decrease in the Activation Energies for Adsorption and Desorption in Wet Conditions (E_{aw}) Compared to Dry Conditions (E_{ad}).

less in humid conditions, implying, of course, that the water molecules are occupying the sites otherwise available for the hydrazine.

The fitted values of $[F_1]_o$, in units of absorbance, can be multiplied by an appropriate conversion factor to render the number of active sites per unit area of Teflon film, provided the Teflon film is the most important source of sites. Given the following values: Teflon surface area - 2.5 meter^2, and approximate conversion between hydrazine absorbance and number of moles - 3.8×10^{-5} mole·Au^{-1} (Au = absorbance units); the number of sites per unit area can be calculated to be .05 Å^{-2}. The reciprocal of this is 20 Å^2. For humid conditions, this number increases to 31 Å^2, in good agreement with the value of 23 Å^2 found by Hayes* for the adsorption of hydrazine hydrate on certain soil components. Of course, there are other surfaces present, such as the mirrors, which also seem to provide adsorption sites.

The value for the parameter, $k_s[S]$, from the permeation model version does increase slightly for the run with the additional 2-mil sheets added (Table 4). However, $k_s[S]$ is significantly larger for the run with the mirrors added. Although the permeation version is not an accurate model version, the fact that $k_s[S]$ is larger is significant. Interactions of hydrazine with surfaces other than Teflon also seem likely in light of the fact that ammonia is produced. It is unlikely that the N-N bond rupture required to form NH_3 will occur either in the gas phase or on Teflon surfaces. Also, the fact that NH_3 production is increased in humid conditions lends support that catalysis on surfaces, unlikely to be Teflon, is occurring, since initial surface adsorption is increased in humid conditions. Moreover, the degree of NH_3 production is insensitive to oxygen content, giving further evidence that hydrazine is adsorbed, or perhaps even chemisorbed, onto a surface which is able to rupture the N-N bond, again unlikely to be Teflon.

---

*Private Communication

Of all gases studied, hydrazine, water, and O_2 are the only gases which seem to interact strongly with Teflon film, evidenced by rapid changes in gas concentration. Gases chemically similar to hydrazine, such as methanol and NH_3, surprisingly do not interact as strongly. Moreover, the molecular size does not correlate with loss rates as indicated by the near identical behavior of CH_4 and SF_6. The exact chemical or physical nature of the interactions of these gases with Teflon is not known at present. However, it is apparent that surface interactions and physical loss processes are the most important loss processes of gaseous hydrazine in Teflon chambers at ambient conditions.

(The reverse of this page is blank.)

REFERENCES

1. Sotaniemi, E., Hirvonen, J., Isomaki, H., Takkunen, J., and Kaila, J., "Hydrazine Toxicity in the Human: Report of a Fatal Case," Annals of Clin. Res., 3, 30-33, 1971.

2. Back, K. C. and Thomas, A. A., "Aerospace Problems in Pharmacology and Toxicology," Ann. Rev. Pharmacol., 10, 395-412, 1970.

3. Hannum, J. A. E., ed., Hazards of Chemical Rockets and Propellants, Volume III, Liquid Propellants, Chemical Propulsion Information Agency, CPIA Publication 394, The Johns Hopkins University, Applied Physics Laboratory, Laurel, MD, September 1984.

4. Bowen, E. J. and Birley, A. W., "The Vapour Phase Reaction between Hydrazine and Oxygen," Trans. Faraday Soc., 47, 580-583, 1951.

5. Winning, W. I. H., "The Thermal Oxidation of Hydrazine Vapour," J. Chem. Soc., 926-931, 1954.

6. Stone, D. A., The Autoxidation of Hydrazine Vapor, CEEDO-TR-78-17, Civil and Environmental Engineering Development Office, Tyndall AFB, FL, January 1978.

7. Stone, D. A., The Autoxidation of Monomethylhydrazine Vapor, ESL-TR-79-10, Air Force Engineering and Services Center, Tyndall AFB, FL, April 1979, pp. 39-42.

8. Bellerby, J. M., The Autoxidation of Hydrazine and Alkyl Substituted Hydrazine Vapours, Memorandum 92, Propellants, Explosives and Rocket Motor Establishment. Westcott, Aylesbury, Bucks. May 1980.

9. Bellerby, J. M., The Effect of Reaction Vessel Surfaces on the Vapour Phase Autoxidation of Hydrazines at Ambient Temperature, Memorandum 117, Propellants, Explosives and Rocket Motor Establishment. Westcott, Aylesbury, Bucks. August 1980.

10. Moody, K. N., The Vapour Phase Oxidation of Hydrazine, Ph.D. Thesis, The University of Leeds, April 1985.

11. Pitts, J. N., Jr., Tuazon, E. C., Carter, W. P. L., Winer, A. M., Harris, G. W., Atkinson, R., and Graham, R. A., Atmospheric Chemistry of Hydrazines: Gas Phase Kinetics and Mechanistic Studies, ESL-TR-80-39, Air Force Engineering and Services Center, Tyndall AFB, FL, August 1980.

12. Tuazon, E. C., Carter, W. P. L., Brown, R. V., Atkinson, R., Winer, A. M., and Pitts, J. N., Jr., Atmospheric Reaction Mechanisms of Amine Fuels, ESL-TR-82-17, Air Force Engineering and Services Center, Tyndall AFB, FL, March 1982.

13. Naik, D. V. and Stone, D. A., Air Oxidation of Hydrazine - A Kinetic Study, Final Report, USAF-SCEEE Summer Faculty Research Program, Tyndall AFB, FL, September 1984.

14. Stone, D. A., Henley, M. V., and Naik, D. V., The Effects of Surfaces on the Air Oxidation of Hydrazine, Chemical Propulsion Information Agency Publication No. 436, November 1985, pp. 151-159.

15. Lin, S. F., The Decay of Hydrazine in Air, Final Report, USAF-SCEEE Research Initiation in Science Program, North Carolina Central University, Durham, NC, January 1985.

16. Naik, D. V., Kinetics of Homogeneous Gas Phase Oxidation of Hydrazine in Air, Final Report, USAF-SCEEE Research Initiation in Science Program, Monmouth College, West Long Branch, NJ, March 1986.

17. Horn, D. and Pimentel, G. C., "2.5-km Low-Temperature Multiple-Reflection Cell", Appl. Opt., 10, 1892, (1971).

18. Johnson, B. A., Macros for Net Absorbance Measurement, FT-IR Spectral Lines, Vol. II, No. 1, pp. 8-9, March 1980, Nicolet Instrument Corp., Madison, WI.

19. Crank, J. and Park, G.S., Diffusion in Polymers, Academic Press, Inc., 1968, Chapter 2.

20. Aueyard, R. and Hajden, D.A., An Introduction to the Principles of Surface Chemistry, Cambridge University Press, 1973, Chapter 5.

21. Cotton, F. A. and Wilkinson, G., Advanced Inorganic Chemistry, Interscience Publishers, New York, 1966, p.335.

22. Teflon Film, Bulletin E-67603, E.I. du Pont de Nemours & Co., Inc., Polymer Products Dept., Wilmington, DE, Table 7, p. 14.

23. Coulter, L.V., "The Native of the Vapor State of Hydrazine Monohydrate and Ethylenediamine Monohydrate", J. Chem. Soc., 3505 (1951).

APPENDIX A

LISTING OF MACRO PROGRAM (AND SUB-MACRO PROGRAMS) TO AUTOMATICALLY ACQUIRE, PROCESS, STORE, PRINT AND PLOT FT-IR DATA

This program is called TS3. It was written in the Nicolet MACRO language by using the TED editor and then compiling with the Nicolet utility program MACCRT. This procedure allows remarks to be included in the program for documentation and user assistance.

The main MACRO program (TS3) calls several SUB-MACRO programs. Most of these were written and compiled as subsections of TS3. Each program ends with the statement END. Each new program begins with "!" followed by the program name.

```
!TS3                \MACRO TO ACQUIRE, PRINT, AND PLOT SPECTRA
                    \AUTOMATICALLY
BFN
DFN
NSD
OMD
============================================================
OMD
SELECT BEGINNING AND ENDING FREQUENCIES FOR PPK, REGION 1
VI0
VI1
THR=0.005
OMD
SELECT BEGINNING AND ENDING FREQUENCIES FOR PPK, REGION 2
VI2
VI3
OMD
------4 INITIAL, SHORTER INTERVAL SPECTRA WILL BE ACQUIRED
OMD
ENTER THE DELAY TIME (MIN) BETWEEN THESE INITIAL SPECTRA
VF1
OMD
---THE REMAINING SPECTRA WILL BE ACQUIRED AT A LONGER INTERVAL
TSX
END
                    \\\\\\\


!TSX                \MACRO TSX:  (TS3 WAS TOO LONG, TSX IS
                    \THE 2ND PART)
OMD
ENTER THE DELAY TIME (MIN) BETWEEN REMAINING SPECTRA
VF0
OMD
```

```
====================
OMD
PRESS "RETURN" TO BEGIN
OMD
====================
PAU
CSN=0                \SET THE DUMMY VARIABLE CSN TO ZERO
ISS                  \RUN THE SUB-MACRO ISS
CSN=0                \SET THE DUMMY VARIABLE CSN TO ZERO
TSS                  \RUN THE SUB-MACRO TSS
END


!ISS                 \SUB-MACRO TO ACQUIRE, PROCESS AND PLOT THE
                     \FIRST 4 SPECTRA
                     \
CSN=17               \SET DUMMY VARIABLE FOR UPCOMING CMR COMMAND
FOR BBB=1 TIL 4
AQ2                  \SUB-MACRO TO ACQUIRE, PROCESS AND PRINT DATA
CMP=CSN              \SET CONDITIONAL MACRO PARAMETER FOR EACH PLOT
CMR
DFN=DFN+1
CSN=CSN+1
DL1                  \SUB-MACRO TO EXECUTE SOFTWARE TIME DELAY
NXT BBB
END


!DL1                 \SUB-MACRO TO GIVE TIME DELAY FOR INITIAL 4
                     \SPECTRA IN "TS3"
OMD
            ==================================
OMD
            =                                =
OMD
            =      DELAY IN PROGRESS         =
OMD
            =                                =
OMD
            ==================================
DCL=204445           \SET NEW DISPLAY COLORS
DCX                  \CHANGE DISPLAY TO NEW COLORS
FOR III=1 TIL VF1
FOR AAA=0 TIL 60000            \LOOP TO DELAY FOR 1 MIN
NXT AAA
NXT III
DCL=210414           \RETURN COLORS TO DEFAULT VALUES
DCX                  \EXECUTE COLOR CHANGE
END
```

```
!M17                    \SUB-MACRO TO PLOT UPPER LEFT SPECTRUM
                        \PART OF TS3
                        \

XSP=VF2
XEP=VF3
PLO=100
ZPN
XPN=1
YPN=5.5
PEN
XSL=3
YSL=4
PAG=NO
TIT=NO
PLS
XPN=.5
YPN=4.5
PEN
PON
PRN DFN
STD
POF
END


!M18                    \SUB-MACRO TO PLOT UPPER RIGHT SPECTRUM
                        \PART OF TS3

XSP=VF2
XEP=VF3
XPN=3.5
YPN=-4.5
PEN
PLS
XPN=.5
YPN=4.5
PEN
PON
PRN DFN
STD
POF
ZPN
XPN=-4.5
PEN
ZPN
END


!M19                    \SUB-MACRO TO PLOT LOWER LEFT SPECTRUM
                        \PART OF TS3
```

```
XSP=VF2
XEP=VF3
PLS
XPN=.5
YPN=4.5
PEN
PON
PRN DFN
STD
POF
XPN=3.5
YPN=-4.5
PEN
END


!M20                    \SUB-MACRO TO PLOT LOWER RIGHT SPECTRUM
                        \PART OF TS3
XSP=VF2
XEP=VF3
PLS
XPN=.5
YPN=4.5
PEN
PON
PRN DFN
STD
POF
ZPN
XPN=3
PEN
ZPN
END


!TSS                    \SUB-MACRO TO COMPLETE DATA ACQUISITION
                        \AND HARD COPY OUTPUT FOR "TS3"
                        \
FOR AAA=1 TIL 100       \LOOP TO ACQUIRE AND PROCESS 100 FILES
CSN=17
FOR CCC=1 TIL 4         \LOOP TO ACQUIRE, PROCESS, PRINT AND
                        \PLOT 4 SPECTRA
AQ2                     \SUB-MACRO TO ACQUIRE AND PRINT DATA
CMP=CSN
CMR
DFN=DFN+1
CSN=CSN+1
DL2                     \SUB-MACRO TO EXECUTE THE DESIRED DELAY
                        \BETWEEN SETS OF SCANS
NXT CCC
```

```
NXT AAA
END


!DL2                \SUB-MACRO TO EXECUTE THE DESIRED DELAY
                    \BETWEEN SETS OF SCANS
                    \PART OF TS2
OMD
                   ========================================
OMD
                   =                                      =
OMD
                   =          DELAY IN PROGRESS           =
OMD
                   =                                      =
OMD
                   ========================================
DCL=204445
DCX
FOR III=1 TIL VF0
FOR AAA=0 TIL 60000
NXT AAA
NXT III
DCL=210414
DCX
END
!!
```

The SUB-MACRO AQ2 was written and compiled separately and is listed below.

```
!AQ2                \SUB-MACRO TO ACQUIRE, DO A PPK AND PRINT PPK VALUES
                    \
TEM=4               \SET TEM TO TOGGLE PRINTER ON
NPR                 \TURN ON PRINTER
SCD
PRN DFN
STD
SFN=2
RFN=DFN
OFN=DFN
MOS
RAS
ABS
DFN=SFN
XSP=VI0
XBP=VI1
PPK
XSP=VI2
```

```
XEP=VI3
PPK
OMD
-------------------------------------------------------------------------------
DFN=RFN
XSP=4000
XEP=400
YSP=-.1
YEP=1.1
DSS
TEM=4                   \SET TEM TO TOGGLE PRINTER OFF
NPR                     \TURN PRINTER OFF
END
!!
```

APPENDIX B

LISTING OF MACRO PROGRAM (AND SUB-MACRO PROGRAMS) TO CALCULATE BASELINE-CORRECTED ABSORBANCE VALUES FOR HYDRAZINE, METHANE AND SULFUR HEXAFLUORIDE

This program is called MPK. It was written in the Nicolet MACRO language by using the TED editor and then compiling with the Nicolet utility program MACCRT. This procedure allows remarks to be included in the program for documentation and user assistance.

The main MACRO program (MPK) calls several conditional MACRO programs which were written and compiled as subsections of MPK. Each program ends with the statement END. Each new program begins with "!" followed by the program name. The final program in the series is terminated with "!!" after its END statement.

This listing also includes the FORTRAN program BASE1, which is called by the MACRO during the baseline correction routine.

```
!MPK                \MACRO TO MEASURE NEW ABSORBANCE BY CHOOSING A
                    \BASELINE FOR EACH ANALYTICAL BAND FOR EACH SPECIES
                    \
OMD
CHOOSE SPECIES TO BE ANALYZED:        HYDRAZINE = 30
OMD
                                        METHANE = 31
OMD
                                            SF6 = 32
CMP
OMD
ENTER BACKGROUND FILE NO. FOR THIS ANALYSIS
BFN
OMD
ENTER BEGINNING FILE TO BE ANALYZED
DFN
OMD
ENTER NO. OF FILES TO BE ANALYZED
QIT
QIT=QIT+DFN
SRT=DFN
SFN=2
FOR XXX=SRT TIL QIT
RAD
ABD
ASD
OMD
FILE CURRENTLY BEING ANALYZED IS:
PRN DFN
```

```
DSD
CMR
DFN=DFN+1
NXT XXX
END


!M30                \CONDITIONAL MACRO, PART OF MPK
                    \THIS MACRO DETERMINES THE BASELINE AND NET
                    \ABSORBANCE FOR HYDRAZINE AT ~958 CM-1
OMD
BASE1 FREQ=DBB= 1170 CM-1 (HYDRAZINE)
OMD
BASE2 FREQ=RBB=  860 CM-1 (   "    )
OMD
BASE1 ABSORBANCE=VF1, BASE2 ABSORBANCE=TBB
XSP=1180
XEP=1160
DSD
TEM=6               \TURN ON PRINTER
NPR
PAU
TEM=8               \RECORD ABSORBANCE AND FREQ. VALUES WITH CTRL-W
NPR
PAU
TEM=7               \TURN OFF CURSOR
NPR
PAU
DBB=PXA             \STORE VALUE OF PXA IN DUMMY VARIABLE DBB
VF1=PYA             \STORE VALUE OF PYA IN DUMMY VARIABLE VF1
TEM=4
NPR
XSP=860
XEP=840
DSD
TEM=6               \TURN ON CURSOR
NPR
PAU
TEM=8               \RECORD ABSORBANCE AND CM-1
NPR
PAU
TEM=7               \TURN OFF CURSOR
NPR
PAU
RBB=PXA               \STORE   NEW   PXA   VALUE   IN   DUMMY   VARIABLE   RBB
TBB=PYA
XSP=958             \SET X-AXIS VALUES TO BRACKET
XEP=957             \   THE HYDRAZINE ANALYTICAL PEAK
THR=0
PPK
```

```
OCE=PXA              \STORE NEW PXA VALUE IN DUMMY VARIABLE PXA
RAN=PYA              \STORE NEW PYA VALUE IN DUMMY VARIABLE PYA
GFN
BASE1.FTN            \CALL THE FORTRAN BASELINE CORRECTION PROGRAM
SID
FTN                  \RUN THE FORTRAN PROGRAM
TEM=4
NPR
END


!M31                 \CONDITIONAL MACRO, PART OF MPK
                     \THIS MACRO DETERMINES THE BASELINE AND NET
                     \ABSORBANCE FOR METHANE AT ~1306 CM-1
OMD
BASE1 FREQ=DBB= 1320 CM-1 (METHANE)
OMD
BASE2 FREQ=RBB= 1310 CM-1 (   "   )
OMD
BASE1 ABSORBANCE=VF1, BASE2 ABSORBANCE=TBB
XSP=1330
XEP=1310
DSD
TEM=6                \TURN ON PRINTER
NPR
PAU
TEM=8                \RECORD ABSORBANCE AND FREQ. VALUES WITH CTRL-W
NPR
PAU
TEM=7                \TURN OFF CURSOR
NPR
PAU
DBB=PXA              \STORE VALUE OF PXA IN DUMMY VARIABLE DBB
VF1=PYA              \STORE VALUE OF PYA IN DUMMY VARIABLE VF1
TEM=4
NPR
XSP=1295
XEP=1275
DSD
TEM=6                \TURN ON CURSOR
NPR
PAU
TEM=8                \RECORD ABSORBANCE AND CM-1
NPR
PAU
TEM=7                \TURN OFF CURSOR
NPR
PAU
RBB=PXA              \STORE NEW PXA VALUE IN DUMMY VARIABLE RBB
TBB=PYA              \STORE NEW PYA VALUE IN DUMMY VARIABLE TBB
```

```
XSP=1306            \SET X-AXIS VALUES TO BRACKET
XEP=1305            \   THE METHANE ANALYTICAL PEAK
THR=0
PPK
OGN=PXA             \STORE NEW PXA VALUE IN DUMMY VARIABLE PXA
RAN=PYA             \STORE NEW PYA VALUE IN DUMMY VARIABLE PYA
GFN
BASE1.FTN           \CALL THE FORTRAN BASELINE CORRECTION PROGRAM
STD
FRN                 \RUN THE FORTRAN PROGRAM
TEM=4
NPR
END


:M32                \CONDITIONAL MACRO, PART OF MPK
                    \THIS MACRO REPLACED THE BASELINE/NET ABSORBANCE
                    \METHOD (AS IN M31 AND M32) WITH THE STANDARD
                    \NICOLET INTEGRATION ROUTINE, SET TO COVER THE
                    \948 CM-1 BAND OF SF6.
OMD
INTEGRATION MACRO
SFN=2
ENTER BACKGROUND AND DESTINATION FILES
BFN
DFN
OFN=DFN
MOS
RAS
ABS
FXF=1000
LXF=900
BAS=YS
SMS
TEM=4
NPR
PRN DFN
STD
PRN FCS
TEM=4
NPR
END
```

The final listing is the FORTRAN program BASE1.FTN.

```
CCCCCCCCCCCCCCCCCCCCCCCCCCCCCCCCCCCCCCCCCCCCCCCCCCCCCCCCCCCCCCCCCCCCCCCC
C
C    PROGRAM BASE1:  TAKES ABSORBANCE AND FREQUENCY VALUES
```

```
C                    FROM FT-IR AND DOES A LINEAR INTERPOLATION
C                    TO DETERMINE NET ABSORBANCE FOR AN
C                    ANALYTICAL PEAK.
C
C234567
      REAL  DBB,VF1,OGN,RAN,RBB,TBB,VF0,VF2,VF3,VF4,FOV
C
C  RETRIEVE BASELINE AND ABSORBANCE VALUES FROM FT-IR
C  USING THE RVAL FUNCTION
C
      DBB=RVAL(6216,1)
      VF1=RVAL(6136,1)
      OGN=RVAL(6249,1)
      RAN=RVAL(6247,1)
      RBB=RVAL(6218,1)
      TBB=RVAL(6214,1)
C
C  CALCULATE NET ABSORBANCE VALUE
C
C  NET ABSORBANCE (FOV) = PEAK ABSORBANCE (RAN) - EXTRAPOLATED
C                         BASELINE ABSORBANCE (VF4)
C
C  VF4 = (VF1-TBB) X (OGN-RBB)/(DBB-RBB)
C
      VF0=ABS(TBB-VF1)
      VF3=ABS(DBB-RBB)
      VF2=ABS(DBB-OGN)
      VF4=VF2/VF3
      VF4=VF4+VF1
      FOV=RAN-VF4
C
C  PRINT OUT RESULTS IN FT-IR
C
      WRITE (2,40) FOV
   40 FORMAT (40('-'),/,' ',' PEAK ABS=',F9.3,/,40('-'),/)
C
C  RETURN TO FT-IR
C
      CALL IREXIT
      END
```

APPENDIX C

LISTING OF MACRO PROGRAM TO CALCULATE THE BASELINE-CORRECTED ABSORBANCE VALUES FOR HYDRAZINE (957.3 CM-1 BAND), INCLUDING THE FORTRAN PROGRAM GET2.FTN

This program is called BC1. It was written in the Nicolet MACRO language by using the TED editor and then compiling with the Nicolet utility program MACCRT. This procedure allows remarks to be included in the program for documentation and user assistance.

The main MACRO program (BC1) calls the FORTRAN program GET2.FTN, which, in turn calls a FORTRAN subroutine called FGETOF. These programs are listed, in sequence, below.

```
!BC1                \MACRO TO COMPUTE BASELINE-CORRECTED ABSORBANCE
                    \VALUES FOR HYDRAZINE (957.3 CM-1 BAND)
                    \---USED WITH SINGLE BEAM SPECTRA
BFN
OMD
ENTER BEGINNING AND ENDING DFN'S
SRT
QIT
DFN=SRT
SFN=2
FOR AAA=SRT TIL QIT
TEM=4
NPR
PRN DFN
STD
TEM=4
NPR
OFN=DFN
MOS
RAS
ABS
DFN=SFN
XSP=958
XEP=957
THR=-.5
PPK
XSP=4000
XEP=0
TEM=4
NPR
GFN
GET2.FTN
FRN
TEM=4
```

```
NPR
DFN=OFN
DFN=DFN+1
NXT AAA
END
!!
```

The FORTRAN program GET2.FTN is listed below.

```
CCCCCCCCCCCCCCCCCCCCCCCCCCCCCCCCCCCCCCCCCCCCCCCCCCCCCCCCCCCCCCCCCCCCCCCCCCC
C
C
C      PROGRAM GET2.ASC
C
C      THIS PROGRAM RETRIEVES ABSORBANCE DATA FOR HYDRAZINE
C      FROM THE DESTINATION FILE AND STORES IT IN A REAL
C      FORTRAN ARRAY, RDATA(I), FOR USE IN BASELINE
C      CORRECTIONS.  IT IS CALLED FROM THE FT-IR MACRO BC1.
C
C      THE BASELINE CORRECTION ROUTINE IS AN EXTENSION OF THE
C      LINEAR CORRECTION GIVEN IN "FT-IR SPECTRAL LINES", VOL.
C      II, NO. 1, PP. 8-9.
C
C               (D.A.S.    22 DEC 86)
C
C
CCCCCCCCCCCCCCCCCCCCCCCCCCCCCCCCCCCCCCCCCCCCCCCCCCCCCCCCCCCCCCCCCCCCCCCCCCC

C234567
             PROGRAM GET2
             INTEGER IHEAD(512),ISTP,IENP,NP
             REAL  RDATA(23000),BP1,LBP,PXA,PYA,CABS,XDIF,XDIF2
     1,YDIF,FAC1,FAC2,EP,SP
             COMMON  / BUFBL / IDA(23000),IBUF(512)
             NPMAX=23000
C
C      GET THE DESIRED REGION OF THE DFN INTO A REAL FORTRAN ARRAY
C
      CALL FGETOF(IHEAD,ISTP,IENP,NP,NPMAX,FXAX,RDATA)
C
C      RETRIEVE THE FILE HEADER INFORMATION AND CHECK FOR
C      CORRECT SPECTRUM FORMAT AND ARRAY SIZE.

          IF (IHEAD(10).NE.0) THEN
             PRINT 100
  100 FORMAT (' ','SPECTRUM NOT ABSORBANCE',/)
             CALL IREXIT
          ELSEIF (NP.GT.NPMAX) THEN
             PRINT 101, NPMAX
```

```
  101 FORMAT (' ','NO. OF PTS. REQUESTED IS MORE THAN  ',I7,/)
            CALL IREXIT
          ENDIF

C
C       COMPUTE THE BASELINE CORRECTED ABSORBANCE VALUE FOR THE
C       ANALYTICAL PEAK OF THE DESIRED SUBSTANCE:
C
C             THE STARTING AND ENDING POINTS FOR DETERMINING THE
C             BASELINE ARE FOUND BY AVERAGING THE ABSORBANCE VALUES
C             IN A SPECIFIC RANGE FOR THE BEGINNING AND ENDING
C             POINTS OF THE BASELINE.  THE LOCATION OF THESE
C             POINTS IN THE SCRATCH FILE IS DETERMINED FROM THE
C             FACT THAT THE DATA FILE IS 44 SECTORS LONG WITH 512
C             POINTS (OR WORDS) PER SECTOR, I.E., 22528 POINTS
C             (THE VALUE OF FSZ FOR A 1.0 CM-1 SPECTRUM).  HOWEVER,
C             ONLY 16384 POINTS ARE NECESSARY TO DEFINE A 1.0 CM-1
C             SPECTRUM.  IN ADDITION, WITH A SAMPLE SPACING (SSP)
C             OF 2, THE FREQUENCY RANGE COVERED BY THE DATA IS
C             ZERO TO 1/2 THE LASER FREQUENCY (0-7899.1 CM-1).
C             THUS, WITH 16384 DATA POINTS TO COVER 7899.1 CM-1,
C             THERE ARE (7899.1/16384) 0.482 CM-1 PER DATA POINT
C             IN THE FT-IR SCRATCH FILE.  NOW, TO DETERMINE THE
C             DATA POINT VALUES FOR A GIVEN WAVENUMBER RANGE, THE
C             ABOVE RELATIONSHIP IS USED.  FOR EXAMPLE, IN THE
C             HYDRAZINE BASELINE, THE FIRST BASELINE POINT WILL
C             BE THE AVERAGE VALUE OF THE POINTS FROM 1160 TO 1180
C             CM-1, OR 2406 TO 2488 IN THE DATA FILE.  SO THE
C             AVERAGE OF THE POINTS (43) ION THIS PART OF THE DATA
C             FILE WILL BE DETERMINED BY ADDING THEM UP AND
C             DIVIDING BY 43.
C
C
C       AVERAGE THE POINTS FOR THE FIRST BASELINE VALUE
C
              SP=0
              BP1=0
              COUNT=0
              XFAC=7899.1/16384
              DO 200 I=2406,2448
              WAVE=XFAC*(I+1)
              SP=SP+RDATA(I)
              COUNT=COUNT+1
  200 CONTINUE
              BP1=SP/COUNT
C
C       AVERAGE THE POINTS FOR THE SECOND BASELINE VALUE
C
              EP=0
              LBP=0
```

```
              COUNT=0
              DO 201 I=1742,1784
              WAVE1=XFAC*(I+1)
              EP=EP+RDATA(I)
              COUNT=COUNT+1
  201 CONTINUE
              LBP=EP/COUNT
C
C       RETRIEVE THE FT-IR VALUES FOR FREQUENCY AND ABSORBANCE
C       FROM TH PEAK PICK ROUTING.  (THEY ARE STORED AS FLOATING
C       POINT VALUES IN PXA AND PYA)
C
              PXA=RVAL(6112,1)
              PYA=RVAL(6116,1)
C
C       CALCULATE BASELINE CORRECTION.  THERE ARE TWO POSSIBLE
C       CASES;  (A) POSITIVE SLOPING BASELINE OR (B) NEGATIVE
C       SLOPING BASELINE.
C
C                     CASE A - POSITIVE SLOPING BASELINE
                              (I.E., BP1 < LBP)
C
C       SKIP TO CASE (B) IF BASELINE SLOPE IS NEGATIVE
C
              IF(BPZ.GT.LBP) GOTO 3000
C
C       OTHERWISE, PROCEED WITH THE CORRECTION

C
              YDIF=LBP-BP1
              XDIF=1170-850
              XDIF2=1170-PXA
              FAC1=XDIF2/XDIF
              FAC2=FAC1*YDIF
              FAC2=FAC2+BP1
                GOTO 3500
C
C                     CASE B - NEGATIVE SLOPING BASELINE
C                              (I.E., BP1 > LBP)
C
C
 3000 CONTINUE
       YDIF=BP1-LBP
       XDIF=1170-850
       XDIF2=PXA-1170
       FAC1=XDIF2/XDIF
       FAC2=FAC1*YDIF
       FAC2=FAC2+LBP
C
 3500 CONTINUE
```

```
C
C       APPLY CORRECTION TO ABSORBANCE VALUE FROM PPK
C
        CABS=PYA-FAC2
C
C       PRINT OUT CORRECTED ABSORBANCE VALUE
C
        WRITE (2,550) CABS
  550 FORMAT(40('-'),/,' ','PEAK ABS= ',F9.3,/,40('-'),/)
C
C       RETURN TO FTIR
C
        CALL IREXIT
        END
```

The final listing is the FORTRAN subroutine FGETOF.

```
CCCCCCCCCCCCCCCCCCCCCCCCCCCCCCCCCCCCCCCCCCCCCCCCCCCCCCCCCCCCCCCCCCCCCCCCCCCCCCC
C
C       SUBROUTINE FGETOF
C
C  Gets a file status block IHEAD and piece of spectrum RDATA
C  from FT-IR data, using XSP, XEP, OFN, and FSZS (in sectors).
C
C  DWV, Nicolet  -  Dec. 1981  (revised Jan, 1982, DWV)
C
C                -  Revision attached to NICOLET letter dated
C                   28 Aug 86 (completed 2 Dec 86), D.A.S.
C
C                -  Revised to have a form compatible with
C                   the original FGETOF program (Nicolet
C                   FORTRAN 77, pp. 61-62), D.A.S. 9 Dec 86

C
CCCCCCCCCCCCCCCCCCCCCCCCCCCCCCCCCCCCCCCCCCCCCCCCCCCCCCCCCCCCCCCCCCCCCCCCCCCCCC
C
C234567
      SUBROUTINE FGETOF (IHEAD,ISTP,IENP,NP,NPMAX, FXAX, AND RDATA)
              COMMON  /  BUFBL  /  IDA(23000)
            REAL RDATA(23000)
            INTEGER IHEAD(512),DFN,FSZS
            FLASER=15798.2
C
C       Use IRVAL to load necessary values from FTIR parameters
C
              IXSP = IRVAL(6165,1)
              IXEP = IRVAL(6166,1)
              DFN  = IRVAL(6162,1)
```

```
            FSZS = IRVAL(6145,1)
            INODE= IRVAL(13003,0)
C
C       Now get file status block of DFN file and call it IHEAD
C
        CALL IRTISK(IHEAD,352,87+(DFN+1)*FSZS,INODE)
        NPTS = IHEAD(15)*128
        IFGF = IHEAD(8)
        FEXP = 2**(19-IHEAD(6))
        FXAX = FLASER/(NPTS*IHEAD(17))
C
C       Now calculate ISTP and IENP for interferogram or wavenumber case
C
        IF (IFGF.EQ.0) THEN
           FXAX = 1.
           IF (IXSP.LE.IXEP) THEN
              ISTP = ISXP
              IENP = IXEP
           ELSE
              ISTP = IXEP
              IENP = IXSP
           ENDIF
        ELSEIF (ISEP.GT.IXEP) THEN
              ISTP = IXEP/FXAX+0.5
              IENP = IXSP/FXAX+0.5
           ELSE
              ISTP = IXSP/FXAX+0.5
              IENP = IXEP/FXAX+0.5
           ENDIF
           NP = IENP-ISTP+1
C
C       Check for a reasonable number of points in NP
C
        IF (NP.GT.NPMAX) THEN
           PRINT 901,NPMAX,NP
           NP = NPMAX
        ELSEIF (NP.LT.5) THEN
           PRINT 902,NP
        ENDIF
C
C       Now read data from scratch DFN into array IDA
C
        IN = 1
        NDONE = ISTP/512
        NSKIP = ISTP-NDONE*512

        IF (NSKIP.GT.0) THEN
              CALL IRTISK(IDA,512,88+DFN*FSZ+NDONE,INODE)
              DO 10 I=NSKIP+1,512
                IDA(IN) = IDA(I)
```

```
                IN = IN+1
   10 CONTINUE
      NDONE = NDONE+1
      ENDIF
      NPREM = NP-IN+1
      IF (NPREM.GT.0) THEN
      CALL IRTISK(IDA(IN),NPREM,88+DFN*FSZ+NDONE,INODE)
      ENDIF
C
C     In FTIR, (-524288) is the "official ridiculous value" which
C     is used in blanking spectral areas.  Since FORTRAN doesn't
C     and shouldn't recognize this value, a trick is used to create
C     this value in IRID in order to excise it from RDATA.
C
      IRID = -524287-1
C
C     Now float IDA into RDATA, checking for IRID and zeroing.
C
      DO 50 I=1,NP
         IDAS = IDA(I)
         IF (IDAS.EQ.IRID) IDAS = 0
         RDATA(I) = IDAS/FEXP
   50 CONTINUE

      RETURN

  901 FORMAT (1X,'Only dimensioned to ',I6,' points, not ',I6/)
  902 FORMAT (1X,'Why are there only',I6,'points requested?'/)

      END
```

APPENDIX D

THE PERMEATION MODEL VERSION AND THE BASIC SUBROUTINE USED IN THE MARQUARDT NONLINEAR LEAST SQUARES ROUTINE

The permeation model allows for permeation through the chamber walls as the only kinetic process. Hence, from Equation (11), the model reduces to:

$$d[G]/dt = -k_s[S][G] + k_{-s}[G\text{-}S_1]$$

$$d[G\text{-}S_1]/dt = k_s[S][G] - k_{-s}[G\text{-}S_1] + k_D[S]([G\text{-}S_2] - [G\text{-}S_1])$$

For $i = 2$ to $N-1$ (if $N \geq 3$);

$$d[G\text{-}S_i]/dt = k_D[S]([G\text{-}S_{i-1}] + [G\text{-}S_{i+1}] - 2[G\text{-}S_i])$$

$$d[G\text{-}S_N]/dt = k_D[S]([G\text{-}S_{N-1}] - [G\text{-}S_N]) - k_{-s}[G\text{-}S_N].$$

Since it is assumed that $[S] \gg [G]$, $[S]$ is essentially constant and the only three parameters are $k_s[S]$, k_{-s}, and $k_D[S]$. N is a predetermined integer. Although in theory N is quite large, in practice it is normally set to 2 for expediency in calculations. Making N larger does alter the parameters, but does not severely affect the goodness of the fit. For $N = 2$, the dependent variables are $[G]$, $[G\text{-}S_1]$, and $[G\text{-}S_2]$.

The actual differential equations which have been used in the routine are:

$$dL_1/dt = c_1(g - L_1) - c_2(L_1 - L_2)$$

For $i = 2$ to N;

$$dL_i/dt = c_3(L_{i-1} + L_{i+1} - 2L_i)$$

$$dL_{N+1}/dt = c_2(L_N - L_{N+1}),$$

in which $c_1 = k_s[S]$, $c_2 = k_{-s}$, $c_3 = k_D[S]$, and the Ls are given in the following expressions:

$$[G] = g - L_i$$

For i = 1 to N;

$$[G\text{-}S_i] = L_i - L_{i+1}.$$

These equations are generated from the following analysis:

$$\underset{g - L_1}{G} + \underset{L_1}{S_1} \underset{k_{-s}}{\overset{k_s}{\rightleftharpoons}} \underset{L_1}{G\text{-}S_1}$$

For i = 2 to N;

$$\underset{L_{i-1} - L_i}{G\text{-}S_{i-1}} + \underset{L_i}{S_i} \underset{k_D}{\overset{k_D}{\rightleftharpoons}} \underset{L_i}{G\text{-}S_i} + \underset{L_{i-1}}{S_{i-1}}$$

$$\underset{L_N - L_{N+1}}{G\text{-}S_N} \xrightarrow{k_{-s}} \underset{L_{N+1}}{G \text{ (outside chamber)}} + S_N.$$

Note that [G], which is proportional to the absorbance according to Beer's Law, is the variable being monitored. This analysis allows for a direct monitoring of how much of G is lost from the chamber system. It can easily be seen that:

$$g - L_{N+1} = [G] + \sum_{i=1}^{N} [G\text{-}S_i].$$

L_{N+1} is the concentration, in moles per unit chamber volume of gas lost from the system. It cannot be interpreted as the concentration outside the system, since all concentration terms must have a common reference point, in this case the chamber volume.

The following is the subroutine, which starts on 1100 of the program, used to perform the numeric integration:

1100 If I > 1, then 1125

```
1101 Dt = .01
1102 Nm = 2
1103 Dim L(Nm+1)
1104 For E = 1 to Nm + 1
1105     L(E) = 0
1106 Next E
1107 T = 0
1108 T = T + Dt
1109 L(1) = L(1) + C(1)*(G - L(1))*Dt - C(2)*(L(1) - L(2))*Dt
1110 For E = 2 to Nm
1111     L(E) = L(E) + C(3)*(L(E-1) + L(E+1) - 2*L(E))*Dt
1112 Next E
1113 L(Nm+1) = L(Nm+1) + C(2)*(L(Nm) - L(Nm+1))*Dt
1114 If T < 0.1 Then 1108
1115 If ABS(G - L(1) - "initial absorbance value") < 0.001 then 1118
1116 G = L(1) + "initial absorbance value"
1117 Go to 1104
1118 Y1 = G - L(1)
1119 T = 0
1120 Go to 1140
1125 T = T + Dt
1126 L(1) = L(1) + C(1)*(G - L(1))*Dt - C(2)*(L(1) - L(2)*Dt
1127 For E = 2 to Nm
1128     L(E) = L(E) + C(3)*(L(E-1) + L(E+1) - 2*L(E))*Dt
1129 Next E
1130 L(Nm+1) = L(Nm+1) + C(2)*(L(Nm) - L(Nm+1))*Dt
1131 If T < X(I,1) then 1125
1132 Y1 = G - L(1)
1140 Return
```

The terms are defined as:

Nm - number of pore layers

Y1 - dependent variable, in this case the absorbance readings

T - time

Dt - differential time element, Δt

X(I,1) - independent variable, in this case the Ith time reading. The "1" refers to this being the first, and in this case the only, independent variable.

The subroutine operates in the following manner. Initially I is set to one, so the program first goes through lines 1101 to 1120. These lines define the parameters Dt, Nm, and T, and set first conditions. In the experimental runs, the gas is mixed in the chamber between 5 and 10 minutes before the first absorbance reading is taken. This is the mixing time. Hence, enough time has elapsed to allow for some surface adsorption, and consequently G in lines 1109 and 1126 is not the initial absorbance reading, but is slightly larger. Lines 1108 through 1117 allow integration to occur for the mixing time, which is usually set at 0.1 hour for convenience. Since G is not known exactly at the beginning of the program, it is generally set to the initial absorbance reading or slightly larger before program execution. Line 1116 readjusts G and the numeric integration for the mixing time is repeated. This is done sufficient times so as to make the quantity, G - L(1), within a certain tolerance (.001 absorbance unit) of the initial absorbance value. Once this condition has been met, T is reset to zero, I is set to 2 and the program goes to line 1125 of the subroutine. Here the integration begins with T = 0 and goes to the full time of the run. The main part of the program then calculates the sum of squares, readjusts the parameters, and goes through the entire integration subroutine again. The intent of the program is of course to minimize the sum of squares.

APPENDIX E

ANALYSIS OF SEVERAL KINETIC SYSTEMS

1. System: $G \xrightarrow{k_1}$ Products

$$2G \xrightarrow{k_2} \text{Products}$$

Differential equation: $d[G]/dt = -(k_2[G] + k_1)[G]$.

Integration:

$$\int_g^{[G]} d[G]/\{[G](k_2[G] + k_1)\} = -\int_0^t dt,$$

$$[G] = [k_1 g \exp(-k_1 t)]/\{k_2 g[1 - \exp(-k_1 t)] + k_1\}$$

2. System: $\underset{g-x}{G} + \underset{a-x}{A} \xrightarrow{k_1} \underset{x}{B}$

$$\underset{g-x-y}{G} + \underset{x-y}{B} \xrightarrow{k_2} \underset{y}{\text{Products}}$$

Differential equations:

$d[A]/dt = -k_1[G][A]$, or $dx/dt = k_1(g - x - y)(a - x)$

$d[B]/dt = -k_2[G][B] + k_1[G][A]$, or

$dx/dt - dy/dt = -k_2(g - x - y)(x - y) + k_1(g - x - y)(a - x)$

Therefore, $dy/dt = k_2(g - x - y)(x - y)$. Y can be solved in terms of x as follows:

$dy/dt/dx/dt = dy/dx = k_2(x - y)/[k_1(a - x)]$.

Let $\alpha = k_2/k_1$. If dy/dx is written as $dy/dx = -\alpha y/(a - x) + \alpha x/(a - x)$ an integrating factor can be easily introduced to aid in the integration. This factor is:

$$\exp[\alpha \int dx/(a - x)] = (a - x)^{-\alpha}.$$

Hence, $(a - x)^{-\alpha} dy/dx + (a - x)^{-\alpha-1} \alpha y = (a - x)^{-\alpha-1} \alpha x$, or $d[y(a - x)^{-\alpha}] = (a - x)^{-\alpha-1} \alpha x dx$. The expression, $(a - x)^{-\alpha-1} \alpha x dx$, can be integrated by parts to yield:

$$\alpha \int (a-x)^{-\alpha-1} x dx = x(a - x)^{-\alpha} - \int (a - x)^{-\alpha} dx.$$

The overall expression can now be integrated for the following two cases:

Case 1: $\alpha = 1$;

$$\int d[y/(a - x)] = x/(a - x) - \int dx/(a - x) + C,$$

in which C is the integration constant. At $t = 0$, $x = y = 0$. Hence, $C = -\ln a$ and y is:

$$y = x + (a - x)\ln(1 - x/a).$$

[G] and [B] can now be put in terms of [A]:

$$[G] = g - 2(a - [A]) - [A]\ln([A]/a),$$

$$[B] = [A]\ln(a/[A]).$$

Case 2: $\alpha \neq 1$;

$$\int d[y(a - x)^{-\alpha}] = x/(a - x)^{\alpha} - \int (a - x)^{-\alpha} dx + C.$$

In this case, $C = a^{1-\alpha}/(\alpha - 1)$. Therefore y is:

$$y = [a - \alpha x - a^{1-\alpha}(a - x)^{\alpha}]/(1 - \alpha).$$

[G] and [B] can be shown to be:

$$[G] = g - a[1 - ([A]/a)^{\alpha} + (1 - 2\alpha)(1 - [A]/a)]/(1 - \alpha)$$

$$[B] = [([A]/a)^{\alpha-1} - 1][A]/(1 - \alpha).$$

The differential equations in time can be analytically integrated easily when $\alpha = 1/2$. In this case, the equation for $d[A]/dt$ is:

$$d[A]/dt = -k_1[A]\{g - 2a[1 - ([A]/a)^{1/2}]\}.$$

If $g = 2a$, $d[A]/dt = -2k_1a[A]([A]/a)^{1/2}$ and integration yields:

$$\int_a^{[A]} a^{-1/2}\,[A]^{-3/2}\,d[A] = -2k_1 \int_0^t dt,$$

$$[A] = a/[(1 + k_1at)^2]$$

$$[G] = 2a(1 - k_1at)/(1 + k_1at)$$

$$[B] = 2k_1a^2t/[(1 + k_1at)^2].$$

If $g \neq 2a$, making the substitution, $\theta = ([A]/a)^{1/2}$, yields the following simplified equation:

$$d\theta = -k_1\theta[g - 2a(1 - \theta)]dt/2.$$

Integration within limits yields:

$$\int_1^{\theta} d\theta/\{\theta[g - 2a(1 - \theta)]\} = -(k_1/2) \int_0^t dt,$$

$$\theta = (2a - g)/[2a - gf(t)],$$

in which $f(t) = \exp[(g/2 - a)k_1t]$. The concentrations can be shown to be:

$$[A] = a\{(2a - g)/[2a - gf(t)]\}^2$$

$$[G] = g + 2ag[f(t) - 1]/[2a - gf(t)]$$

$$[B] = 2ag(2a - g)[1 - f(t)]/[2a - gf(t)]^2.$$

3. System: $\underset{g-x}{G} + \underset{a-x}{A} \underset{k_{-1}}{\overset{k_1}{\rightleftharpoons}} \underset{x}{B}$

Differential equation:

$$d[G]/dt = -k_1[G][A] + k_{-1}[B], \text{ or } dx/dt = k_1(g - x)(a - x) - k_{-1}x.$$

The integral within limits is:

$$\int_0^x dx/[k_1(g - x)(a - x) - k_{-1}x] = \int_0^t dt.$$

This integral can be found in mathematics handbooks. The integration yields:

$$(1/\sqrt{q})\ln[(2x - a - g - k_{-1}/k_1 - \sqrt{q})/(2x - a - g - k_{-1}/k_1 + \sqrt{q})]\Big|_0^x = t,$$

in which $q = (a + g + k_{-1}/k_1)^2 - 4ag$, which is always positive unless $a = g$ and $k_{-1} = 0$. In this case it is zero. X can be shown to be:

$$x = Z_1Z_2[\exp(k_1\sqrt{q}t) - 1]/\{2[Z_1 - Z_2\exp(k_1\sqrt{q}t)]\},$$

in which $Z_1 = \sqrt{q} - a - g - k_{-1}/k_1$ and $Z_2 = -(\sqrt{q} + a + g + k_{-1}/k_1)$.

The concentrations are:

$$[B] = 2ag[f(t) - 1]/[Z_1 - Z_2f(t)]$$

$$[A] = a\{1 - 2g[f(t) - 1]/[Z_1 - Z_2f(t)]\}$$

$$[G] = g\{1 - 2a[f(t) - 1]/[Z_1 - Z_2f(t)]\},$$

in which $f(t) = \exp(k_1\sqrt{q}t)$.

4. System: $\underset{g-x}{G} + \underset{a-x}{A} \underset{k_{-1}}{\overset{k_1}{\rightleftharpoons}} \underset{x}{B} + \underset{x}{C}$

Differential equation:

$$d[G]/dt = -k_1[G][A] + k_{-1}[B][C], \text{ or } dx/dt = k_1(g - x)(a - x) - k_{-1}x^2.$$

Integration within limits yields:

$$\int_0^x dx/[(k_1 - k_{-1})x^2 - (a + g)k_1x + k_1ag] = t.$$

If $k_1 = k_{-1}$, x can be shown to be:

$$x = ag\{1 - \exp[-(a + g)k_1t]\}/(a + g).$$

The concentrations are:

$$[B] = [C] = ag[1 - f(t)]/(a + g)$$

$$[G] = g[g + af(t)]/(a + g)$$

$$[A] = a[a + gf(t)]/(a + g),$$

in which $f(t) = \exp[-(a + g)k_1t]$. If $k_1 \neq k_{-1}$, the form of the integral is identical to that of system 3. Therefore, the concentrations can be shown to be:

$$[B] = [C] = 2ag[f(t) - 1]/[Z_1 - Z_2f(t)]$$

$$[G] = g\{1 - 2a[f(t) - 1]/[Z_1 - Z_2f(t)]\}$$

$$[A] = a\{1 - 2g[f(t) - 1]/[Z_1 - Z_2f(t)]\},$$

in which $f(t) = \exp(k_1\sqrt{q}t)$, $q = (a - g)^2 + 4agk_{-1}/k_1$, $Z_1 = \sqrt{q} - a - g$, and $Z_2 = -(\sqrt{q} + a + g)$.

5. System: $G + A \underset{k_{-1}}{\overset{k_1}{\rightleftharpoons}} B$ (g-x, a, k_{-1}, x) Assumption: $a \gg g$

$$A + B \underset{k_{-2}}{\overset{k_2}{\rightleftharpoons}} C \quad (a,\ x-y,\ k_{-2},\ y)$$

Differential equations:

$$d[G]/dt = -k_1a[G] + k_{-1}[B], \text{ or } dx/dt = k_1a(g - x) - k_{-1}(x - y)$$

$$d[C]/dt = k_2a[B] - k_{-2}[C], \text{ or } dy/dt = k_2a(x - y) - k_{-2}y$$

X and y can be put in terms of one another as follows:

$$dx/dt/dy/dt = dx/dy =$$

$$[k_1a(g - x) - k_{-1}(x - y)]/[k_2a(x - y) - k_{-2}y],$$

The differential equation can be solved by making the following substitutions:

$$k_2ax - (k_2a + k_{-2})y = c_1(x + c_2) + c_3(y + c_4)$$

$$k_1ag - (k_1a + k_{-1})x + k_{-1}y = c_5(x + c_2) + c_6(y + c_4),$$

in which the constants can be shown to be:

$$c_1 = k_2a$$

$$c_2 = -k_1ag(k_2a + k_{-2})/[k_1a(k_2a + k_{-2}) + k_{-1}k_{-2}]$$

$$c_3 = -k_2a - k_{-2}$$

$$c_4 = -k_1k_2a^2g/[k_1a(k_2a + k_{-2}) + k_{-1}k_{-2}]$$

$$c_5 = -k_1a - k_{-1}$$

$$c_6 = k_{-1}.$$

The differential equation reduces to :

$$dy'/y' = (K_2s - K_2 - 1)ds/\{-K_2s^2 + [K_2 - 1 - a(1 + K_1)]s + a\},$$

in which $y' = y + c_4$, $a = k_{-1}/k_{-2}$, $K_1 = k_1a/k_{-1}$, $K_2 = k_2a/k_{-2}$, $x' = sy'$, and $x' = x + c_2$. The variable, s, has been introduced to allow for variable separation in the equation. It can be shown that the numerator of the right-hand side of the equation above is

never the derivative of the denominator. The integral of this expression can be found in mathematics handbooks, and is:

$$\ln y' = -(1/2)\ln(-K_2 s^2 + \theta s + \alpha) + [(\theta/2 - K_2 - 1)/\sqrt{q}]\ln[(2K_2 s - \theta + \sqrt{q})/(2K_2 s - \theta - \sqrt{q})] + C,$$

In which $\theta = K_2 - 1 - \alpha(1 + K_1)$, $q = \theta^2 + 4K_2\alpha$, and C is the integration constant. At $t = 0$, $x = y = 0$. Solving for C and substituting back into the expression yields:

$$y = K_1 K_2 g[1 - f(s)]/[K_1(K_2 + 1) + 1],$$

in which $f(s) = \{[K_2(1 + 1/K_2)^2 - \theta(1 + 1/K_2) - \alpha]/(K_2 s^2 - \theta s - \alpha)\}^{1/2}\{(2K_2 s - \theta + \sqrt{q})(2 + 2K_2 - \theta - \sqrt{q})/[(2 + 2K_2 - \theta + \sqrt{q})(2K_2 s - \theta - \sqrt{q})]\}^{\Phi}$, and $\Phi = (\theta/2 - K_2 - 1)/\sqrt{q}$. Noting that $x = s(y + c_4) - c_2$, the concentrations can be put in terms of s as:

$$[B] = K_1 K_2 g(1 - s)f(s)/[K_1(K_2 + 1) + 1] + K_1 g/[K_1(K_2 + 1) + 1]$$

$$[C] = K_1 K_2 g[1 - f(s)]/[K_1(K_2 + 1) + 1]$$

$$[G] = K_1 K_2 g s f(s)/[K_1(K_2 + 1) + 1] + g/[K_1(K_2 + 1) + 1].$$

Relative values for these concentrations can be calculated by inputting the appropriate values for s. The upper value of s is the value at $t = 0$. At $t = 0$, $s = 1 + 1/K_2$. At $t = \infty$, the concentrations are all at their equilibrium values. The equilibrium concentrations can be shown to be:

$$[B]_e = K_1 g/[K_1(K_2 + 1) + 1]$$

$$[C]_e = K_1 K_2 g/[K_1(K_2 + 1) + 1]$$

$$[G]_e = g/[K_1(K_2 + 1) + 1],$$

in which the subscript "e" denotes equilibrium. Equilibrium conditions are met where $f(s) = 0$. Since Φ is always negative, $f(s) = 0$ where $2K_2 s - \theta + \sqrt{q} = 0$. Hence, $s_e = (\theta + \sqrt{q})/2K_2$. The range for s is:

$$1 + 1/K_2 \geq s \geq (\theta + \sqrt{q})/(2K_2).$$

It is true that the term, $K_2s^2 - \theta s - \alpha$, is zero where $s = s_e$. Even though this term appears in the denominator, the term, $2K_2s - \theta + \sqrt{q}$, is in the numerator, and f(s) does approach zero as s approaches s_e.

The differential equations in time can be solved by assuming a general exponential form of the solution to the differential equations in time. This is done in several kinetics textbooks and will not be done here.

APPENDIX F

ADAPTATION OF THE MODEL FOR DESCRIBING EFFUSION AND PERMEATION INTO THE CHAMBER

For a gas coming into the chamber, one can write the following series of steps:

$$\underset{g}{G(\text{outside})} \underset{ke}{\overset{ke}{\rightleftharpoons}} \underset{L_e}{G(\text{inside})}$$

$$\underset{g}{G(\text{outside})} + S_N \underset{k_{-s}}{\overset{k_s}{\rightleftharpoons}} \underset{L_{N+1}}{G\text{-}S_N}$$

For i = 1 to N - 1;

$$\underset{\substack{L_{N+2-i} - \\ L_{N+1-i}}}{G\text{-}S_{N+1-i}} + S_{N-i} \underset{k_D}{\overset{k_D}{\rightleftharpoons}} \underset{L_{N+1-i}}{G\text{-}S_{N-i}} + S_{N+1-i}$$

$$\underset{L_2 - L_1}{G\text{-}S_1} \underset{k_s}{\overset{k_{-s}}{\rightleftharpoons}} \underset{L_1}{G(\text{inside})} + S_1$$

This model assumes an infinite outside reservoir of the gas. The concentrations are:

$$[G] = L_e + L_1$$

For i = 1 the N;

$$[G\text{-}S_i] = L_{i+1} - L_i.$$

The differential equations are:

$$dL_e/dt = k_e(g - L_e - L_1)$$

$$dL_{N+1}/dt = k_s[S]g - k_{-s}(L_{N+1} - L_N)$$

For $i = 1$ to $N - 1$;

$$dL_{N+1-i}/dt = k_D[S](L_{N+2-i} + L_{N-i} - 2L_{N+1-i})$$

$$dL_1/dt = k_{-s}(L_2 - L_1) - k_s(L_e + L_1).$$

APPENDIX G

ADAPTATION OF THE MODEL FOR DESCRIBING PERMEATION THROUGH CHAMBER WALLS AND THROUGH PERMEABLE SURFACES WITHIN THE CHAMBER

For a gas permeating through the surface of a material placed inside the chamber, the processes are described as:

$$\begin{matrix} G(\text{inside}) + \bar{S}_1 & \underset{\bar{k}_{-s}}{\overset{\bar{k}_s}{\rightleftharpoons}} & G\text{-}\bar{S}_1 \\ g - \bar{L}_1 & & \bar{L}_1 \end{matrix}$$

For $i = 1$ to $\bar{N} - 1$;

$$\begin{matrix} G\text{-}\bar{S}_i + \bar{S}_{i+1} & \underset{\bar{k}_D}{\overset{\bar{k}_D}{\rightleftharpoons}} & G\text{-}\bar{S}_{i+1} + \bar{S}_i \\ \bar{L}_i - \bar{L}_{i+1} & & \bar{L}_{i+1} \end{matrix}$$

$$\begin{matrix} G\text{-}\bar{S}_{\bar{N}} & \underset{\bar{k}_s}{\overset{\bar{k}_{-s}}{\rightleftharpoons}} & G(\text{inside}) + \bar{S}_{\bar{N}}, \\ \bar{L}_{\bar{N}} - \bar{L}_{\bar{N}+1} & & g - \bar{L}_1 + \bar{L}_{\bar{N}+1} \end{matrix}$$

in which the overhead bar refers to the permeable surface inside the chamber. For a gas permeating through the chamber walls, the processes are:

$$\begin{matrix} G(\text{inside}) + S_1 & \underset{k_{-s}}{\overset{k_s}{\rightleftharpoons}} & G\text{-}S_1 \\ g - \bar{L}_1 + \bar{L}_{\bar{N}+1} - L_1 & & L_1 \end{matrix}$$

For $i = 1$ to $N - 1$;

$$\begin{matrix} G\text{-}S_i + S_{i+1} & \underset{k_D}{\overset{k_D}{\rightleftharpoons}} & G\text{-}S_{i+1} + S_i \\ L_i - L_{i+1} & & L_{i+1} \end{matrix}$$

$$\begin{matrix} G\text{-}S_N & \xrightarrow{k_{-s}} & G(\text{outside}) + S_N. \\ L_N - L_{N+1} & & L_{N+1} \end{matrix}$$

The concentrations are:

$$[G] = g - \bar{L}_1 + \bar{L}_{\bar{N}+1} - L_1$$

For $i = 1$ to $\bar{N}$;

$$[G\text{-}\bar{S}_i] = \bar{L}_i - \bar{L}_{i+1}$$

For $i = 1$ to N;

$$[G\text{-}S_i] = L_i - L_{i+1}.$$

The differential equations describing the gas permeation through the inside permeable surfaces are:

$$\begin{aligned} d[G]/dt &= -d\bar{L}_1/dt + d\bar{L}_{\bar{N}+1}/dt - dL_1/dt \\ &= -(2\bar{k}_s[\bar{S}] + k_s[S])(g - \bar{L}_1 + \bar{L}_{\bar{N}+1} - L_1) \\ &\quad + \bar{k}_{-s}(\bar{L}_1 - \bar{L}_2 + \bar{L}_{\bar{N}} - \bar{L}_{\bar{N}+1}) + k_{-s}(L_1 - L_2) \end{aligned}$$

$$\begin{aligned} d[G\text{-}\bar{S}_1]/dt &= d\bar{L}_1/dt - d\bar{L}_2/dt \\ &= \bar{k}_D[\bar{S}](g - \bar{L}_1 + \bar{L}_{\bar{N}+1} - L_1) - \bar{k}_{-s}(\bar{L}_1 - \bar{L}_2) - \bar{k}_D[\bar{S}](\bar{L}_1 - 2\bar{L}_2 + \bar{L}_3) \end{aligned}$$

For $i = 2$ to $\bar{N} - 1$;

$$d[G\text{-}\bar{S}_i]/dt = d\bar{L}_i/dt - d\bar{L}_{i+1}/dt = \bar{k}_D[\bar{S}][\bar{L}_{i-1} - 3(\bar{L}_i - \bar{L}_{i+1}) - \bar{L}_{i+2}]$$

$$\begin{aligned} d[G\text{-}\bar{S}_{\bar{N}}]/dt &= d\bar{L}_{\bar{N}}/dt - d\bar{L}_{\bar{N}+1}/dt \\ &= \bar{k}_s[\bar{S}](g - \bar{L}_1 + \bar{L}_{\bar{N}+1} - L_1) - \bar{k}_{-s}(\bar{L}_{\bar{N}} - \bar{L}_{\bar{N}+1}) \\ &\quad - \bar{k}_D[\bar{S}](\bar{L}_{\bar{N}-1} - 2\bar{L}_{\bar{N}} + \bar{L}_{\bar{N}+1}). \end{aligned}$$

The independent variables can be combined algebraically in pairs and the number of differential equations reduced to yield:

$$d\bar{L}_1/dt = 2\bar{k}_s[\bar{S}](g - L_1 - \bar{L}_1) - \bar{k}_{-s}(\bar{L}_1 - \bar{L}_2)$$

For $i = 2$ to $q + \delta - 1$ (if $\bar{N} \geq 5$);

$$d\bar{L}'_i/dt = \bar{k}_D[\bar{S}](\bar{L}'_{i-1} + \bar{L}'_{i+1} - 2\bar{L}'_i)$$

$$d\bar{L}'_{q+\delta}/dt = \bar{k}_D[\bar{S}][\bar{L}'_{q+\delta-1} - 2(1 + \delta)\bar{L}'_{q+\delta}] \quad \text{(if } \bar{N} \geq 3\text{)},$$

in which, in general, $\bar{L}'_i = \bar{L}_i - \bar{L}_{\bar{N}+2-i}$, $q = \bar{N}/2$, and $\delta = 1/2$ if $\bar{N}$ is odd and zero if $\bar{N}$ is even. The equations for the permeation through the chamber walls are:

$$dL_1/dt = k_s[S](g - L_1 - \bar{L}'_1) - k_{-s}(L_1 - L_2)$$

For $i = 2$ to N;

$$dL_i/dt = k_D[S](L_{i-1} + L_{i+1} - 2L_i)$$

$$dL_{N+1}/dt = k_{-s}(L_N - L_{N+1}).$$

Since $\bar{L}'_1 = \bar{L}_1 - \bar{L}_{\bar{N}+1}$, $[G] = g - L_1 - \bar{L}'_1$.

APPENDIX H

FIT OF HYDRAZINE DECAY DATA FROM STUDIES AT THE UNIVERSITY OF LEEDS

Hydrazine decay studies in Pyrex containers were conducted at the University of Leeds (Reference 10). No attempt was made to model the kinetic data by the researcher at the university. Some of the data from the University of Leeds studies have been modeled in this work. Two models have been used to test the concepts outlined in this report against the data: the adsorption-vapor oxidation model and the surface catalysis model. The adsorption-vapor oxidation model is:

$$N_2H_4 + S \underset{k_{-s}}{\overset{k_s}{\rightleftharpoons}} N_2H_4\text{-}S$$

$$N_2H_4 + O_2 \xrightarrow{k_p} N_2 + 2H_2O,$$

in which the rate constants have their usual meaning. The surface catalysis model is:

$$N_2H_4 + S \underset{k_{-s}}{\overset{k_s}{\rightleftharpoons}} N_2H_4\text{-}S$$

$$N_2H_4\text{-}S + O_2 \xrightarrow{k_p} N_2 + 2H_2O + S$$

If the variable, x, represents the extent of the first reaction in terms of the partial pressure, and y represents the extent of the second reaction, the differential equations for the adsorption-vapor oxidation model can be written as:

$$dx/dt = k_s[S](P_{N_2H_4} - x - y) - k_{-s}x$$

$$dy/dt = k_p(P_{N_2H_4} - x - y)(P_{O_2} - y)$$

in which the Ps represent initial partial pressures. The data was taken as the total pressure vs time. In terms of initial partial pressures and x and y, the total pressure is given from this model as:

$$P_T = P_{N_2H_4} + P_{O_2} - x + y$$

The differential equations for the surface catalysis model are:

$$dx/dt = k_s[S](P_{N_2H_4} - x) - k_{-s}(x - y)$$

$$dy/dt = k_s(x - y)(P_{O_2} - y)$$

The total pressure for this model is given by:

$$P_T = P_{N_2H_4} + P_{O_2} - x + 2y$$

If the approximation is made that $P_{O_2} - y \approx P_{O_2}$ and $k_{-s} \approx 0$, then the surface catalysis model can be analytically integrated to yield:

$$x = P_{N_2H_4}[1 - \exp(-k't)]$$

$$y = P_{N_2H_4\text{-}S} + P_{N_2H_4} - k_p'P_{N_2H_4}\exp(-K't)/(k_p' - k')$$

$$+ [k'P_{N_2H_4}/(k_p' - k') - P_{N_2H_4\text{-}S}]\exp(-k_p't)$$

in which $k' = k_s[S]$, $k_p' = k_pP_{O_2}$, and $P_{N_2H_4\text{-}S}$ is the partial pressure equivalent of the initial surface concentration of N_2H_4-S.

Both models were fitted to representative data. Figure H-1 shows a data set with model fits. As can be seen, the surface catalysis model fits the data much better. Results of the fit for the surface catalysis yield: $k' = .014(.002)$ minute^{-1}, $k_pP_{O_2} = .0325(.008)$ minute^{-1}, and $P_{N_2H_4\text{-}S} = .18(.05)$ mm Hg.

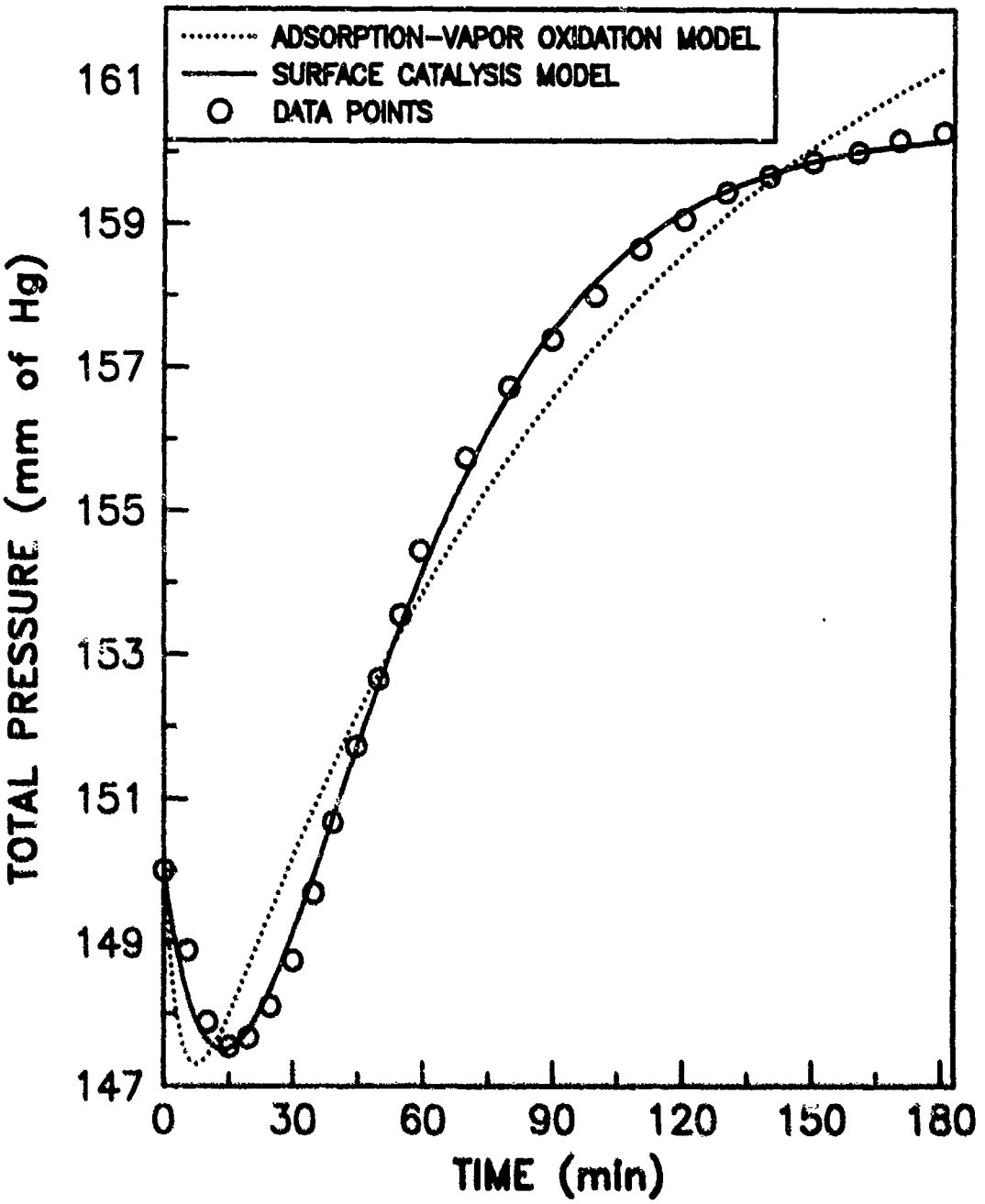

Figure H-1. Model Fits to University of Leeds Hydrazine Decay Data. Conditions: $P_{N_2H_4}$ = 10 mm Hg, P_{O_2} = 140 mm Hg, Temperature = 26 °C, Surface-to-Volume Ratio (Pyrex Vessel) = 1.38 cm^{-1}.